CHARACTERIZATION OF SEQUENCE VARIANTS IN THE CARDIAC ION CHANNEL GENES *KCNH2* AND *SCN5A*

Vom Fachbereich Biologie der Technischen Universität Darmstadt

zur Erlangung des akademischen Grades

eines Doctor rerum naturalium

genehmigte Dissertation von

Dipl.-Biol. Tina Jenewein

aus Frankfurt am Main

1. Referent/Referentin: Prof. Dr. Gerhard Thiel

2. Referent/Referentin: Prof. Dr. Ralf Galuske

3. Referent/Referentin: PD Dr. Silke Kauferstein

Tag der Einreichung: 05.05.2017

Tag der mündlichen Prüfung: 11.08.2017

Darmstadt 2017

D17

1. CHAPTER 1 – A MUTATION (L69P) IN THE PAS DOMAIN OF THE HERG CHANNEL IMPAIRS CHANNEL FUNCTION AND LEADS TO TRAFFICKING DEFECTS

1.1. Abstract

The congenital long QT syndrome (LQTS) is a cardiac disorder characterized by a prolonged QT interval on the electrocardiogram and an increased susceptibility to ventricular arrhythmias and sudden cardiac death. Mutations in the *KCNH2* gene (also known as the *human ether-a-go-go-related gene* or *hERG*) can cause a reduction in the potassium current I_{Kr}, which is responsible for cardiac repolarization.

In a patient with a clinically diagnosed LQTS we identified the mutation L69P in the PAS (Per-Arnt-Sim) domain of the hERG channel. Functional expression of mutant channels in HEK293 cells unveiled a reduced hERG channel function and an impaired trafficking to the plasma membrane compared to the wild type (WT) channel. Lowering the incubation temperature of hERG-L69P mutant expressing HEK293 cells to 27°C, a measure which should promote folding of the channel, did not appreciably improve channel trafficking. Three additional hERG channel variants with mutations at the same position exhibited larger currents than the hERG-L69P mutant but with different inactivation/deactivation kinetics compared to the WT channel. In conclusion, the results imply that the loss of the conserved amino acid leucine at position 69 in the PAS domain of the hERG protein has a negative effect on the functional properties of the channel as well as on its trafficking to the plasma membrane. Therefore, the functional and trafficking defects of this mutant support the clinical diagnosis of a LQTS.

1.2. Introduction

The *KCNH2* or *hERG* (*human ether-a-go-go-related gene*) gene encodes the α-subunit of a voltage-gated potassium channel Kv11.1, which conducts the rapidly activating delayed rectifier potassium current (I_{Kr}). With these properties it is an important component in the repolarization of the cardiac action potential [1,2]. The hERG channel is a multi-domain protein, which contains an amino-terminal Per-Arnt-Sim (PAS) domain [3], the voltage sensor (S1-4) and pore domains (S5-6) [4] and a carboxy terminus with the cyclic-nucleotide-binding homology domain (CNBD) [5]; the part of the channel between S1 and S6 is located in the membrane (Fig. 1). Loss of hERG channel function due to inherited mutations is a frequent cause of the long QT syndrome type 2 (congenital LQTS), which is characterized by a delayed ventricular repolarization (prolonged QT interval on the ECG) and an increased risk for fatal arrhythmias and sudden cardiac death (SCD) [6]. In addition, loss of hERG channel functionality can be caused by off-target drug effects (acquired LQTS) [7].

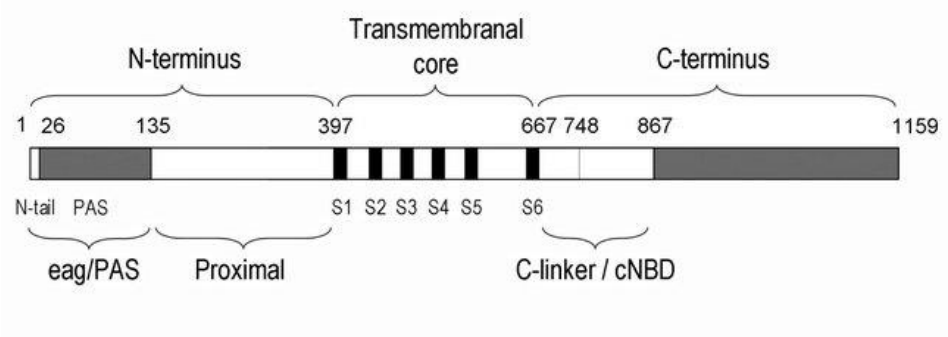

Fig. 1: Schematic linear topology of the hERG channel protein.

The hERG protein consists of following domains: The N-terminal eag/PAS (Per-Arnt-Sim) domain (amino acids 1-135), the proximal domain (residues 136-397), the transmembrane domain with six transmembrane helices S1-6 (amino acids 398-667) and the carboxy terminus with the CNB domain (residues 668-867) (Modified from de la Pena et al. [8]).

Over 300 suspected LQTS-causing missense mutations have by now been identified, but only half of them have been studied in heterologous expression systems [9,10]. Most of these missense mutations are leading to a reduction of the repolarizing outward potassium current (I_{Kr}) and cause a prolonged repolarization of the cardiac action potential. The dominant molecular mechanisms by which *KCNH2* mutations cause a loss of hERG channel function are a disruption of channel gating and reduction of intracellular transport or trafficking to the plasma membrane [11]. The latter has been suggested early on as the predominant cause, but only recently a comprehensive study [10] could show that 88% of *KCNH2* missense mutations in the PAS domain, CNB domain and pore domain produce trafficking deficient hERG channels. Additionally, this study showed that 70% of pore domain mutations produce a dominant negative effect, whereas PAS and CNB domain mutations did not [10].

In the present work, we identified a missense mutation in the *KCNH2* gene in a case of LQTS. The mutation is located in the N-terminal PAS domain of the hERG channel and leads to a non-conservative amino acid substitution L69P. To test the impact of the natural L69P mutation and three experimentally constructed variants at this position on channel kinetics, we performed patch-clamp measurements HEK293 cells. Furthermore, we examined the trafficking of the hERG-L69P channel by imaging using intact HEK293 cells as well as isolated membrane patches.

1.3. Material and Methods

1.3.1. Genetic analysis

Genomic DNA was extracted from blood samples using standard phenol chloroform procedures. Polymerase chain reaction (PCR) was used to amplify 15 exons of *KCNH2* with published [12] and own primers (see Appendix 2.7.1.). Direct sequencing of the amplicons was performed in the presence of fluorescence–labeled dideoxynucleotides (BigDye® Terminator Cycle Sequencing Kit, Life Technologies, Germany) and primers in both sense and antisense direction. Sequencing products were examined with a 3130xl Genetic Analyzer (Applied Biosystems, Germany). Sequence Data were analyzed with SeqScape v2.5 (Applied Biosystems, Germany) and compared to the NCBI (National Center of Biotechnology) reference sequence NG_008916.

1.3.2. Cloning of the *KCNH2* mutations

QuickChange®II XL Site-Directed Mutagenesis Kit (Stratagene, Agilent Technologies) was used to introduce the *KCNH2*-L69P, *KCNH2*-L69A, *KCNH2*-L69D and *KCNH2*-L69G mutations into the pEGFP-N2 vector with hERG *(KCNH2)*. All constructs were verified by sequencing (Eurofins, Ebersberg, Germany).

1.3.3. Expression of hERG channels in HEK293 cells

Human Embryonic Kidney (HEK293) cells were cultured in Dulbecco's Modified Eagle Medium (DMEM/Ham's F-12, Biochrom AG, Berlin, Germany) supplemented with 2 mM glutamine, 10% fetal calf serum (Sigma-Aldrich GmbH, Taufkirchen, Germany) and 1% penicillin/streptomycine solution (Sigma-Aldrich GmbH, Taufkirchen, Germany) under 5% CO_2 and at 37°C. For patch clamp measurements, the HEK293 cells were grown in 35 mm plates to a confluency of 60-70% and transiently transfected with 1 µg plasmid DNA using Gene Juice (Novagen, Merck, Darmstadt) or Turbofect (Thermo Fischer Scientifics, Waltham, MA, USA) according to the manufacturer's protocol. One day after transfection the cells were isolated and transferred to new 35 mm plates in different concentrations. For confocal laser scanning microscopy (CLSM) the HEK293 cells were grown and transfected as mentioned above but on 25 mm round glass coverslips.

1.3.4. Patch clamp measurements in HEK293 cells

Patch clamp recordings were performed 48 h after transfection with an EPC-9 amplifier (HEKA, Lambrecht, Germany) in the whole cell configuration using borosilicate glass pipettes (Tube capillary, Melting point, 1,5-1,8 mm, Kimble Chase, Gerresheimer, Vineland, USA) with a tip resistance of 2-5 MΩ. The extracellular bath solution contained 140 mM NaCl, 5,6 mM KCl, 1,2 mM $MgCl_2$, 2,6 mM $CaCl_2$ and 10 mM HEPES (pH 7,4, adjusted with NaOH). The internal pipette solution contained 140 mM KCl, 10 mM EGTA, 5 mM $MgCl_2$, 2 mM $CaCl_2$, 5 mM HEPES (pH 7,2, adjusted with KOH) and 5 mM ATP. All currents were recorded at room temperature. The voltage protocols are presented in the respective Figure legends.

1.3.5. Plasma membrane preparation

HEK293 cells were cultivated and transfected as described in section 2.3.3. Plasma membrane preparation was performed according to [13]. 24 h after transfection the cells were detached by swilling with phosphate buffered saline (PBS) and centrifuged for 4 minutes at 2.500 rpm (Biofuge pico, Heraeus, Hanau, Germany). The cell pellet was resuspended in 1 ml PBS. 300 µl of the cell suspension was transferred on a poly-D-lysine (PDL) coated, 25 mm round glass coverslip that was placed in a 35 mm round culture dish. After filling with 2 ml PBS the cells were incubated for 15 minutes. During this incubation step the cells attached to the poly-D-lysine surface of the pre-treated coverslip. The PBS solution was then replaced by 2 ml ice-cold ddH_2O and incubated for 5 minutes. The osmotic stress led the cells to burst open. By following washing steps with ddH_2O cell debris and organelles were removed and only plasma membrane patches firmly attached to the coverslip remained.

1.3.6. Confocal Laser Scanning Microscopy (CLSM)

Confocal images were obtained 24-48 h after transfection on a Leica TCS SP5 II Confocal System equipped with an argon laser. Enhanced green fluorescent protein (EGFP) was excited with 488 nm and the emission was detected through a band pass filter between 500 and 530 nm. The fluorescent marker Cellmask™ DeepRed (Invitrogen GmbH, Karlsruhe, Germany) was used for staining the plasma membrane of isolated membrane patches. Cellmask™ DeepRed was excited with 633 nm and the emission was recorded at 655-700 nm. Image acquisition was made with the HCX PL APO CS 100x1.44 OIL UV objective. The images were analysed using the LAS AF software version 2.60 (Leica Microsystems CMS GmbH, Heidelberg, Germany) and further edited with the open source software ImageJ (http://rsb.info.nih.gov/ij).

1.3.7. Data analysis and statistics

Electrophysiological data acquisition and analysis was performed with Patchmaster and Fitmaster software (HEKA, Lambrecht, Germany). Graphics of the current recordings and the corresponding I-V relationships were created with Igor Pro 6.03 software (WaveMetrics, Lake Oswego, OR). Data are expressed as mean ± standard deviation (SD) of n experiments. An unpaired student-t-test was used to evaluate the significance of differences in the relative fluorescence intensity between hERG-WT and hERG-L69P cells.

1.4. Results

1.4.1. *KCNH2* mutation analysis

Genetic analysis was performed in the work of Kiehne [14]. Direct sequencing of the exon spanning region of *KCNH2* revealed a heterozygous mutation L69P (c.206T>C, rs199473665) in a 35-year-old women suffering from dizziness and tachycardia in resting periods after physical stress (Fig. 2). A cardiological examination revealed no morphological abnormalities but the electrocardiogram (ECG) showed supraventricular systoles and tachycardia. First a Brugada syndrome (BrS) was assumed but further investigations unveiled a prolonged QT interval.

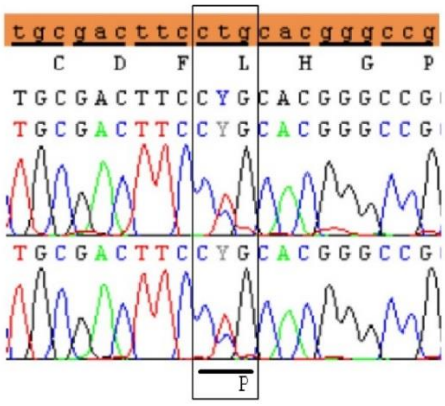

Fig. 2: Electropherogram showing the heterozygous nucleotide change.

Sequencing of the coding region of *KCNH2* revealed a heterozygous nucleotide change at position 206 from thymine to cytosine (C**T**G → C**C**G) leading to an amino acid substitution on position 69 in the resulting protein. Highlighted in orange is the *KCNH2* reference sequence. L = Leucine, P = Proline.

The *KCNH2* L69P mutation has been previously associated with the Long-QT Syndrome (LQTS) [9]; the mutation is located in the N-terminal PAS domain of the hERG protein (Fig. 3). As can be seen in Fig. 4 the amino acid position 69 is highly conserved among different species. The PAS domain in hERG channels is crucial for maintaining normal cardiac activity. Previous studies have shown that mutations, which disrupt the PAS domain structure, can cause functional or trafficking defects associated with the LQTS [15–17].

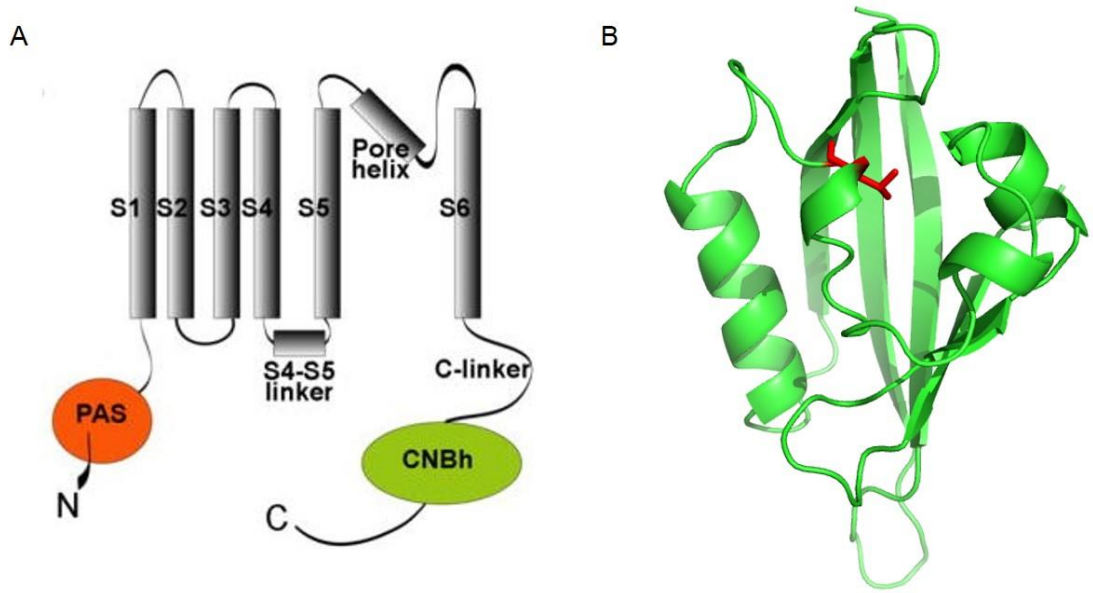

Fig. 3: Schematic topology of the hERG channel and PAS domain structure.

(A) Schematic representation of a hERG channel α-subunit showing the relative positioning of channel regions and domains. Transmembrane helices are labelled S1 to S6. PAS = Per-Arnt-Sim domain, CNBh = Cyclic Nucleotide Binding homology domain (modified from Morais-Cabral *et al.* [18]). (B) PAS domain structure including the position of the mutated amino acid leucine shown in red (PDB code: 1BYW [19]).

Q12809	HUMAN	… QRPCTCDF**L**HGPRTQRRAA …
I0FG57	MACAQUE	… QRPCTCDF**L**HGPRTQRRAA …
Q8WNY2	RABBIT	… QRPCTCDF**L**HGPRTQRRAA …
Q9TSZ3	DOG	… QRPCTCDF**L**HGPRTQRRAA …
O35219	MOUSE	… QRPCTCDF**L**HGPRTQRRAA …
O08962	RAT	… QRPCTCDF**L**HGPRTQRRAA …

Fig. 4: Alignment of a part of the N-terminal hERG amino acid sequence from different species.

Each amino acid sequence is preceded by its UniProt accession number. The mutated amino acid (L69P) is indicated in red.

An additional evaluation of the mutation pathogenicity of *KCNH2* L69P was performed using the sequence based programs PolyPhen-2 (Polymorphism Phenotyping v2), SIFT (Sorts

Intolerant From Tolerant), KvSNP (Single Nucleotide Polymorphism Prediction of Kv channels) and SNPs&Go. These tools are based on comparing sequence homologies and predict whether an amino acid substitution in a protein will have a phenotypic effect. The results are presented in table 1 and underline a potential detrimental effect of the L69P mutation.

Table 1: Summary of pathogenicity prediction results.

Protein	CDS	Prediction tool			
		PolyPhen-2	SIFT	KvSNP	SNPs&Go
p.L69P	c.206T>C	Probably damaging (1.000)	Damaging	Disease (0,959)	Disease (8)

Values in parentheses (0-1 for PolyPhen-2 and KvSNP and 1-10 for SNPs&Go) are a reliability index with larger values more reliable. CDS = coding sequences.

1.4.2. Functional expression of hERG-WT and hERG mutants in HEK293 cells

1.4.2.1. Voltage dependent hERG-WT and mutant hERG channel activation

To investigate the voltage-dependent properties of the currents generated by the hERG-L69P mutant compared to the hERG-WT, the channels were transiently expressed in HEK293 cells and whole cell patch clamp recordings were performed (Bachelor thesis Johanna Schäfer, 2014). The cells were therefore clamped from a holding potential of -80 mV to depolarizing voltages between -40 and +40 mV for 4 s to activate the hERG channel. For recording of the tail currents the cells were then clamped to -40 mV for 4 s (Fig. 5A).

The endogenous currents of the non-transfected HEK293 cells were only elicited by depolarizing step more positive than -20 mV. The resulting small outward currents decreased after several milliseconds to a constant value (Fig. 5B). Figs. 5C and D show in comparison to this the voltage dependence of activation of hERG-WT and hERG-L69P, respectively. At depolarizing steps hERG-WT transfected cells exhibited large outward currents, which decreased at positive voltages due to the inherent inactivation of the hERG channel. During the repolarizing pulse (-40 mV) the channels recovered from inactivation and opened again. This transient opening generated the typical tail currents (Fig. 5C).

The current response of the cell expressing the hERG-L69P mutant channel was clearly different from that recorded from the hERG-WT channel. The hERG-L69P transfected cells (Fig 5D) only generated small currents, which were much smaller than those recorded in the hERG-WT transfected cells (Fig. 5C). However, compared to the non-transfected HEK293 cell (Fig. 5A), the hERG-L69P cell exhibited a minimal tail current. This hERG typical tail current underscores that the mutant is active in the HEK293 cells.

A plot of the steady state current as a function of the clamp voltage reports the corresponding current/voltage (I-V) relation of the measured cells (Fig. 5E). The I-V data show that the hERG-WT channel was activated at voltages positive to -50 mV; the maximum outward current was present in response to voltage steps to +10 mV. At more positive voltages the I-V relation exhibited a negative slope conductance which has been attributed to the hERG typical voltage-dependent channel inactivation [20,21]. The I-V relation of cells expressing the hERG-L69P mutant show an almost linear increasing curve with no apparent maximum. The current amplitude at the reference voltage of +10 mV was 565 pA for cells expressing the hERG-WT, 126 pA for cells with the hERG-L69P mutant and 62 pA for non-transfected HEK293 cells.

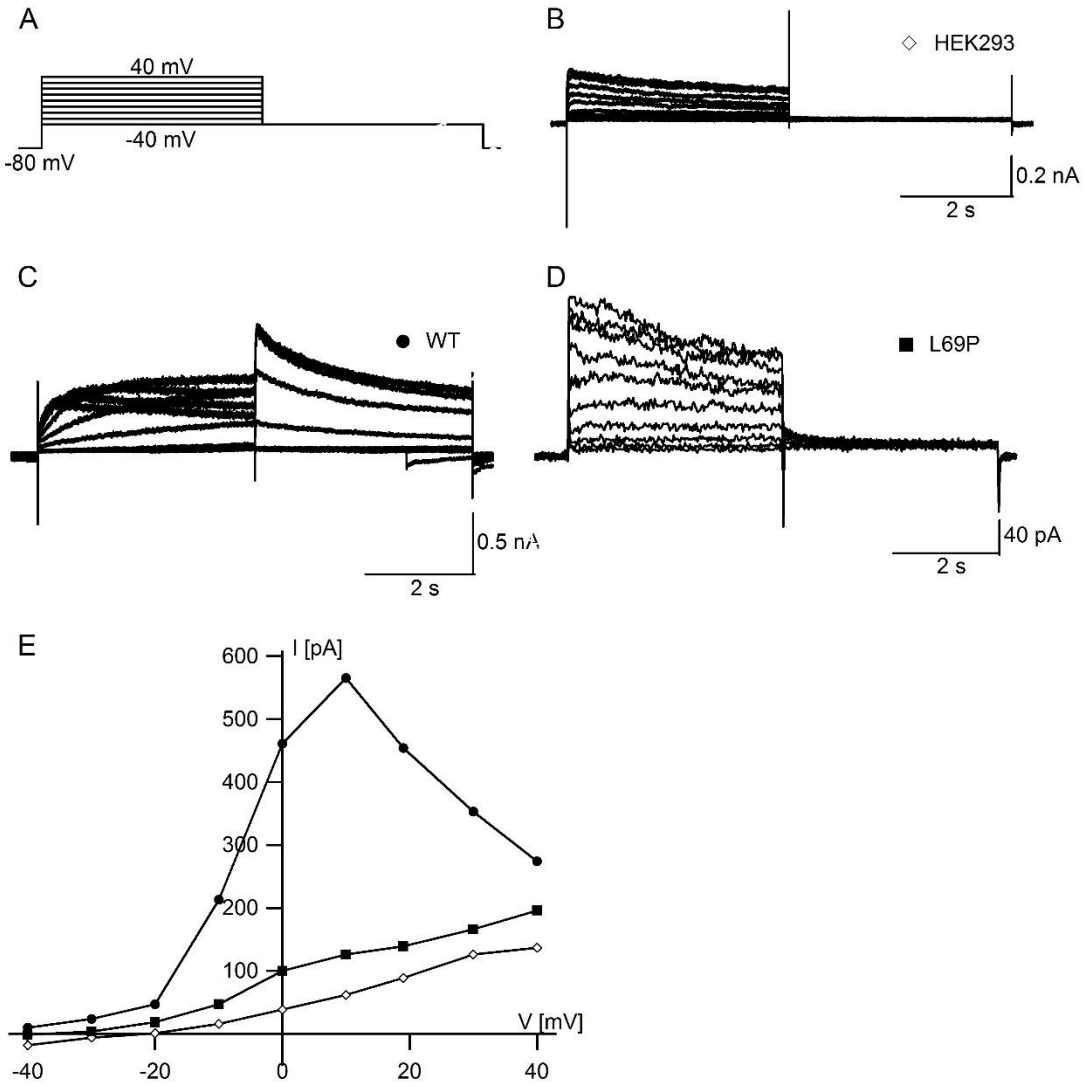

Fig. 5: Voltage dependent activation of hERG-WT channel and its hERG-L69P mutant.

(A) Voltage clamp protocol. The cell was first clamped for 2 s to a holding potential (-80 mV); the hERG current was then activated by 4 s long depolarizing steps between -40 and +40 mV, and then clamped to -40 mV for 4s to elicit tail currents. Currents recorded from a non-transfected HEK293 cell (B), a cell transfected with hERG-WT (C) and a hERG-L69P expressing cell (D). (E) Corresponding steady state I-V relationship of cells in B-D; data were collected at the end of the depolarizing test pulses (◇ HEK293, ● hERG-WT, ■ hERG-L69P).

The tail current is a characteristic property of hERG channels and is induced at a clamp step from positive to negative voltages [22]. This transient current is a result of a conformational change of the hERG channel from an inactive state via an open state to the closed state. In a total of sixteen measurements, which were performed with hERG-L69P transfected cells, we observed two different populations with respect to the tail currents. Seven cells showed a minimal tail current (population 1) and nine cells displayed no measurable tail current (population 2) (Fig. 6A). The current recordings of the latter population rather resembled those from non-transfected HEK293 cells. The mean tail current in response to the voltage step from +40 mV to -40 mV was 546 ± 246 pA for hERG-WT, 40 ± 35 pA for hERG-L69P (population 1), -23 ± 29 pA for hERG-L69P (population 2) and -16 ± 9 pA for non-transfected HEK293 cells.

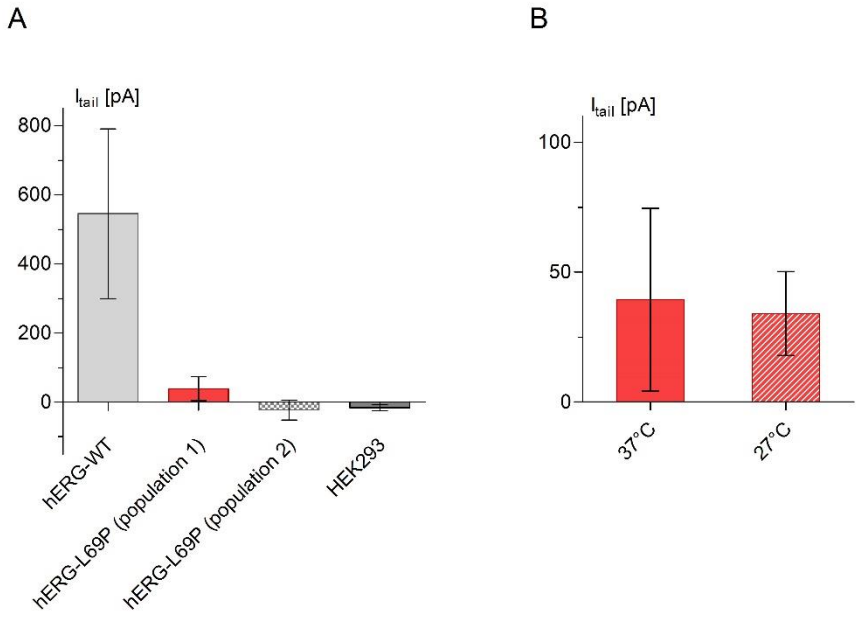

Fig. 6: Comparison of mean tail currents.

Each plot represents the mean tail currents (±SD) determined from current recordings as in Fig. 5 at the voltage step from +40 mV to -40 mV. (A) hERG-WT n = 6, hERG-L69P (population 1) n = 7, hERG-L69P (population 2) n = 9, HEK293 n = 3. (B) Mean tail currents of hERG-L69P cells cultivated at 37°C or 27°C. 37°C n = 7, 27°C n = 4.

Collectively the data show that the current responses of the hERG-L69P mutant were very small and the mutant channel did not show the voltage-dependent channel activation. Nonetheless some hERG-L69P expressing cells exhibited a minimal tail current (Fig. 6, population 1), therefore it can be concluded, that a few functional channels are presumably located in the plasma membrane.

Previous studies have shown that PAS domain mutations result in folding and hence trafficking defects of the hERG channel [17,23]. Recently, Anderson et al. [10] demonstrated that the protein-trafficking for 80% of the mutations in the PAS domain could be rescued by lower incubation temperatures. To examine whether the trafficking of the hERG-L69P mutant channel is temperature-sensitive the HEK293 cells were incubated at 27°C. However, the current responses of these cells did not differ from cells incubated at 37°C (Bachelor thesis Johanna Schäfer, 2014, data not shown). Also, the mean tail current was not increased by lowering the incubation temperature (Fig. 6B).

The replacement of the nonpolar amino acid leucine by the nonpolar, aliphatic amino acid proline seems to disturb the structural integrity of the PAS domain structure resulting in either a trafficking or a functional defect of the hERG channel, or both. Three additional point mutations at position 69 were constructed to determine the effect on hERG channel activation. The leucine was substituted with alanine (A), aspartic acid (D) or glycine (G). Alanine is also nonpolar but significantly smaller than leucine, whereas aspartic acid contains a negatively charged side chain. Glycine, without any side chain, is small and allows higher flexibility in contrast to the other amino acids. The mutants were expressed in HEK293 cells and analysed as described above. The patch clamp recordings revealed three different current responses: cells which were similar to non-transfected cells (“HEK293-like”), cells exhibiting a minimal tail

current and cells which generated a “hERG-like” current; in the latter case, the typical activation and deactivation properties of hERG channels have been recognized (Fig. 7). For further data analysis, only those cells were considered, which exhibited either the “hERG-like” phenotype or, in case of hERG-L69P, a minimal tail current.

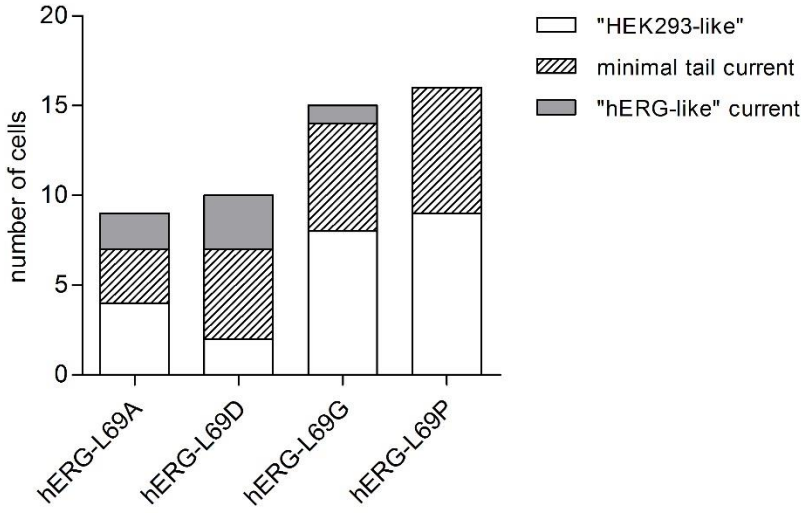

Fig. 7: Histogram showing the different current response phenotypes of the hERG mutants.

The current recordings as in Fig. 5A with the four hERG mutants elicited three different current phenotypes. hERG-L69A: HEK293-like n = 4, minimal tail current n = 3, hERG-like n = 2, hERG-L69D: HEK293-like n = 2, minimal tail current n = 5, hERG-like n = 3, hERG-L69G: HEK293-like n = 8, minimal tail current n = 6, hERG-like n = 1, hERG-L69P: HEK293-like n = 9, minimal tail current n = 7.

The current responses (Fig. 8A) and the corresponding I-V relation (Fig. 8B) show that the three additional hERG mutants (L69A, L69D and L69G) generated larger outward currents than the hERG-L69P mutant channel. Except for the hERG-L69G mutant, which exhibited even larger currents than the hERG-WT channel, the current amplitudes of the other two mutant channels were similar to the WT. The maximum outward current was at 0 mV: 404 pA for hERG-L69A and 594 pA for hERG-L69D. At +30 mV 1210 pA was measured for hERG-L69G.

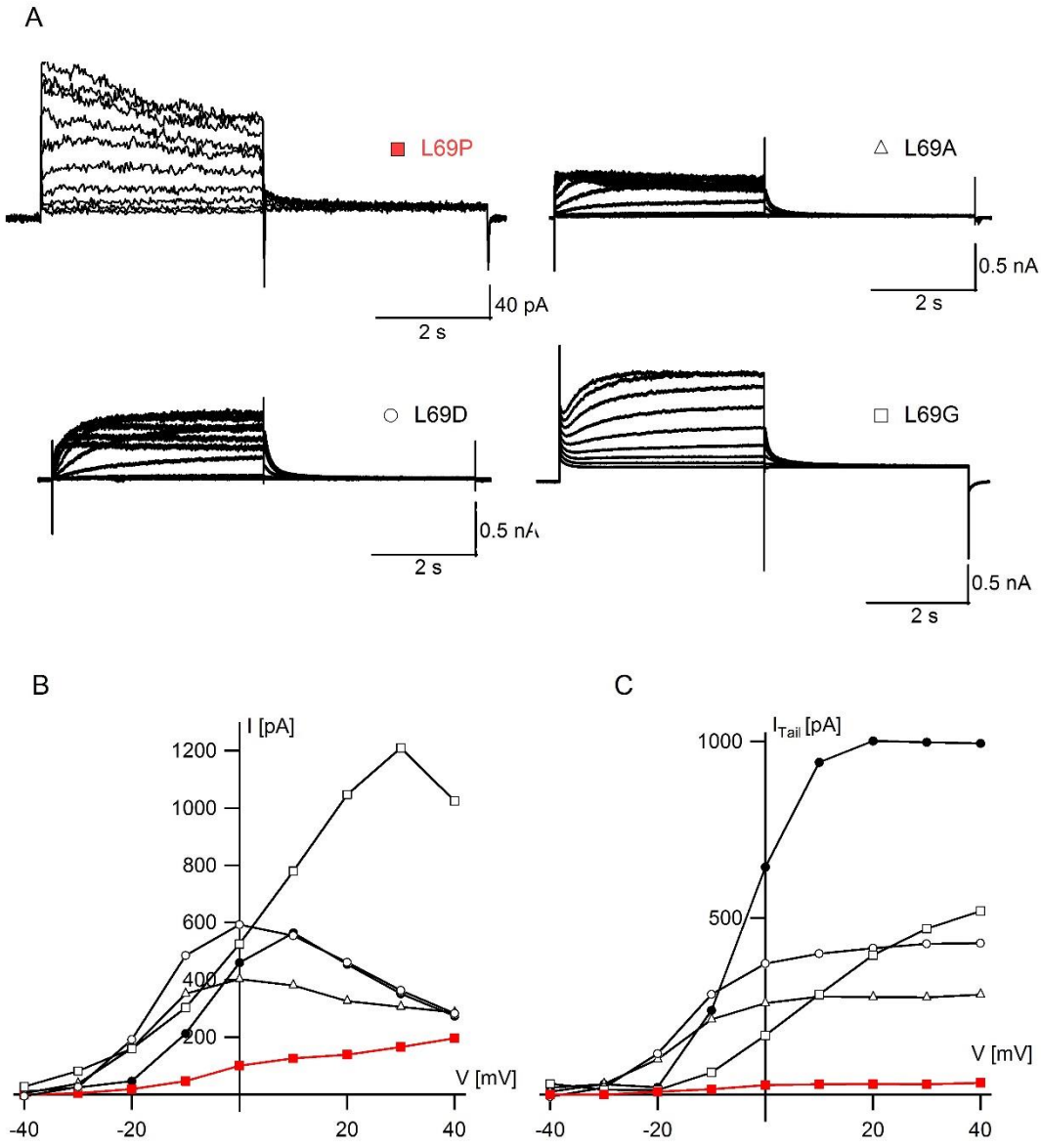

Fig. 8: Voltage dependent activation of hERG-L69P and three other mutant hERG channels.

Currents were measured as in Fig. 5A. (A) Current responses of cells expressing the mutant hERG channels specified along the current traces. (B) Corresponding steady state I-V relation of hERG-WT and hERG mutants; currents were measured at the end of the depolarizing clamp steps (Data of hERG-WT and hERG-L69P are the same as in Fig. 5E). (C) Corresponding tail currents for hERG-WT and hERG mutants in response to different conditioning voltages. ● hERG-WT, ■ hERG-L69P, ∆ hERG-L69A, ○ hERG-L69D, □ hERG-L69G.

The corresponding peak tail currents obtained for hERG-WT and the four hERG mutants at -40 mV following a depolarization pulse to different voltages are depicted in Fig. 8C. The hERG channel mutants L69A, L69D and L69G generated larger tail currents than the hERG-L69P mutant but not as large as the hERG-WT channel. In the case of the hERG-WT channel and the mutant channels L69A and L69D the curves reach saturation at voltages ≥ 20 mV while the hERG mutant L69G did not reach saturation.

In summary, the results demonstrate that all three mutated channel variants (L69A/-D/-G) are functional. They all exhibited currents, which are smaller than the WT channel but larger than the hERG-L69P mutant. Since some of the tested mutants generate, different from the hERG-

L69P mutant, a “hERG-like” current (Fig. 7), it can be assumed that the effect of these variants on channel function is not as dramatic as for L69P.

1.4.2.2. The fully activated I-V relation of hERG mutant channels compared to the WT channel

The fully activated I-V relation for hERG-transfected cells expressing either mutant (L69P/-A/-D/-G) or WT channels was obtained by applying the pulse protocol shown in Fig. 9A. The hERG current was activated and partially inactivated by a depolarizing step to 60 mV for 1 s, followed by repolarizing steps to different voltages. With repolarizing steps to more negative voltages, the hERG current recovered from inactivation and reached a peak value from which it underwent a voltage-dependent decrease (Fig. 9B). Fig. 9C shows the corresponding I-V relation of the peak current recorded during repolarization for hERG-WT and mutant channels. The maximum outward current for hERG-WT was obtained at -30 mV followed by a decrease at more positive voltages. In cells expressing the hERG-L69P mutant channel the current did not reach a maximum and the I-V relation had the same shape as that from non-transfected HEK293 cells. The hERG-L69A and hERG-L69D transfected cells exhibited a small reduction in absolute current amplitudes compared to the hERG-WT transfected cell, with a current maximum at -10 mV. The I-V relation obtained for the hERG-L69G mutant is clearly shifted to more positive voltages with a current maximum at 20 mV.

This shift of the I-V curve of the fully activated channel is difficult to explain. It could mean that the mutation has an effect on the selectivity of the channel. This explanation is rather unlikely since the PAS domain is far away from the selectivity filter, which dictates the K^+ selectivity of the channel. Another explanation may suggest that the mutation alters the kinetics of the channel in such a way that it is not fully activated by the voltage protocol. This interpretation seems more likely considering the fact that the currents, which were conducted by this mutant exhibited strong differences in the kinetics compared to the other mutants (see for example Fig. 11).

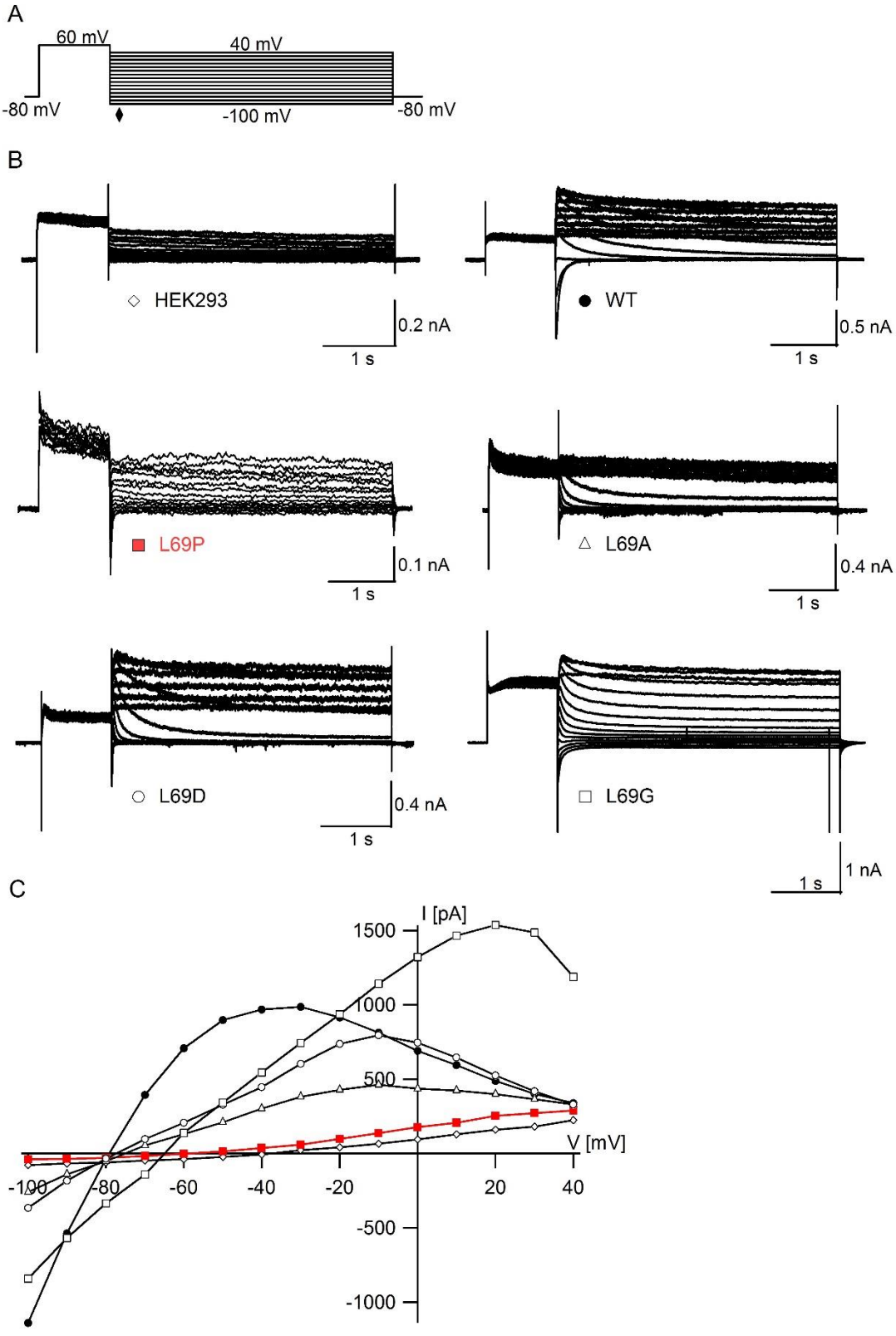

Fig. 9: The fully activated I-V relation of hERG-WT and hERG mutant currents.

(A) Voltage clamp protocol. A cell was depolarized to 60 mV for 1 s to activate and partially inactivate the hERG current. This step was followed by repolarizing steps between -100 and 40 mV. (B) Typical current responses of a non-transfected HEK293 cell, a cell expressing either hERG-WT or the hERG mutants (L69P/-A/-D/-G). (C) Corresponding fully activated I-V plot of the peak currents during repolarization (measuring point indicated by ♦). ◇ HEK293, ● hERG-WT, ■ hERG-L69P, Δ hERG-L69A, ○ hERG-L69D, □ hERG-L69G.

1.4.2.3. Inactivation properties of mutant hERG channels (L69A/-D/-G)

To determine the rates of inactivation of cells expressing WT and mutant hERG channels a three-step pulse protocol was used (Fig. 10A, see also [22]). The cells were depolarized to 60 mV for 200 ms to ensure that all hERG channels were fully inactivated. By applying a short pulse (-100 mV for 2 ms) the channels recovered from inactivation without significant deactivation. To observe the inactivation of the hERG current a series of test pulses (between -20 and 60 mV) was applied. The rates of inactivation could only be determined for cells expressing the mutant hERG channels L69A, L69D and L69G, which exhibited the characteristic hERG current. In Fig. 10B exemplary current responses of hERG-WT and the three mutant hERG channels are shown. The rate of inactivation at different voltages was measured by fitting a single exponential function to the decay of the different current traces. The resulting time constants were plotted as a function of the membrane potential (Fig. 10C). The time constants of hERG inactivation at -20 mV are presented in Fig. 10D. Considering the individual measurements there is no difference in inactivation kinetics at -20 mV between hERG-WT and the mutant channels hERG-L69A and hERG-L69D in the range of experimental error. For the cell expressing the hERG-L69G mutant the exponential fitting of the current traces at -20 and 0 mV was not possible, because inactivation at these voltage steps was hardly visible.

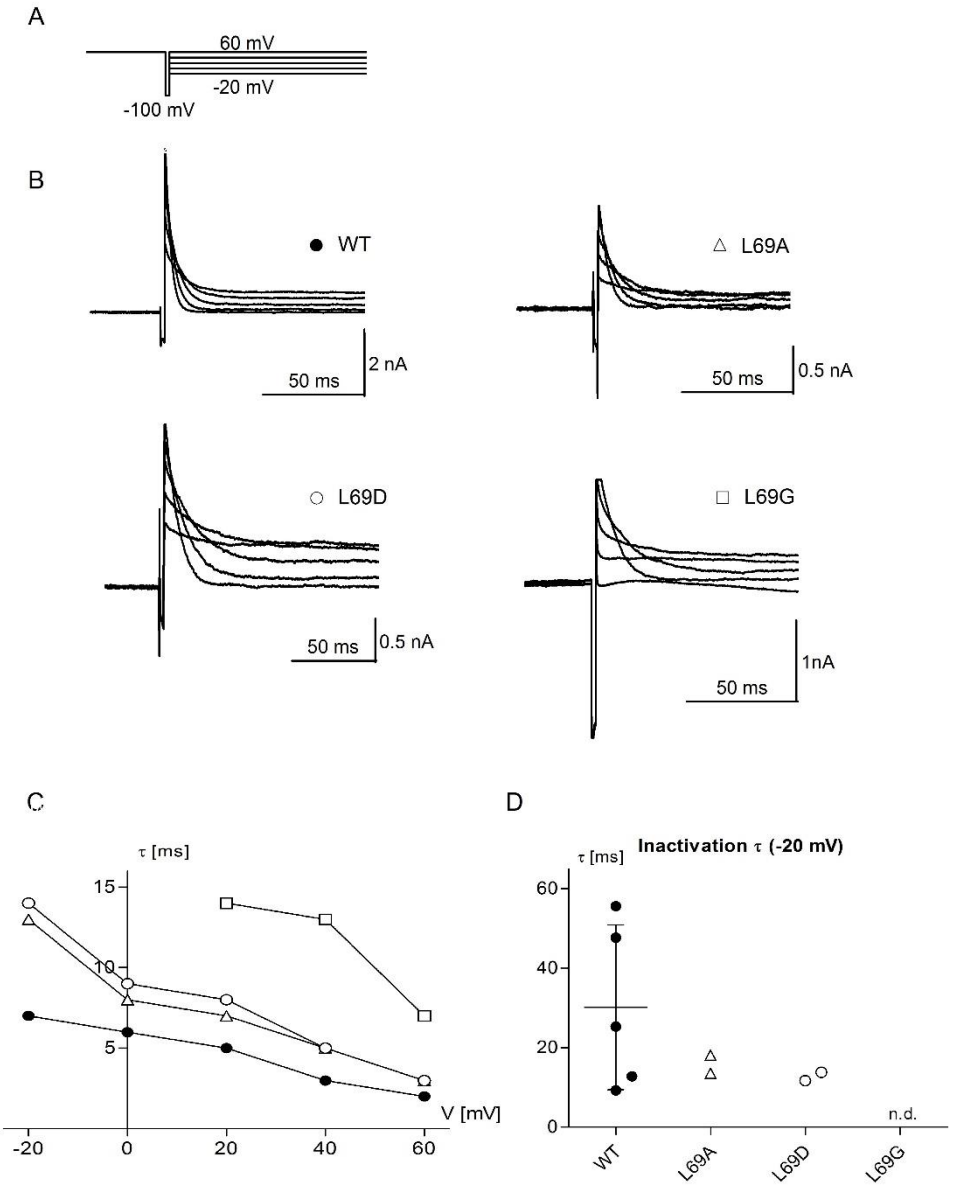

Fig. 10: Rates of inactivation of WT and mutant hERG channels.

(A) A triple pulse protocol was used to determine the rate of channel inactivation at different voltages. The hERG current was activated and inactivated by a 200 ms long depolarizing pulse to 60 mV. A short repolarizing pulse (-100 mV for 2 ms) was used to allow the channels to recover from inactivation without appreciable deactivation. The membrane was then stepped to test voltages ranging from -20 to 60 mV during which the channels re-inactivated. (B) Current traces of hERG-WT and three hERG mutants (L69A/-D/-G) in response to the triple pulse protocol. (C) The corresponding time constants at the individual test voltages were determined by fitting the current traces with a single exponential function. The time constants (τ) are plotted as a function of the membrane potential (V). (D) Time constants of hERG inactivation at -20 mV: ● hERG-WT (n = 5): 30.1 ± 20.7 ms, ∆ hERG-L69A: 13.6 and 18.1 ms, ○ hERG-L69D: 11.8 and 13.8 ms, □ hERG-L69G: not determined (n.d.).

1.4.2.4 Deactivation rates of mutant hERG channels (L69A/-D/-G)

The deactivation rates of hERG-WT and hERG mutant (L69A/-D/-G) channels were measured using the voltage clamp protocol shown in Fig. 11A. The hERG channels were activated by applying a pulse of 60 mV followed by a series of test pulses ranging from -100 to -20 mV during which the cells elicited tail currents. The respective current traces of hERG-WT and mutant channels were biphasic (Fig. 11B). A scrutiny of the current trace at -100 mV shows a rapid increase in current in the first phase; this reflects the fast recovery of channels from inactivation. In the second phase the tail currents decayed due to channel deactivation. The rate of current deactivation was determined by fitting these tail currents with the sum of two exponential functions. The time constants of the fast and slow component of deactivation measured at -100 mV are shown in Fig. 11C. The time constants for the fast component of deactivation were similar for hERG-WT (1.5 ± 0.6 ms) and the hERG mutants L69A (1.6 and 1.9 ms) and L69D (1.4 ± 0.2 ms). In case of the mutant channel hERG-L69G the fast component could not be identified. Considering the time constants for the slow deactivating component there was an apparent difference between hERG-WT and its mutant channels. The time constants were 73.4 ± 51.6 ms for hERG-WT, 8.9 and 9.5 ms for hERG-L69A, 11.6 ± 2.5 ms for hERG-L69D and 31.7 ms for hERG-L69G (only one current recording). Due to the fact that sample size of hERG mutants was very small, a statistical analysis of the time constants for the slow deactivating component was not possible. Hence, evaluating more samples might confirm the apparent difference in deactivation kinetics between hERG WT and hERG mutant channels.

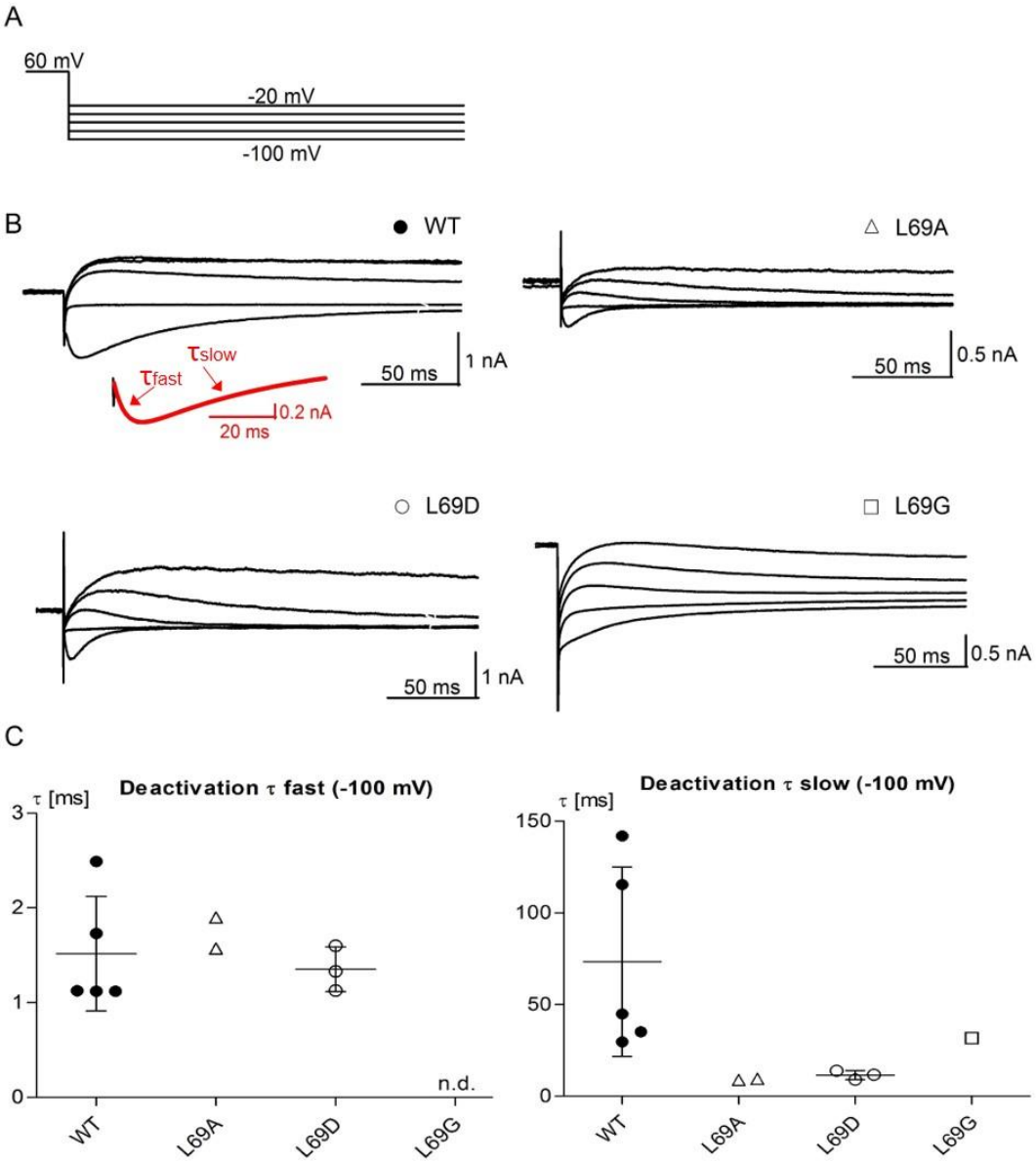

Fig. 11: Deactivation properties of hERG-WT and hERG-L69A/-D/-G.

(A) The deactivation kinetics were determined using the following pulse protocol: After applying an activating pulse of 60 mV the tail currents were recorded at potentials ranging from -100 to -20 mV. The tail currents at -100 mV were fitted with the sum of two-exponential functions. (B) Representative hERG current recordings of WT and mutant channels. WT current trace in *inset* shows the fitting with the sum of two exponential functions (red trace) to illustrate the calculation of the time constants for recovery from inactivation (τ_{fast}) and deactivation (τ_{slow}). (C) Time constants of the fast and slow components of deactivation. τ_{fast}: ● WT (n = 5): 1.5 ± 0.6 ms, Δ L69A (n = 2): 1.6 and 1.9 ms, ○ L69D (n= 3): 1.4 ± 0.2 ms, □ L69G not determined (n.d.); τ_{slow}: ● WT (n = 5): 73.4 ± 51.6 ms, Δ L69A (n = 2): 8.9 and 9.5 ms, ○ L69D (n= 3): 11.6 ± 2.5 ms, □ L69G (n = 1): 31.7 ms.

1.4.3. Confocal microscopy

The results of the functional characterization of the hERG-L69P mutation, which is located in the N-terminal PAS domain of the protein, imply that the mutation has considerable impact on hERG current when expressed in HEK293 cells. Furthermore, also cells expressing three additional hERG channel variants (L69A/-D/-G) with mutations in the same site exhibited different kinetic properties (slow deactivation) compared to the hERG-WT channel.

The reduction of the hERG current in case of the L69P mutation may be due to abnormal channel gating/kinetics or deficient protein trafficking to the cell membrane. Several studies have shown that mutations, which disrupt PAS domain structure, mainly cause trafficking defects [10,17,23–25]. To examine this possibility, the WT and mutant channels were tagged with EGFP and the cellular distribution of these constructs was monitored by CLSM. Representative images of HEK293 cells expressing the hERG-WT and mutant channels are depicted in Fig. 12. The cell expressing the hERG-WT channel exhibited a clear GFP fluorescence in the plasma membrane (Fig. 12A and B). Whereas in cells expressing the hERG mutants (Fig. 12A) the GFP fluorescence was stronger in intracellular compartments, like the perinuclear ring and the endoplasmatic reticulum, than in the plasma membrane (Fig. 12B).

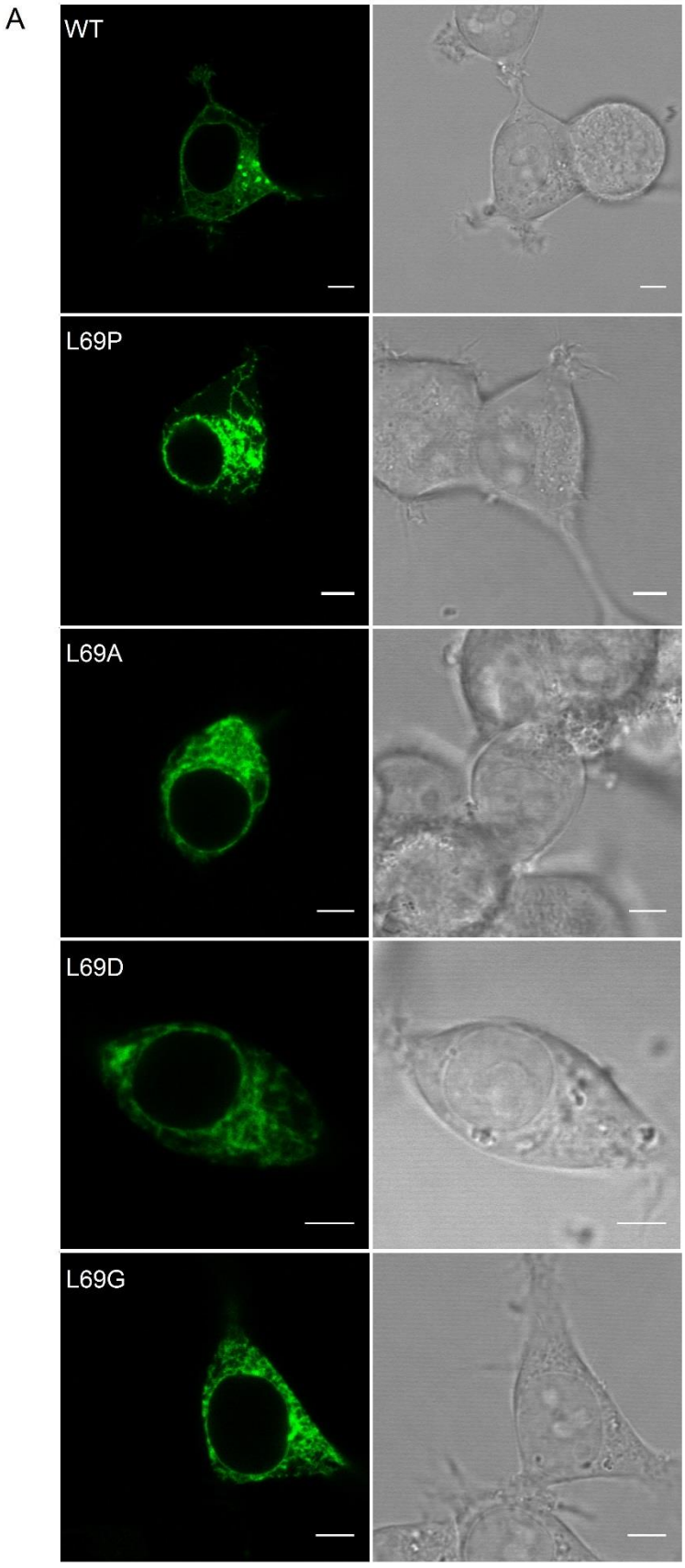
A
WT
L69P
L69A
L69D
L69G

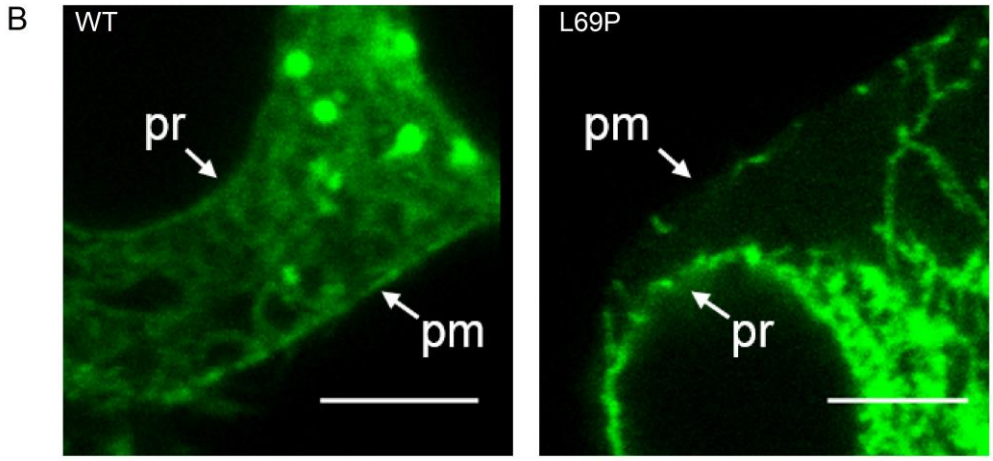

Fig. 12: Cellular distribution of hERG-WT:EGFP and four EGFP-tagged hERG mutants.

(A) CLSM images of HEK293 cells transfected with hERG-WT, hERG-L69P, hERG-L69A, hERG-L69D and hERG-L69G. Left are the EGFP fluorescent and right the transmitted light images. Scale bar 5 µm. (B) Zoomed part of the fluorescent images of HEK293 cells expressing hERG-WT and hERG-L69P, respectively. pr = perinuclear ring, pm = plasma membrane. Scale bar 5 µm.

A differentiation between a GFP-labelled protein in the plasma membrane, in the cortical endoplasmatic reticulum or in vesicles close to the plasma membrane is very difficult with the resolution of a confocal microscope. Therefore isolated membrane patches as described by Guthmann [13] were examined by CLSM. With this method, it is possible to detect GFP-tagged proteins exclusively in the plasma membrane without the interference of intracellular compartments. Fig. 13 shows exemplary images of isolated plasma membrane patches of HEK293 cells expressing hERG-WT and hERG-L69P. The membrane patches were obtained from cells incubated at 37°C as well as 27°C to determine whether the trafficking of the hERG-L69P mutant is temperature sensitive. The images show that all membrane patches, which were stained and identified with Cellmask^{TM} DeepRed (panel b), contained GFP fluorescence (panel a). In all cases the co-localization of both fluorescent signals was evident in the top (panel c) as well as in the side view (panel d) of the membrane patches. The confocal images demonstrate that both channels, WT and mutant, were positively targeted to the plasma membrane. However, considering panel a in Fig. 13, the membrane patch with hERG-L69P at 37°C (image 2a) exhibited a lower GFP fluorescence intensity.

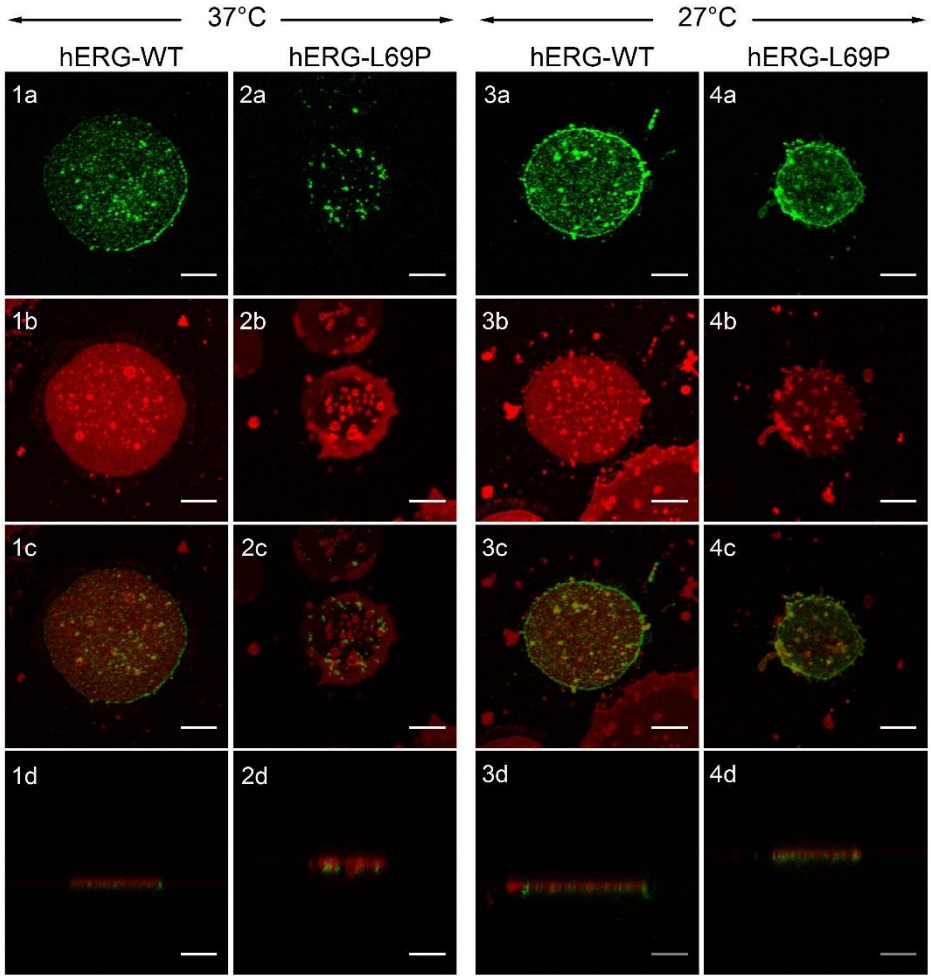

Fig. 13: Isolated plasma membrane patches of hERG-WT:EGFP and hERG-L69P:EGFP

HEK293 cells expressing either hERG-WT:EGFP or hERG-L69P:EGFP were incubated at 37°C or 27°C. Panel a and b show the fluorescence signal of GFP and Cellmask™ DeepRed in top view, respectively. Panel c shows an overlay of panel a and b. Panel d is a side view of panel c. Overlay images were created with ImageJ. Scale bar 5 µm.

To compare the relative GFP fluorescence of the membrane patches the green fluorescence in a defined area was measured using the software ImageJ. In a second step the relative value of the green fluorescence was divided by the corresponding value of the red channel; this normalized the data with respect to different laser intensities. The results of this analysis are shown in Fig. 14. A comparison of the relative fluorescence intensity of hERG-L69P at 37°C with that of hERG-WT at 37°C confirms the visual impression in that the mutant exhibits on average less GFP fluorescence in the plasma membrane than the WT. The difference is of moderate statistical significance ($p = 0.046$).

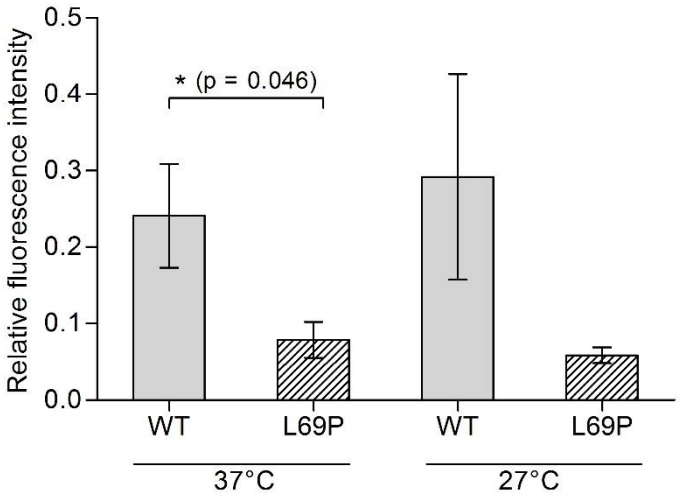

Fig. 14: Relative fluorescence intensities of isolated membrane patches.

The images of membrane patches exhibiting EGFP fluorescence (Fig. 13, panel a) were analysed as described in the text. The relative fluorescence intensity (± SEM) was 0.24 ± 0.07 for hERG-WT 37°C (n= 10), 0.08 ± 0.02 for hERG-L69P 37°C (n = 8), 0.29 ± 0.13 for hERG-WT 27°C (n= 5) and 0.06 ± 0.01 for hERG-L69P 27°C (n= 7).

The results of these experiments confirm that the hERG-L69P mutant with an altered PAS domain is positively targeted to the plasma membrane. But the data also stress that the mutation seems to interfere with the trafficking of the channel to the plasma membrane. In both growth conditions (37°C and 27°C) the relative density of the mutant channel in the plasma membrane is only about half of that seen for the hERG-WT channel. This 50% reduction in channel density can, however, not explain the electrical measurements, in which the current generated by the mutant is barely measurable. The results of these experiments stress that the L69P mutation affects not only the trafficking of the channel to the plasma membrane but also functional properties of the hERG channel (see 1.4.2.1., Fig. 6).

1.5. Discussion

Here we describe the functional characterization of the *KCNH2* mutation L69P, which was identified in a female LQTS patient. The L69P mutation resides in the amino-terminal PAS domain of the hERG protein. The hERG PAS domain is a hot spot for missense mutations that result in a decreased trafficking of the channel [17,24] or in an accelerated rate of deactivation [15,26]. Both defects may lead to a prolongation of the QT interval resulting in long QT syndrome type 2 (LQTS2).

The PAS domain (residues 1-135) contains the PAS core (residues 26-135), an N-terminal cap with an amphipathic helix (N-cap helix, residues 13-25) and a flexible N-terminal tail (residues 1-12) [26–28]. In a recent study, it has been shown that the interaction between the N-cap amphipathic helix the core of the PAS domain plays a critical role in stabilizing the isolated PAS domain [29]. The authors therefore suggested that mutations in the PAS core, which disrupt this self-liganded structure, will lead to trafficking defects of the hERG channel. Furthermore, they demonstrated that channels lacking the PAS domain (∆2-135) traffic perfectly well. Thus, if the PAS domain is present, it must be intact and properly folded. In addition of being important for channel trafficking, the integrity of the PAS domain is essential for normal channel gating [30]. At least 61 PAS domain mutations have by now been linked to LQTS2 [10]. Only 13 (D16A, K28E, F29L, N33T, Y43C, G53R, R56Q, T65P, C66G, H70R, A78P, L86R and M124R) were so far characterized with electrophysiological recordings. The tested mutants revealed altered deactivation kinetics as well as defects in the biogenesis of the channel [15,16,23,26,31–33].

In the present study, we performed patch-clamp measurements of mutant hERG channels in HEK293 cells. The hERG-L69P mutant channels only generated small currents compared to those recorded from hERG-WT channels. Nevertheless, this small current was still distinguishable from the endogenous currents in HEK293 cells. The current amplitudes of cells expressing the hERG mutants were slightly larger than those from non-transfected HEK293 cells and most importantly some of the hERG-L69P transfected cells exhibited a minimal tail current, e.g. a current, which is typical for hERG channels. From these data, it can be concluded that some of the mutant hERG channels must have reached the plasma membrane and were able to conduct currents. The reduced current of the hERG-L69P mutant channel may be either explained by an abnormal channel gating or a deficient trafficking to the plasma membrane. It has been shown that defective protein trafficking is the dominant mechanism responsible for LQTS2 caused by *KCNH2* missense mutations [10].

To visualise the cellular distribution of hERG-WT and hERG-L69P mutant channels in HEK293 cells, EGFP-tagged channels were monitored by CLSM. While cells expressing the hERG-WT channel exhibited a clear GFP signal in the plasma membrane, the GFP fluorescence in hERG-L69P expressing cells was stronger in intracellular compartments than in the plasma membrane. This impression was supported by the analysis of isolated plasma membrane patches. A comparative quantification of membrane patches showed that the relative fluorescence intensity of the hERG-L69P mutant was about 50% reduced compared to that of hERG-WT. The results of these experiments strongly suggest that the mutation causes a reduced trafficking of the channel protein to the plasma membrane. Previous studies have shown that such a deficient trafficking of hERG channels with missense mutations in the PAS core, which are located next to amino acid position 69 (T65P, C66G, F68L and H70R) can be improved by lowering the incubation temperature to 27°C [10,23]. A lower temperature presumably supports a correct folding of the protein. However, in the present study, the relative channel density at the plasma membrane as well as the current response of cells expressing the hERG-L69P mutant were not temperature-sensitive. These results indicate that the replacement of the conserved amino acid leucine with proline on position 69 seems deleterious

for the highly-ordered structure of the PAS domain. The consequence is an impaired trafficking and effects on the functional properties of the hERG channel.

The crystal structure of the hERG PAS domain (PDB: 1BYW) [19] contains a five-stranded antiparallel β-sheet packed against a strand comprising a coil and a single turn of a 3_{10} helix flanked by three α-helices. When mapped on this structure the L69P mutation is located at the C-terminal end of the single turn of this 3_{10} helix (Fig. 15).

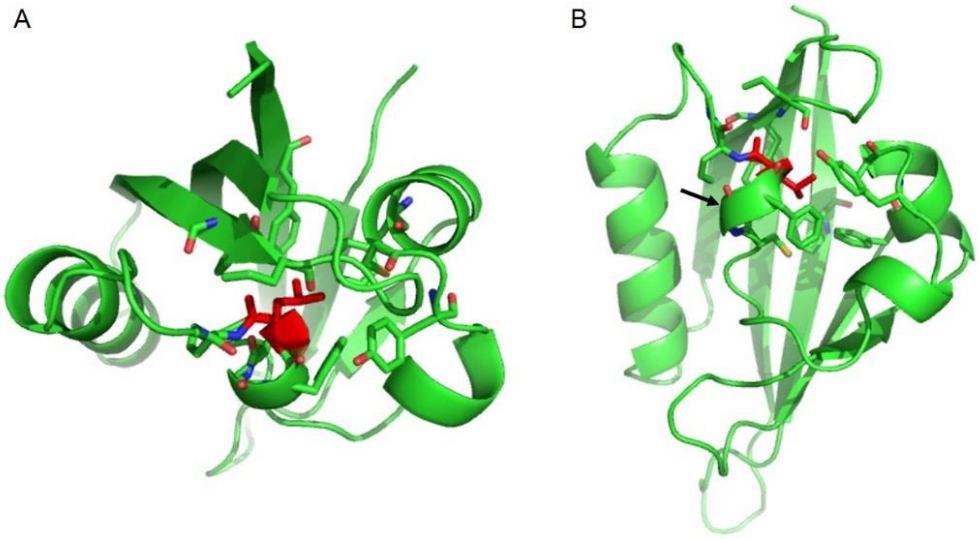

Fig. 15: hERG PAS domain structure.

Ribbon diagram with secondary structure elements. (A) Top view (from the membrane) and (B) side view with the 3_{10} helix nicely presented (arrow). The leucine 69 is visualised as red stick. Side chains of surrounding amino acids in a radius of 10 Å of leucine 69 are shown as green sticks.

The side chain of leucine 69 intrudes into the hydrophobic core of the PAS domain (Fig. 15) and is additionally stabilized by hydrogen bonding to the backbone carbonyl of Y99 and C66. The presence of proline at the C-terminal cap of 3_{10} helices is energetically disfavoured and might induce distortions [34]. Proline is a unique amino acid in that the side chain is cyclized back on to the backbone amide position. As a general consequence proline is unable to function as a hydrogen bond donor and this can function to introduce kinks into α-helices [35]. For this particular mutation, the kinking could affect the interaction to the β-sheet via the hydrogen bond to Y99; it might further abolish the 3_{10} helix internal hydrogen bond to C66. Thus, it is very likely that the area around the L69P mutation is less structured than in the wild type protein. In contrast to other missense mutations, such as T65P, C66G, F68L and H70R, trafficking of the hERG-L69P mutant channel could not be restored by lowering the incubation temperature (27°C) indicating here a more serious structural effect.

Three additional mutated channel variants (L69A, L69D and L69G) were constructed to further examine the effect of amino acid substitutions at this position on hERG channel trafficking and kinetics. CLSM images of HEK293 cells expressing the EGFP-tagged constructs indicated that, like in hERG-L69P expressing cells, all three channel variants exhibited a stronger GFP signal in intracellular compartments than in the plasma membrane. Considering the kinetic properties of these variants, HEK293 cells expressing hERG-L69A, -L69D and -L69G mutant channels generated larger currents than the hERG-L69P mutant channel; moreover, in contrast to hERG-L69P expressing cells, some of these mutated channel variants generated

a “hERG-like” current with the typical inactivation and deactivation properties of hERG channels. The results of these experiments suggest that the position L69 is sensitive to any kind of amino acid exchange. However, the substitution by a proline with the consequent kink formation of the amino acid chain seems to have the most deleterious effects.

The PAS domain is crucial for regulation of deactivation in the gating of hERG channels [30]. Several studies showed that hERG channels with deletion of the N-terminal cap (Δ2-25, [26]), the entire PAS domain (Δ2-135, [19]) or most of the N-terminal region (Δ2-354, [36]) result in 5 to 10-fold faster deactivation rates compared to wild type channels. hERG channels with point mutations in the PAS domain also have accelerated deactivation kinetics [15,19,33]. In the present study, the hERG-L69A, -L69D and -L69G mutant channels revealed some accelerating effect on the slow deactivating component of the channel. However, due to the small sample size of additional hERG mutants, this trend could not be verified statistically.

In summary, the characterization of the L69P mutant of hERG indicates that the replacement of the amino acid leucine in the highly-conserved region of the PAS domain has appreciable impact on trafficking and gating of the hERG channel. The fact that hERG channels with an alanine, aspartic acid or glycine at position 69 formed functional channels at the plasma membrane suggest that these substitutions did not have a gross effect on PAS domain structure like the substitution with proline. It is not known whether the functional or the trafficking defect of the hERG-L69P mutant cause the clinical phenotype, however, both defects support the diagnosis of a LQTS.

1.6. References

1. Sanguinetti MC, Jiang C, Curran ME, Keating MT. A mechanistic link between an inherited and an acquired cardiac arrhythmia. HERG encodes the IKr potassium channel. Cell. 1995; 81: 299–307.
2. Trudeau M, Warmke J, Ganetzky B, Robertson G. HERG, a human inward rectifier in the voltage-gated potassium channel family. Science. 1995; 269: 92–95.
3. Cabral JH, Lee A, Cohen SL, Chait BT, Li M, Mackinnon R. Crystal Structure and Functional Analysis of the HERG Potassium Channel N Terminus. Cell. 1998; 95: 649–655.
4. Doyle DA. The Structure of the Potassium Channel. Molecular Basis of K+ Conduction and Selectivity. Science. 1998; 280: 69–77.
5. Brelidze TI, Carlson AE, Sankaran B, Zagotta WN. Structure of the carboxy-terminal region of a KCNH channel. Nature. 2012; 481: 530–533.
6. Curran ME, Splawski I, Timothy KW, Vincen G, Green ED, Keating MT. A molecular basis for cardiac arrhythmia. HERG mutations cause long QT syndrome. Cell. 1995; 80: 795–803.
7. Sanguinetti MC, Tristani-Firouzi M. hERG potassium channels and cardiac arrhythmia. Nature. 2006; 440: 463–469.
8. La Pena P de, Machin A, Fernandez-Trillo J, Dominguez P, Barros F. Mapping of interactions between the N- and C-termini and the channel core in HERG K+ channels. Biochem J. 2013; 451: 463–474.
9. Hedley PL, Jørgensen P, Schlamowitz S, Wangari R, Moolman-Smook J, Brink PA, et al. The genetic basis of long QT and short QT syndromes: a mutation update. Hum Mutat. 2009; 30: 1486–1511.
10. Anderson CL, Kuzmicki CE, Childs RR, Hintz CJ, Delisle BP, January CT. Large-scale mutational analysis of Kv11.1 reveals molecular insights into type 2 long QT syndrome. Nat Commun. 2014; 5: 5535.
11. Vandenberg JI, Perry MD, Perrin MJ, Mann SA, Ke Y, Hill AP. hERG K+ Channels: Structure, Function, and Clinical Significance. Physiological Reviews. 2012; 92: 1393–1478.
12. Splawski I, Shen J, Timothy KW, Vincent GM, Lehmann MH, Keating MT. Genomic structure of three long QT syndrome genes: KVLQT1, HERG, and KCNE1. Genomics. 1998; 51: 86–97.
13. Guthmann T. The outer transmembrane domain of the Kesv channel determines its intracellular localization. Dissrtation, TU Darmstadt. 2013.
14. Kiehne N. Molekulare Grundlagen zur Diagnostik und Ätiologie genetisch bedingter kardiovaskulärer Erkrankungen als Auslöser des plötzlichen Herztodes. Dissertation, TU Darmstadt. 2011.
15. Chen J, Zou A, Splawski I, Keating MT, Sanguinetti MC. Long QT Syndrome-associated Mutations in the Per-Arnt-Sim (PAS) Domain of HERG Potassium Channels Accelerate Channel Deactivation. Journal of Biological Chemistry. 1999; 274: 10113–10118.
16. Gianulis EC, Trudeau MC. Rescue of aberrant gating by a genetically encoded PAS (Per-Arnt-Sim) domain in several long QT syndrome mutant human ether-á-go-go-related gene potassium channels. J. Biol. Chem. 2011; 286: 22160–22169.
17. Harley CA, Jesus CSH, Carvalho R, Brito RMM, Morais-Cabral JH. Changes in channel trafficking and protein stability caused by LQT2 mutations in the PAS domain of the HERG channel. PLoS ONE. 2012; 7: e32654.
18. Morais-Cabral JH, Robertson GA. The Enigmatic Cytoplasmic Regions of KCNH Channels. J. Mol. Biol. 2015; 427: 67–76.

19. Morais Cabral JH, Lee A, Cohen SL, Chait BT, Li M, Mackinnon R. Crystal Structure and Functional Analysis of the HERG Potassium Channel N Terminus: A Eukaryotic PAS Domain. Cell. 1998; 95: 649–655.
20. Michael C Sanguinetti, Changan Jiang, Mark E Curran, Mark T Keating. A mechanistic link between an inherited and an acquird cardiac arrthytmia: HERG encodes the IKr potassium channel. Cell. 1995; 81: 299–307.
21. MC Trudeau, JW Warmke, B Ganetzky, GA Robertson. HERG, a human inward rectifier in the voltage-gated potassium channel family. Science. 1995; 269: 92–95.
22. Smith PL, Baukrowitz T, Yellen G. The inward rectification mechanism of the HERG cardiac potassium channel. Nature. 1996; 379: 833–836.
23. Paulussen A. A Novel Mutation (T65P) in the PAS Domain of the Human Potassium Channel HERG Results in the Long QT Syndrome by Trafficking Deficiency. Journal of Biological Chemistry. 2002; 277: 48610–48616.
24. Ke Y, Ng CA, Hunter MJ, Mann SA, Heide J, Hill AP, et al. Trafficking defects in PAS domain mutant K v 11.1 channels: roles of reduced domain stability and altered domain–domain interactions. Biochem. J. 2013; 454: 69–77.
25. Smith JL, Anderson CL, Burgess DE, Elayi CS, January CT, Delisle BP. Molecular pathogenesis of long QT syndrome type 2. Journal of Arrhythmia. 2016; 32: 373–380.
26. Ng CA, Hunter MJ, Perry MD, Mobli M, Ke Y, Kuchel PW, et al. The N–Terminal Tail of hERG Contains an Amphipathic α–Helix That Regulates Channel Deactivation. PLoS ONE. 2011; 6: e16191.
27. Li Q, Ng HQ, Yoon HS, Kang C. Insight into the molecular interaction between the cyclic nucleotide-binding homology domain and the eag domain of the hERG channel. FEBS Lett. 2014; 588: 2782–2788.
28. Muskett FW, Thouta S, Thomson SJ, Bowen A, Stansfeld PJ, Mitcheson JS. Mechanistic insight into human ether-a-go-go-related gene (hERG) K+ channel deactivation gating from the solution structure of the EAG domain. J. Biol. Chem. 2011; 286: 6184–6191.
29. Ke Y, Hunter MJ, Ng CA, Perry MD, Vandenberg JI. Role of the cytoplasmic N-terminal Cap and Per-Arnt-Sim (PAS) domain in trafficking and stabilization of Kv11.1 channels. J. Biol. Chem. 2014; 289: 13782–13791.
30. Gustina AS, Trudeau MC. HERG potassium channel regulation by the N-terminal eag domain. Cell Signal. 2012; 24: 1592–1598.
31. Shushi L, Kerem B, Goldmit M, Peretz A, Attali B, Medina A, et al. Clinical, genetic, and electrophysiologic characteristics of a new PAS-domain HERG mutation (M124R) causing Long QT syndrome. Ann Noninvasive Electrocardiol. 2005; 10: 334–341.
32. Rossenbacker T, Mubagwa K, Jongbloed RJ, Vereecke J, Devriendt K, Gewillig M, et al. Novel mutation in the Per-Arnt-Sim domain of KCNH2 causes a malignant form of long-QT syndrome. Circulation. 2005; 111: 961–968.
33. Gustina AS, Trudeau MC. A recombinant N-terminal domain fully restores deactivation gating in N-truncated and long QT syndrome mutant hERG potassium channels. Proc Natl Acad Sci U S A. 2009; 106: 13082–13087.
34. Karpen ME, Haseth PL de, Neet KE. Differences in the amino acid distributions of 3(10)-helices and alpha-helices. Protein Sci. 1992; 1: 1333–1342.
35. Betts MJ, Russell RB. Amino Acid Properties and Consequences of Substitutions. In Bioinformatics for geneticists, Barnes MR, Gray IC (editors): Wiley; 2003.
36. Wang J, Trudeau MC, Zappia AM, Robertson GA. Regulation of Deactivation by an Amino Terminal Domain in Human Ether-à-go-go –related Gene Potassium Channels. J Gen Physiol. 1998; 112: 637–647.

1.7. Appendix

1.7.1. *KCNH2* Primer Sequences

The coding region of the *KCNH2* gene was amplified with published [12] and redesigned primers. The PCR conditions were partial modified by using dimethyl sulfoxide (5%/10% DMSO) or a GC PCR Kit (AmpliTaq Gold® 360 DNA Polymerase Kit, Applied Biosystems, Germany).

Exon	*Forward Primer (5' → 3')*	*Reverse Primer (5' → 3')*	*Amplicon length (bp)*	*Add on*
1	GCG CCC GCA GTC CAG TCT	GAC TCG CAC TTG CCG ACG CA	335	GC PCR
2	GGT CCC CGC TCA CGC GCA CTC TC	TTG ACC CCG CCC CTG GTC GT	231	5% DMSO
3	GCC CAC TGA GTG GGT GCC AAG	CCA CGA ACC CCT GAG CCT GCC	165	
4	CTC CGG GGC TGC TCG CGA T	CAC CAG CGC ACG CCG CTC CT	200	10% DMSO
	GCC ATG GAC AAC CAC GTG GCA	CCC AGA ATG CAG CAA GCC TG	283	10% DMSO
5	GGC CTG ACC ACG CTG CCT CT	CCC TCT CCA AGC TCC TCC AA	212	
6	CAG AGA TGT CAT CGC TCC TG	CAG GCG TAG CCA CAC TCG GTA G	196	
	TTC CTG CTG AAG GAG ACG GAA G	TAC ACC ACC TGC CTC CTT GCT GA	245	
7	TGC CCC ATC AAC GGA ATG TGC	CAG CCA GCC GAT GCG TGA GTC CA	178	
	TAG CCT GCA TCT GGT ACG C	GCC CGC CCC TGG GCA CAC TCA	236	
8	TGG GGT CCC TGC AGA GGC TGA C	CTT CCC AGC CTG CCA CCC ACT G	200	
9	GGC CTG GAG GTT GAG ATT TC	GCG GTG CAT GTG TGG TCT TG	188	
	GCA CTG CAA ACC CTT CCG AG	GGC ATT TCC AGT CCA GTG C	165	
10	TGA GCT CCC TGT CCT CTC CAT G	CTC AGG GCA GCC AAC TCA CAT C	194	
11	GGT GGG GCA GGA GAG CAC TG	TCC CCC GCC TCA CCC TTG TC	93	
12	CTC TGT TTC CCA CAG ACA CG	CTG GGT GAG CGG GGT AGA CG	360	GC PCR
13	CCG CTC ACC CAG CTC TGC TCT C	CAG GGC GTG CCC CCC CAC CCC	227	
14	ACT CCC GGT GGA GGC TGT CA	GAA CAA GCG GGT CAC GGT AC	178	

15	TCC TGT CCT CCC GTC CAT C	TGT CCA CAC TGG GCA G	155	

1.7.2. pEGFP-N2 Vector Information

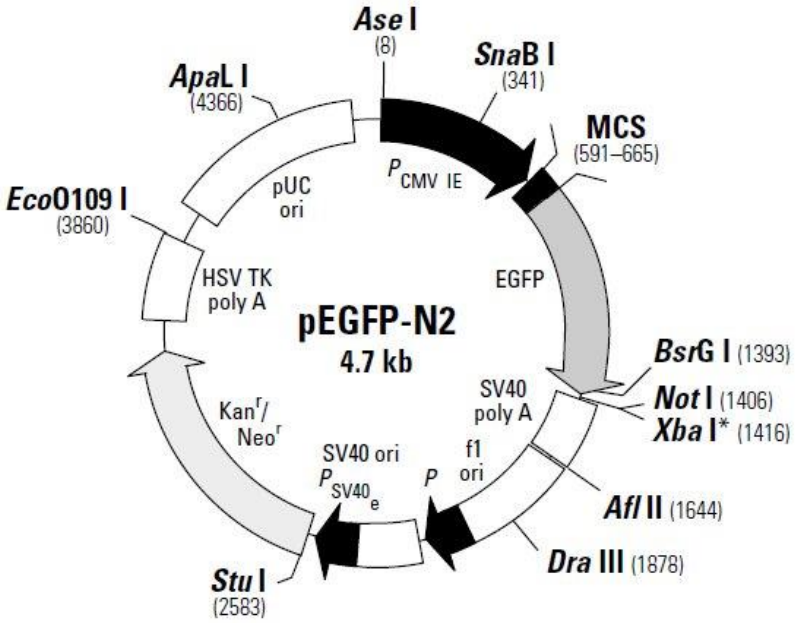

Fig. 16: Vector map of pEGFP-N2

(www.bdbiosciences.com)

1.7.3. Mutagenesis Primer Sequences

***KCNH2*-L69P**	
forward	5'-CCC TGC ACC TGC GAC TTC CCG CAC GGG CCG CGC ACG CAG C-3'
reverse	5'-GCT GCG TGC GCG GCC CGT GCG GGA AGT CGC AGG TGC AGG G-3'

***KCNH2*-L69A**	
forward	5'-CCC TGC ACC TGC GAC TTC GCT CAC GGG CCG CGC ACG CAG-3'
reverse	5'-CTG CGT GCG CGG CCC GTG AGC GAA GTC GCA GGT GCA GGG-3'

***KCNH2*-L69D**	
forward	5'-CCC TGC ACC TGC GAC TTC GAC CAC GGG CCG CGC ACG CAG-3'
reverse	5'-CTG CGT GCG CGG CCC GTG GTC GAA GTC GCA GGT GCA GGG-3'

***KCNH2*-L69G**	
forward	5'-CCC TGC ACC TGC GAC TTC GGA CAC GGG CCG CGC ACG CAG-3'
reverse	5'-CTG CGT GCG CGG CCC GTG TCC GAA GTC GCA GGT GCA GGG-3'

1.7.4. Amino acids

A	Ala	Alanine
C	Cys	Cysteine
D	Asp	Aspartic acid
E	Glu	Glutamic acid
F	Phe	Phenylalanine
G	Gly	Glycine
H	His	Histidine
I	Ile	Isoleucine
K	Lys	Lysine
L	Leu	Leucine
M	Met	Methionine
N	Asn	Asparagine
P	Pro	Proline
Q	Gln	Glutamine
R	Arg	Arginine
S	Ser	Serine
T	Thr	Threonine
V	Val	Valine
W	Trp	Tryptophan
Y	Tyr	Tyrosine

2. CHAPTER 2 – GENOTYPE-PHENOTYPE DILEMMA IN A CASE OF SUDDEN CARDIAC DEATH WITH THE E1053K MUTATION AND A DELETION IN THE SCN5A GENE

2.1. Abstract

Mutations in the cardiac sodium channel gene *SCN5A* may result in various arrhythmia syndromes such as long QT syndrome type 3 (LQTS), Brugada syndrome (BrS), sick sinus syndrome (SSS), cardiac conduction diseases (CCD) and possibly dilated cardiomyopathy (DCM). In most of these inherited cardiac arrhythmia syndromes the phenotypical expression may range from asymptomatic phenotypes to sudden cardiac death (SCD).

A 16-year-old female died during sleep. Autopsy did not reveal any explanation for her death and a genetic analysis was performed. A variant in the *SCN5A* gene (E1053K) that was previously described as disease causing was detected. Family members are carriers of the same E1053K variant, some even in a homozygous state, but surprisingly did not exhibit any pathological cardiac phenotype. Due to the lack of genotype-phenotype correlation further genetic studies were performed. A novel deletion in the promoter region of *SCN5A* was identified in the sudden death victim but was absent in other family members.

These findings demonstrate the difficulties in interpreting the results of a family-based genetic screening and underline the phenotypic variability of *SCN5A* mutations.

2.2. Introduction

Mutations in the *SCN5A* gene, which encodes the α-subunit of the cardiac sodium channel $Na_v1.5$, may cause either a gain or a loss of channel function. Gain-of-function mutations associated with an increase in the persistent late I_{Na} during the action potential plateau (Fig. 17, phase 2), may lead to the long QT syndrome type 3 (LQTS) [1]. Loss-of-function mutations result in a decrease in peak I_{Na} (Fig. 17, phase 0) and are associated with a spectrum of arrhythmia phenotypes including Brugada syndrome (BrS) [2], sick sinus syndrome (SSS) [3], cardiac conduction diseases (CCD) [4] and possibly dilated cardiomyopathy (DCM) [5]. Most of the inherited cardiac arrhythmia syndromes show variable phenotypic severity ranging from absence of any symptoms to sudden cardiac death (SCD). Mixed phenotypes (overlap syndromes, e.g. presentation of ECG features of Brugada syndrome, conduction disorders and long QT syndrome type 3) have also been described [6,7].

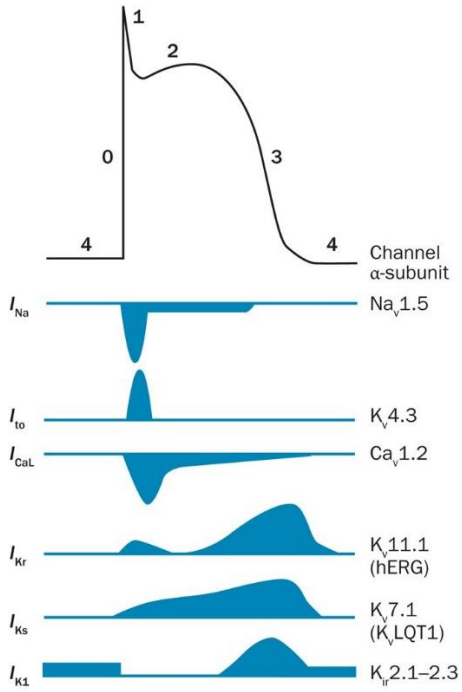

Fig. 17: Major ion channel currents during the cardiac action potential.

In response to a change in membrane potential a rapid influx of Na^+ through voltage-gated channels occurs which generates the fast inward Na^+ current (peak I_{Na}, phase 0, depolarization). Phase 1 is characterized by a transient outward K^+ current (I_{to}) with fast activation and inactivation kinetics. The plateau phase (phase 2) is a result of inward currents as well as components of the outward rectifier current. The inward currents are due to a fraction of Na^+ channels which were not inactivated at the end of phase 0 (late I_{Na}) and L-type Ca^{2+} channels which generate the Ca^{2+} current I_{Ca}. The components of the outward rectifier K^+ currents are rapid I_{Kr} and slow I_{Ks}. During phase 3 (repolarization) outward rectifying K^+ channels are dominant and Na^+ and Ca^{2+} channels are inactivated. At the end of the repolarization phase the inward rectifier channel K_{ir} generates I_{K1}. At negative membrane potentials, this current is conducted more in the inward direction and sets the resting membrane potential close to the K^+ equilibrium potential (-90 mV, phase 4). (Modified from Liu et al. [8])

The Brugada syndrome is an inherited autosomal-dominant arrhythmogenic disorder with characteristic electrocardiogram (ECG) abnormalities (Fig. 18). It is associated with an increased risk for SCD due to polymorphic ventricular tachycardia and/or ventricular fibrillation [9,10]. At present, seventeen genes have been putatively linked to BrS, but mutations in these genes are found only in about 25-35% of BrS cases [11]. Most rare variants are found in *SCN5A* and are present in 11-28% of the cases [12]. The clinical phenotype of a particular variant in the *SCN5A* gene may show a variable penetrance among individuals even within the same family. In some BrS-affected families, Probst et al. [13] found that *SCN5A* gene mutations are not solely causal for the manifestation of BrS and suggested that other factors beyond mutant sodium channels (e.g. genetic variation in other genes, alteration in transcription/translation, RNA processing and protein degradation) may contribute to different BrS phenotypes. More recent data present evidence that BrS might actually have an oligogenic basis [14].

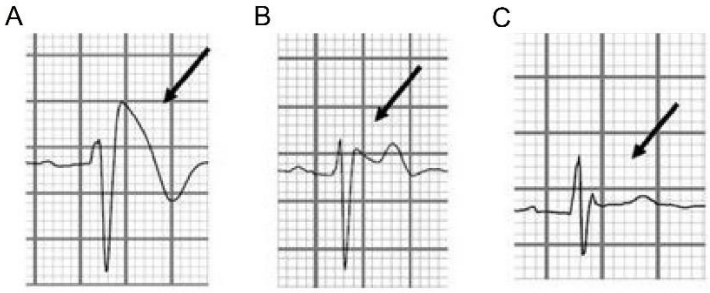

Fig. 18: Brugada syndrome ECG abnormalities.

Typical BrS ECG abnormalities in the right precordial leads. (A) Type 1 ECG (diagnostic in BrS) is characterized by a J-wave amplitude or coved-type ST-segment elevation of ≥ 2 mm followed by a negative T-wave. (B) Type 2 ECG is defined as a ≥2 mm J-wave elevation, ≥1 mm ST-segment elevation resulting in a saddle-back configuration, followed by a positive or biphasic T-wave. (C) Type 3 ECG shows a ST-segment elevation < 1 mm with either a coved or saddle-back appearance. Type 2 and 3 ECG patterns are not diagnostic rather than suspicious for BrS. (Modified from Mizusawa and Wilde [15]).

The phenotypic variability associated with *SCN5A* mutations can also be partly explained by the co-inheritance of additional genetic variants in that gene. For example, the common *SCN5A* polymorphism H558R is known to be a disease modifying variant that can alter the effects of gain- or loss-of-function mutations [16–18]. Hoshi et al. [19] showed that several apparently benign (or atypical) *SCN5A* mutations only lead to a BrS phenotype through a reduction in sodium current when expressed in a heterozygous state. Furthermore, *SCN5A* promotor variants, which cause variable transcription of the cardiac sodium channel gene, may contribute to the phenotypic variability of BrS. Bezzina et al. [20] studied the role of the genetic variation in the *SCN5A* promotor and identified six variants in close linkage disequilibrium, that could be associated with a reduced expression of the sodium channel as demonstrated in functional studies. This haplotype, found in people of Asian origin, could modulate the phenotypic expression of the Brugada syndrome. Additionally, multiple genetic variants in the *SCN5A* core promotor, which were found in BrS patients as well as in apparently healthy individuals, exhibit altered *in vitro* expression activity [21].

Here we describe the difficulties in interpreting results of a postmortem genetic analysis in a case of sudden cardiac death. Besides a variant in the coding area of the *SCN5A* gene, a deletion in the promotor region in that gene was detected. Genetic screening of family members of the deceased revealed the presence of the variant, but not of the deletion; none of them showed clinically cardiac symptoms.

2.3. Material and Methods

2.3.1. Clinical studies/Study subjects

Following the sudden cardiac death (SCD) of a 16 years old female medico-legal autopsy was performed. Since no pathological findings were obtained postmortem, genetic screening was carried out in the context of the research project “molecular basis of diagnosis and etiology of genetic cardiovascular diseases as cause for sudden cardiac death” of the Institute of Forensic Medicine in Frankfurt. As this analysis revealed a potentially pathogenic variant, previously described as disease causing, the first-degree relatives were encouraged to seek genetic counseling. After obtaining informed consent of six family members, blood samples were

collected and analyzed. It was recommended for all family members to undergo cardiological assessment including resting and exercise ECG and Ajmaline testing.

2.3.2. Genetic screening

Genomic DNA was extracted from blood samples using standard phenol chloroform procedures. Polymerase chain reaction (PCR) was used to amplify 28 exons (excluding non-coding exon 1) of *SCN5A* with published [22] and own primers (see Appendix 2.7.1.) Direct sequencing of the amplicons was performed in the presence of fluorescence–labeled dideoxynucleotides (BigDye® Terminator Cycle Sequencing Kit, Life Technologies, Germany) and primer in both sense and antisense direction. Sequencing products were examined with a 3130xl Genetic Analyzer (Applied Biosystems, Germany). Data analysis was done with SeqScape v2.5 (Applied Biosystems, Germany) and the NCBI (National Center of Biotechnology) reference sequence NC_008934. In case of the homozygous carrier of the variant, the exon containing the sequence variant was amplified with a second set of primers to rule out the possibility of a primer binding site mutation in one allele. Variant filtering was performend with the ExAC database (Exome Aggregation Consortium) and a minor allele frequency (MAF) cut-off of <0.1% was used.

2.3.3. Multiplex Ligation-dependent Probe Amplification (MLPA)

MLPA is a semi-quantitative technique for detecting large deletions and duplications in a DNA sample. MLPA was performed on genomic DNA using the SALSA P108 SCN5A kit (MRC-Holland, Amsterdam, the Netherlands) according to the manufacturer's protocol. Three different control samples were included in each MLPA experiment. The SALSA P108 MLPA kit contains probes for each exon of the *SCN5A* gene (29 exons, including non-coding exon 1) and one probe upstream of exon 1. The amplification products were separated and identified by capillary electrophoresis using a 3130xl Genetic Analyzer (Applied Biosystems, Germany). Data analysis of the electropherograms was done with the Coffalyser.Net software (www.mlpa.com) performing two normalization steps of the MLPA peak pattern. Each probe peak of each sample was compared with the peaks of the reference probes (intrasample normalization). By comparing the relative probe peak of the sample to all control samples final probe ratios are calculated (intersample normalization). The resulting probe ratio for a normal DNA sample is ~1.0 (0.8-1.2), for a heterozygous deletion ~0.5 (0.4-0.65).

2.3.4. Analyzing the *SCN5A* promotor region using Real-Time Quantitative PCR

To confirm the deletion in the 5' upstream region of the *SCN5A* gene real-time quantitative PCR (RT-qPCR) using DNA binding SYBR® GreenER™ (EXPRESS SYBR® GreenER™ qPCR SuperMixes and Two-Step qRT-PCR Kit, Invitrogen) and PCR Primers (see Appendix 2.7.2.) flanking the suspected boundaries of the deletion was performed. The method includes amplification of three segments in the 5' upstream sequence of *SCN5A* and two reference loci on chromosome 3 with normal copy number (*GPR15* and *ZNF80* [23]) for normalization. Amplification mixtures (20 µl) contained EXPRESS SYBR® GreenER™ master mix, 200 nM of each forward and reverse primer, 500 nM ROX reference dye and 1,25 ng template DNA. All reactions were performed in triplicates. The Applied Biosystems StepOnePlus™ Real-Time PCR System was used for the PCR reaction and the cycling conditions were as follows: 95°C for 2 min, 40 cycles of 95°C for 15 s and 60°C for 1 min. Melting curve analysis was generated for every amplification product to ensure the specificity of the PCR reaction. Calculation of

copy numbers of the prospected segments was done with the Data Assist™ v3.01 Software (Applied Biosystems, Germany) using the comparative C_T ($\Delta\Delta C_T$) method [24]. Using *GPR15* (G Protein-coupled Receptor 15) and *ZNF80* (Zinc Finger Protein 80) as reference genes with normal copy number, Hoebeek et al. [23] have shown that a copy number of ~1.0 (cut-off value ≥0.8) is expected for a normal sample, while a heterozygous deletion would have a value of ~0.5 (cut-off value ≤0.7).

2.4. Results

2.4.1. Genetic analysis

Sequencing of 28 exons (excluding non-coding exon 1) of the *SCN5A* gene revealed the heterozygous variant E1053K (c.3157G>A, rs137854617) in the deceased female (IV.3 Fig. 19A and B). This rare variant has a minor allele frequency (MAF) of 0.014% in the European population (ExAC database) and has been previously associated with the Brugada [25,26] as well as with the Long-QT syndrome [27]. By cascade family screening the E1053K (heterozygous) variant was identified in the mother (III.4, age 47 years) of the deceased and in one cousin of the mother (III.2, age 57 years). Homozygous carriership of this variant was detected in one aunt (III.6, age 43 years, Fig. 19B) of the SCD victim. The other screened genes did not contain protein-altering variants at the variant-filtering cut-off of <0.1%.

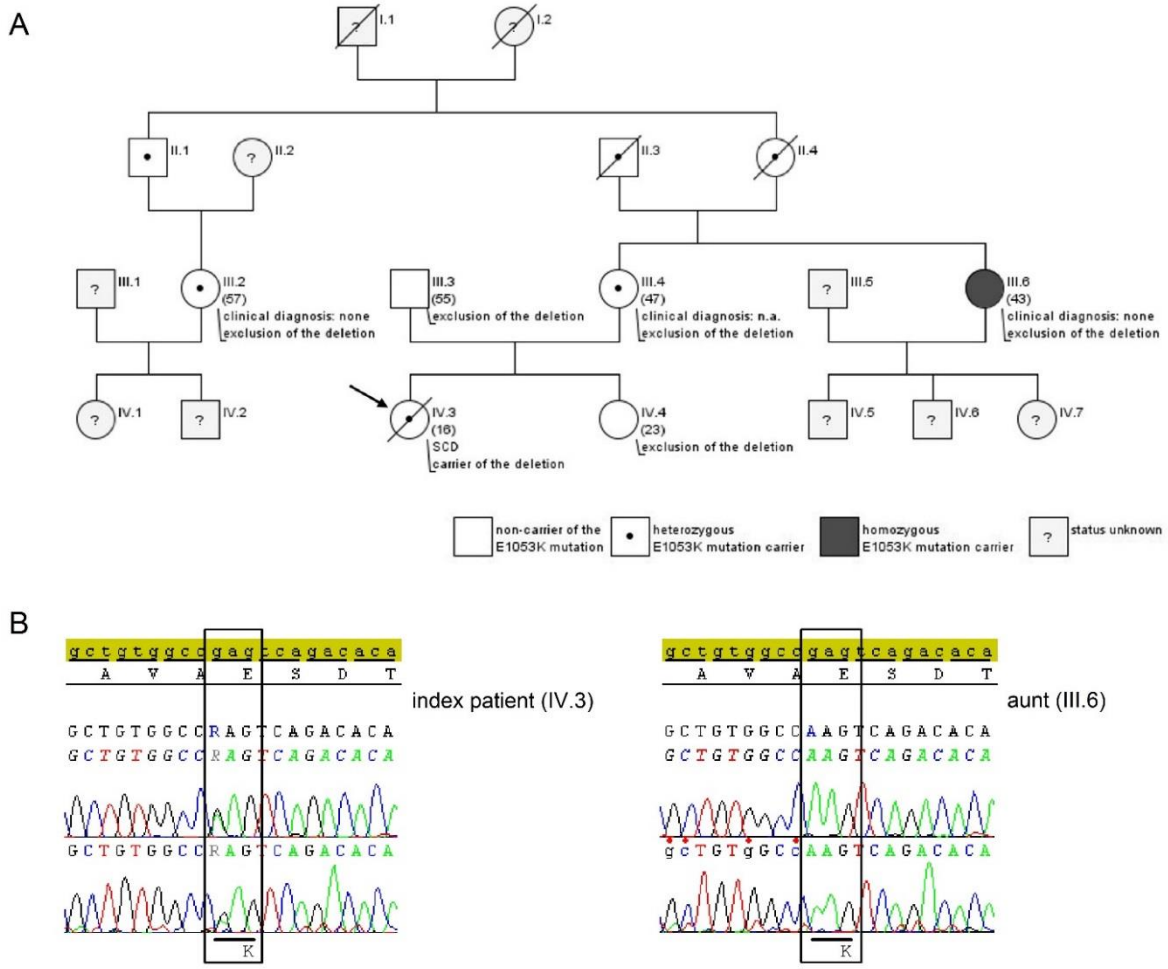

Fig. 19: Identification of *SCN5A* variant E1053K in the family of the deceased.

(A) Pedigree structure of the family of the deceased female. Square symbols indicate males, round symbols females and slashed symbols mark deceased individuals. The Roman numerals indicate the generation number, Arabic numerals each individual in a given generation. The arrow indicates the index patient. SCD = Sudden Cardiac Death, n.a. = not available. (B) Sequencing of the 28 exons of the *SCN5A* gene revealed a heterozygous nucleotide change in the index patient (left) and a homozygous nucleotide change in the aunt of the deceased (right). Highlighted in grey is the *SCN5A* reference sequence. E = glutamic acid, K = lysine.

The *SCN5A* E1053K mutation is localized in the 9-amino acid ankyrin-G-binding motif (VPIAVA[E→K]SD) of the DII-DIII loop of $Na_v1.5$ [26] (Fig. 20). Ankyrin-G belongs to the family of the spectrin-binding proteins. It is required for the targeting of membrane proteins, especially ion channels like Na_v channel isoforms, to excitable membranes [28]. The *SCN5A* variant E1053K inhibits the binding of the $Na_v1.5$ channel to ankyrin-G and, therefore, the mutant channel is not efficiently targeted to cardiomyocyte membranes [26,29].

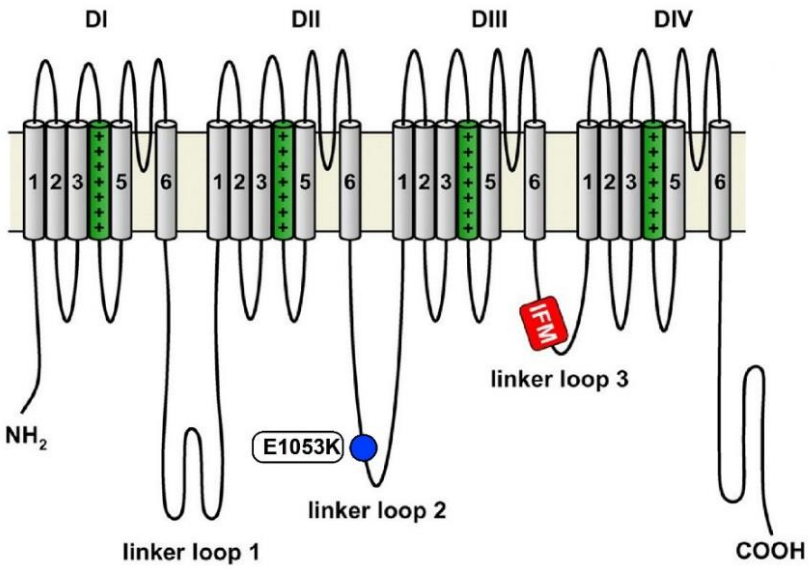

Fig. 20: Schematic topology of the α-subunit of the cardiac sodium channel $Na_v1.5$.

The four homologous domains DI-DIV are connected by extracellular and intracellular loops. The mutation E1053K is located in the intracellular linker loop 2 (modified from Abriel *et al*. [30]).

2.4.2. Clinical examination

A thorough clinical examination which included resting ECG (III.2, III.6 and IV.4), provocation test with the sodium channel blocker Ajmaline (III.2 and III.6), exercise ECG (III.2, III.6 and IV.4) and cardiac MRI (III.6) did not reveal any pathological phenotype neither in the heterozygous (III.2) nor in the homozygous carrier (III.6) of the E1053K variant (Ajmaline provocation test see Fig. 21). Regrettably, the mother (III.4) of the SCD victim refused any clinical examination and her parents had already died due to non-cardiac diseases. Considering the fact that the *SCN5A* variant E1053K did not lead to a pathological phenotype in the homozygous carrier, it is not very likely that this variant is the sole cause of death of the index patient. In addition, the minor allele frequency of 0.014% in the ExAC database is not compatible with being an independent pathogenic variant.

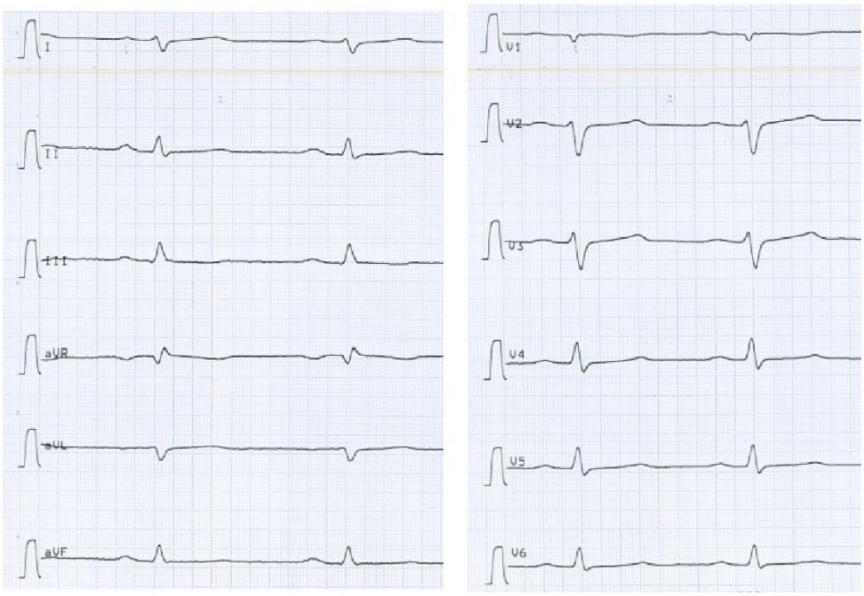

Fig. 21: 12-lead ECG during ajmaline challenge.

12-lead ECG of the homozygous carrier (III.6) of the E1053K variant after intravenous injection of 60 mg ajmaline. No abnormalities were detected.

2.4.3. Detection of a deletion in the promotor region of *SCN5A* using MLPA

By MLPA analysis a heterozygous deletion in the 5' upstream region of *SCN5A* in the index patient was identified (Fig. 22A). This 5' upstream sequence is a part of the *SCN5A* promotor region which has been characterized as an ~2.8 kb segment including ~2.1 kb of 5' upstream sequence, the non-coding exon 1 and a part of the 16 kb intron 1 [31]. In several studies promotor variants functioning as positive and negative *cis*-acting elements have been identified, which are associated with various arrhythmia phenotypes [20,21,31,32]. A point mutation in the sequence detected by the MLPA probe *SCN5A*-up could be excluded, because no differences in the nucleotide sequence were detected by sequencing of this region (primer location see fig. 24). MLPA analysis of the first-degree relatives showed that none of the other family members carries the deletion in the 5' upstream region of *SCN5A*. As an example, figure 22B shows the MLPA result of the homozygous E1053K-carrier (III.6).

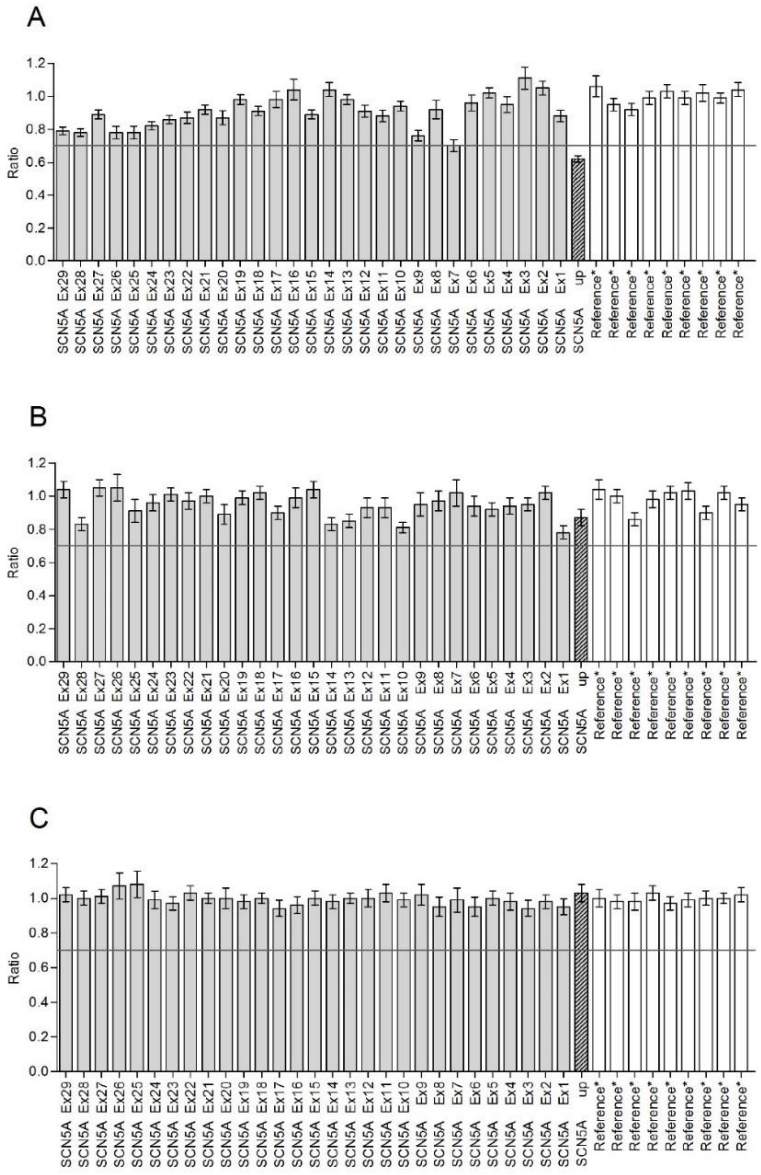

Fig. 22: MLPA analysis results.

Each plot represents the relative peak ratios (±SD) for reference probes (white), *SCN5A* exon probes (grey) and one probe in the 5' upstream region of *SCN5A* (dark). The solid line indicates the cut-off ratio of 0.7. (A) shows a heterozygous deletion of *SCN5A*-up in the index patient (IV.3). (B) and (C) shows the MLPA results for the homozygous carrier (III.6) and a control sample, respectively.

Figure 23 summarizes the results of four MLPA runs for the probe *SCN5A*-up. The mean ratio (±SD) was 0.63±0.01 for the index patient, 0.92±0.04 for the homozygous E1053K-carrier (III.6) and 0.99±0.07 for control sample 1. Two-sample t-test (assuming unequal variation) indicate that the ratio was significantly different between the index patient and III.6 (p=0.0005) as well as between the index patient and control 1 (p=0.0015).

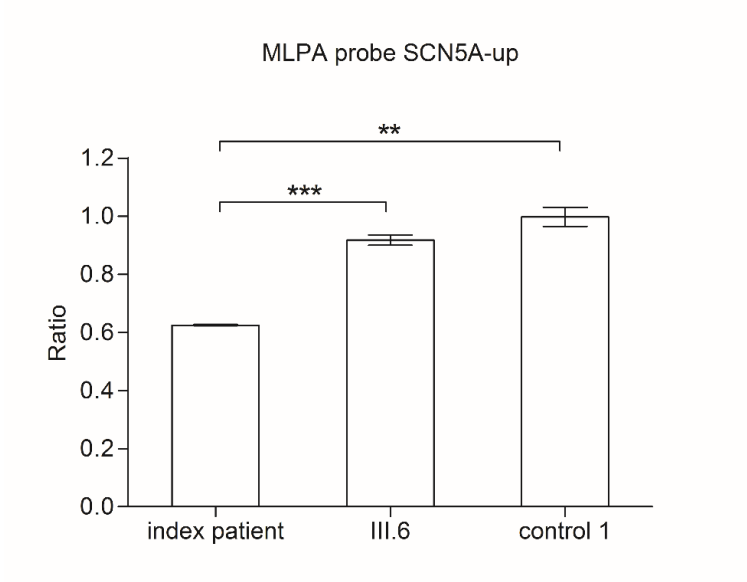

Fig. 23: Diagram showing the relative peak ratios for the MLPA probe *SCN5A*-up (n=4).

Significance: ** p<0.01, *** p<0.001

2.4.4. Real-Time Quantitative PCR

To determine the extent of the deletion detected by MLPA, a real-time quantitative PCR (RT-qPCR) was performed. The nomenclature proposed by Yang et al. [31] was adopted, where position +1 is the major transcription initiation site in *SCN5A* (Fig. 24). Three fragments (I: position -1845 to -1610, II: position -1964 to -1853, III: position -1606 to -1469) in the upstream region of *SCN5A* and two reference genes (*GPR15* and *ZNF80*) for data normalization were amplified. The MLPA probe *SCN5A*-up binds at position -1740 to -1681 therefore fragment I is covering this region (Fig. 24). RT-qPCR was performed on genomic DNA of the index patient and of two healthy controls.

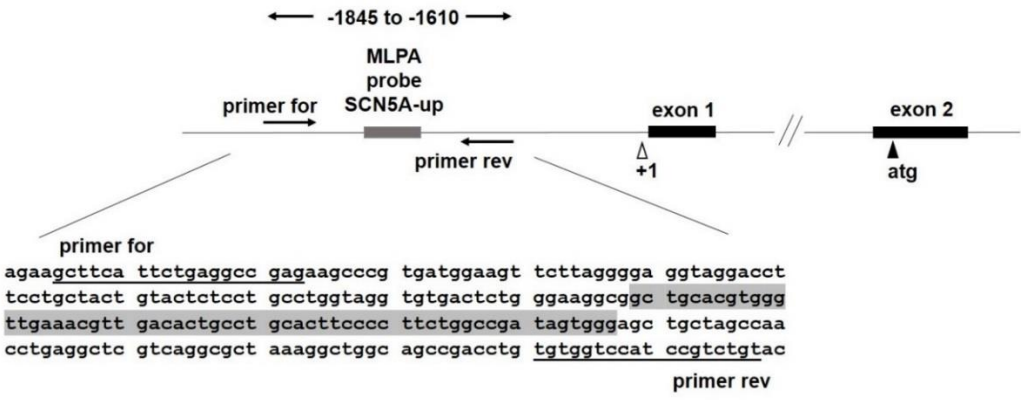

Fig. 24: Locations of the primer used for sequencing and RT-qPCR.

The MLPA probe sequence of SCN5A-up is highlighted in grey. The major transcription initiation site is indicated by Δ. The translation start site is located within exon 2 and is indicated by ▲.

The RT-qPCR revealed a deletion of fragment I (Fig. 25A) in the 5' upstream region of the *SCN5A* gene from the index patient. The mean copy number (±SD) was 0.34 (±0.02) for fragment I, 1.02 (±0.09) for fragment II and 1.41 (±0.28) for fragment III, respectively. The copy numbers of fragment I were compared with the two-sample t-test (unequal variation) which demonstrates that the copy number is significantly different between the index patient and control I as well as control II ($p<0.0001$). In the two adjacent fragments, II and III, no deletion could be detected by RT-qPCR (Fig. 25B and C).

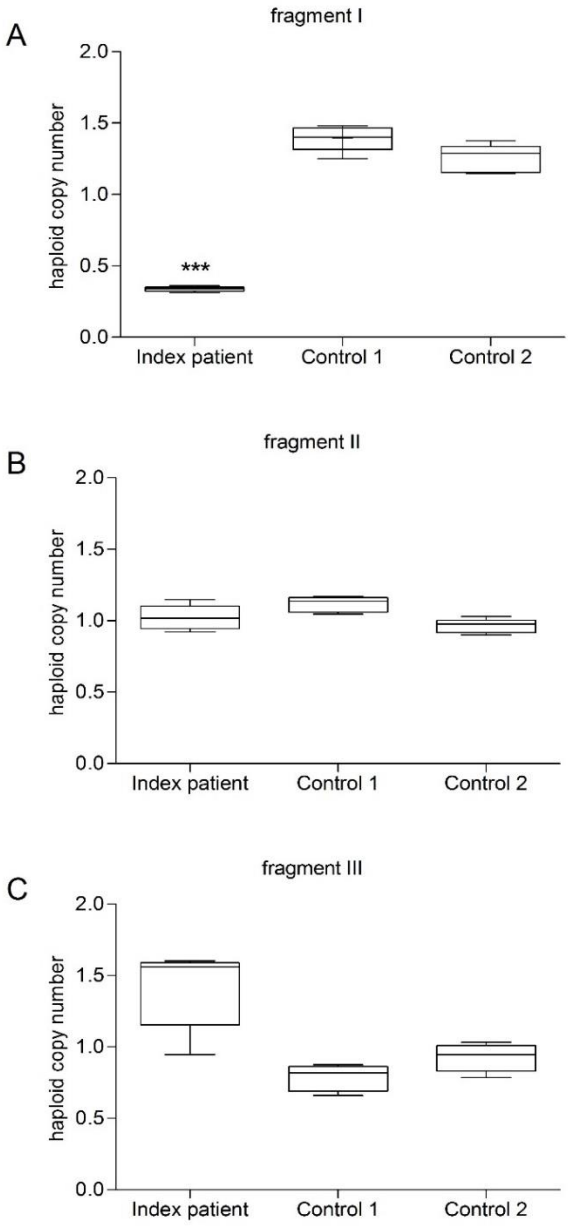

Fig. 25: Haploid copy number values determined by RT-qPCR.

Box-plot representation of copy numbers of fragment I-III obtained for the index patient and two normal controls. (A) The index patient harbours a deletion of fragment I in the upstream region of *SCN5A* (Significance: *** $p<0.001$). No deletion could be detected in the neighbouring fragments II (B) and III (C).

2.5. Discussion

In the present study, a heterozygous variant (E1053K) in the *SCN5A* gene of a 16-year-old female was identified who died suddenly during sleep. Medico-legal autopsy revealed no pathological findings. Genetic screening of the family members of the deceased revealed heterozygous carriership of this variant in her mother and in a cousin of second degree. Her aunt was a homozygous carrier of this variant. The *SCN5A* E1053K variant has been described previously in patients with BrS [25,26] as well as in a patient with LQTS [33]. Hence, a thorough cardiological examination of the relatives was performed, however, to our surprise these tests revealed no pathological phenotype neither in the heterozygous nor in the homozygous carrier of the variant, suggesting that the *SCN5A* E1053K variant alone is not disease causing and additional genetic factors may exist in the *SCN5A* gene of the index patient. Subsequent MLPA analysis and RT-qPCR identified a deletion in the *SCN5A* promotor region. Table 2 summarizes the genetic and clinical findings for the affected family members.

Table 2: Summary of the results of genetic and clinical examination.

	Genetic results	**Clinical diagnosis**
Index patient	E1053K heterozygous Deletion (-1845 to-1610)	SCD
Mother	E1053K heterozygous	n.d.
Aunt	E1053K homozygous	negative
Second cousin	E1053K heterozygous	negative

n.d. not determined

Mohler et al. [26] demonstrated that the *SCN5A* E1053K variant, found in a patient with BrS, impairs binding of $Na_v1.5$ channels to ankyrin-G. This leads to reduced membrane expression of the sodium channel in cardiomyocytes (albeit not in HEK293 cells). In a following study functional experiments had been performed using cardiomyocytes lacking ankyrin-G. The cardiomyocyte membranes exhibited a reduced total Na^+ current, nevertheless, a residual Na^+ current was detected [29]. The authors suggested that this current may reflect residual sodium channel activity or may represent the activity of other sodium channel isoforms.

More recently Hoshi et al. [19] described apparently benign (also referred to as atypical) *SCN5A* BrS mutations, amongst which E1053K, that do not present the typical loss-of-function phenotype when expressed alone in heterologous expression systems such as HEK293 cells, but which lead to a decrease in sodium current when co-expressed with the wild-type sodium channel mimicking the heterozygous genotype in patients. They hypothesized that an impaired dimerization of two different $Na_v1.5$ α-subunits may account for the results they obtained.

Notwithstanding the observation made in vitro, E1053K genotype-phenotype relationships in the family we studied question the role of the E1053K variant in causing SCD, at least in isolation, since relatives carrying this variant heterozygously or homozygously do not exhibit clinical symptoms. The *SCN5A* H558R polymorphism, known to be a disease modifying variant in *SCN5A* mutation carriers [16–18], could be excluded in the index patient as well as in the other family members examined. Furthermore, considering that the *SCN5A* E1053K variant was previously identified in patients with clinical diagnosis of BrS [25,26,34] as well as in a patient with LQTS [33], representing disorders with distinct functional defects, and remembering the frequency in the ExAC database (0.014%) it can be concluded that this variant could not be the sole cause of death.

However, the deletion in the promotor region of the *SCN5A* gene in the index patient may be relevant. The deleted fragment is located in a region extending from position -1845 to -1610 upstream of the major transcription initiation site (numbering based on *SCN5A* promotor RefSeq: AY313163 and according to [31]). Several studies have demonstrated the impact of promotor variants on the transcriptional activity of the *SCN5A* gene and it has been suggested that these variants may contribute to the variability of arrhythmia phenotypes [20,35–38]. Yang et al. [31] cloned and characterized the human *SCN5A* promotor. They identified and characterized various *cis*-acting DNA regulatory elements and described the functional effect of a single nucleotide polymorphism (SNP), which increased transcriptional activity in cardiomyocytes. Furthermore, Yang et al. [21] analysed subjects of various ethnical origins (including BrS patients and normal controls) and demonstrated that DNA variants are not uncommon in the *SCN5A* promotor region. Among the identified promotor variants, the SNP c.-225-1790 G>A significantly reduced the expression activity in cardiomyocytes and was suggested to modulate a putative transcription factor binding site. The described SNP position (c.-225-1790 G>A) is located within the deleted fragment (-1845 to -1610) that was identified in the *SCN5A* upstream region of the index patient. Therefore, this deletion may produce similar effects, although it is not known whether the deletion is present in the wild-type or in the mutant (E1053K) allele. In a recent study Yagihara et al. [38] identified variants in the promoter and in the transcription regulatory region of *SCN5A* which were associated with a variety of arrhythmia phenotypes. They hypothesized that variants in the *SCN5A* promoter may not be the sole cause of arrhythmias but they may modulate the susceptibility to arrhythmia syndromes. Taking this into account, the deletion detected in the index patient may affect the transcriptional activity of the *SCN5A* gene but this should be further elucidated.

In conclusion, the genetic and clinical findings in the family suggest that E1053K-*SCN5A* is not an independent pathogenic variant. In functional studies sodium channels containing the E1053K variant exhibited a dysfunction that might contribute to a heightened risk for arrhythmias in the setting of co-inheritance of additional genetic modifications such as genetic variations in the same or unrelated genes, alteration in transcription/translation, RNA processing or protein degradation [8,13] Interpretation of *SCN5A* mutations should therefore always be correlated carefully with regard to the clinical phenotype and rigorously evaluated considering additional genetic modifications.

Genetic testing in sudden cardiac death cases is emerging as an important forensic tool to explain the cause of death. Based on the present and previous studies, genetic and cardiological assessment of the relatives of a SCD victim is recommended helping to understand genotype-phenotype relationships in this case using the example of a *SCN5A* variant. Elucidation of the cause of sudden cardiac death should always be embedded in a specialized multidisciplinary service with appropriately trained staff.

2.6. References

1. Wang Q, Shen J, Li Z, Timothy K, Vincent G, Priori SG, et al. Cardiac sodium channel mutations in patients with long QT syndrome, an inherited cardiac arrhythmia. Hum Mol Genet. 1995; 4: 1603–1607.
2. Zimmer T, Surber R. SCN5A channelopathies – An update on mutations and mechanisms. Progress in Biophysics and Molecular Biology. 2008; 98: 120–136.
3. Benson DW, Wang DW, Dyment M, Knilans TK, Fish FA, Strieper MJ, et al. Congenital sick sinus syndrome caused by recessive mutations in the cardiac sodium channel gene (SCN5A). J. Clin. Invest. 2003; 112: 1019–1028.
4. Tan HL, Bink-Boelkens MT, Bezzina CR, Viswanathan PC, Beaufort-Krol GC, van Tintelen PJ, et al. A sodium-channel mutation causes isolated cardiac conduction disease. Nature. 2001; 409: 1043–1047.
5. McNair WP, Ku L, Taylor MRG, Fain PR, Dao D, Wolfel E, et al. SCN5A mutation associated with dilated cardiomyopathy, conduction disorder, and arrhythmia. Circulation. 2004; 110: 2163–2167.
6. Ruan Y, Liu N, Priori SG. Sodium channel mutations and arrhythmias. Nat Rev Cardiol. 2009; 6: 337–348.
7. Remme CA, Wilde AA, Bezzina CR. Cardiac Sodium Channel Overlap Syndromes: Different Faces of SCN5A Mutations. Trends in Cardiovascular Medicine. 2008; 18: 78–87.
8. Liu M, Yang K-C, Dudley SC. Cardiac sodium channel mutations: why so many phenotypes. Nat Rev Cardiol. 2014; 11: 607–615.
9. Brugada P, Brugada J. Right bundle branch block, persistent ST segment elevation and sudden cardiac death. A distinct clinical and electrocardiographic syndrome. Journal of the American College of Cardiology. 1992; 20: 1391–1396.
10. Wilde AA. Proposed Diagnostic Criteria for the Brugada Syndrome. Consensus Report. Circulation. 2002; 106: 2514–2519.
11. Nielsen MW, Holst AG, Olesen S-P, Olesen MS. The genetic component of Brugada syndrome. Front Physiol. 2013; 4: 179.
12. Berne P, Brugada J. Brugada Syndrome 2012. Circ J. 2012; 76: 1563–1571.
13. Probst V, Wilde, Arthur A M, Barc J, Sacher F, Babuty D, Mabo P, et al. SCN5A mutations and the role of genetic background in the pathophysiology of Brugada syndrome. Circ Cardiovasc Genet. 2009; 2: 552–557.
14. Bezzina CR, Barc J, Mizusawa Y, Remme CA, Gourraud J-B, Simonet F, et al. Common variants at SCN5A-SCN10A and HEY2 are associated with Brugada syndrome, a rare disease with high risk of sudden cardiac death. Nat Genet. 2013; 45: 1044–1049.
15. Mizusawa Y, Wilde AAM. Brugada syndrome. Circ Arrhythm Electrophysiol. 2012; 5: 606–616.
16. Tester DJ, Valdivia C, Harris-Kerr C, Alders M, Salisbury BA, Wilde AA, et al. Epidemiologic, molecular, and functional evidence suggest A572D-SCN5A should not be considered an independent LQT3-susceptibility mutation. Heart Rhythm. 2010; 7: 912–919.
17. Shinlapawittayatorn K, Du XX, Liu H, Ficker E, Kaufman ES, Deschênes I. A common SCN5A polymorphism modulates the biophysical defects of SCN5A mutations. Heart Rhythm. 2011; 8: 455–462.
18. Kauferstein S, Kiehne N, Peigneur S, Tytgat J, Bratzke H. Cardiac channelopathy causing sudden death as revealed by molecular autopsy. International Journal of Legal Medicine. 2013; 127: 145–151.

19. Hoshi M, Du XX, Shinlapawittayatorn K, Liu H, Chai S, Wan X, et al. Brugada syndrome disease phenotype explained in apparently benign sodium channel mutations. Circ Cardiovasc Genet. 2014; 7: 123–131.
20. Bezzina CR, Shimizu W, Yang P, Koopmann TT, Tanck, Michael W T, Miyamoto Y, et al. Common sodium channel promoter haplotype in asian subjects underlies variability in cardiac conduction. Circulation. 2006; 113: 338–344.
21. Yang P, Koopmann TT, Pfeufer A, Jalilzadeh S, Schulze-Bahr E, Kääb S, Wilde AA, Roden DM and Bezzina CR. Polymorphisms in the cardiac sodium channel promoter displaying variant in vitro expression activity. Eur J Hum Genet. 2008; 16: 350–357.
22. Wang Q, Zhizhong L, Jiaxiang S and Keating MT. Genomic Organization of the Human SCN5A Gene Encoding the Cardiac Sodium Channel. Genomics. 1996; 34: 9–16.
23. Hoebeeck J, van der Luijt, Rob, Poppe B, Smet E de, Yigit N, Claes K, et al. Rapid detection of VHL exon deletions using real-time quantitative PCR. Lab Invest. 2004; 85: 24–33.
24. Schmittgen TD, Livak KJ. Analyzing real-time PCR data by the comparative CT method. Nat. Protocols. 2008; 3: 1101–1108.
25. Priori SG, Napolitano C, Gasparini M, Pappone C, Della Bella P, Brignole M, et al. Clinical and Genetic Heterogeneity of Right Bundle Branch Block and ST-Segment Elevation Syndrome. A Prospective Evaluation of 52 Families. Circulation. 2000; 102: 2509–2515.
26. Mohler PJ, Rivolta I, Napolitano C, LeMaillet G, Lambert S, Priori SG, et al. Nav1.5 E1053K mutation causing Brugada syndrome blocks binding to ankyrin-G and expression of Nav1.5 on the surface of cardiomyocytes. Proc Natl Acad Sci U S A. 2004; 101: 17533–17538.
27. Kapplinger JD, Tester DJ, Salisbury BA, Carr JL, Harris-Kerr C, Pollevick GD, et al. Spectrum and prevalence of mutations from the first 2,500 consecutive unrelated patients referred for the FAMILION® long QT syndrome genetic test. Heart Rhythm. 2009; 6: 1297–1303.
28. Daixing Zhou, Stephen Lambert, Peter L. Malen, Scott Carpenter, Linda M. Boland and Vann Bennett. Ankyrin G Is Required for Clustering of Voltage-gated Na Channels at Axon Initial Segments and for Normal Action Potential Firing. J Cell Biol. 1998; 143: 1295–1304.
29. Lowe JS, Palygin O, Bhasin N, Hund TJ, Boyden PA, Shibata E, et al. Voltage-gated Nav channel targeting in the heart requires an ankyrin-G dependent cellular pathway. J Cell Biol. 2008; 180: 173–186.
30. Abriel H. Roles and regulation of the cardiac sodium channel Na v 1.5: recent insights from experimental studies. Cardiovascular Research. 2007; 76: 381–389.
31. Yang P. Cloning and initial characterization of the human cardiac sodium channel (SCN5A) promoter. Cardiovascular Research. 2004; 61: 56–65.
32. Ji Kwon Park, MD, PhD, Lisa J. Martin, PhD, Xue Zhang, MsPH, PhD, Anil G. Jegga, DVM, MS, D. Woodrow Benson, MD, PhD. Genetic variants in SCN5A promoter are associated with arrhythmia phenotype severity in patients with heterozygous loss-of-function mutation. Heart Rhythm. 2012: 1090–1096.
33. Kapplinger JD, Tester DJ, Salisbury BA, Carr JL, Harris-Kerr C, Pollevick GD, et al. Spectrum and prevalence of mutations from the first 2,500 consecutive unrelated patients referred for the FAMILION long QT syndrome genetic test. Heart Rhythm. 2009; 6: 1297–1303.
34. Priori SG. Natural History of Brugada Syndrome. Insights for Risk Stratification and Management. Circulation. 2002; 105: 1342–1347.

35. Yang P, Koopmann TT, Pfeufer A, Jalilzadeh S, Schulze-Bahr E, Kääb S, et al. Polymorphisms in the cardiac sodium channel promoter displaying variant in vitro expression activity. Eur J Hum Genet. 2008; 16: 350–357.
36. van den Boogaard M, Wong LYE, Tessadori F, Bakker ML, Dreizehnter LK, Wakker V, et al. Genetic variation in T-box binding element functionally affects SCN5A/SCN10A enhancer. J. Clin. Invest. 2012; 122: 2519–2530.
37. Park JK, Martin LJ, Zhang X, Jegga AG, Benson DW. Genetic variants in SCN5A promoter are associated with arrhythmia phenotype severity in patients with heterozygous loss-of-function mutation. Heart Rhythm. 2012; 9: 1090–1096.
38. Yagihara N, Watanabe H, Barnett P, Duboscq-Bidot L, Thomas AC, Yang P, et al. Variants in the SCN5A Promoter Associated With Various Arrhythmia Phenotypes. J Am Heart Assoc. 2016; 5.

2.7. Appendix

2.7.1. *SCN5A* Primer Sequences

References Primer Sequences [22]

Exon	*Forward Primer (5' → 3')*	*Reverse Primer (5' → 3')*	*Amplicon length (bp)*
2	GGT CTG CCC ACC CTG CTC TCT	CCT CTT CCC CCT CTG CTC CAT T	325
3	AGT CCA AGG GCT CTG AGC CAA	GGT ACT CAG CAG GTA TTA ACT GCA A	119
4	GGT AGC ACT GGC CTG GCA GTG AT	CCT GGA CAC AAG CCC CCT TC	90
5	TCA CAC CAC GTA AGG AAC CTG	ATG TGG ACT GCA GGG AGG AAG C	129
6	CCT TTC CTC CTC TGA CTG TGT GT	GGT ATT CTG GTG ACA GGC ACA TTC	92
7	CCA CCT CTG GTT GCC TAC ACT G	GTC TGC TGG TCT CAC AAA GTC TTC	231
8	AGA GTG CCC CTC ACC AGC ATG	GGA GAC TCC CCT GGC AGG ACA A	64
9	GGG AGA CAA GTC CAG CCC AGC AA	AGC CCA CAC TTG CTG TCC CTT G	142
10	ACT TGG AAA TGC CAT AAC CCA GA	CAC CTA TAG GCA CCT ACA GTC AG	198
11	AAA CGT CCG TTC CTC CAC TCT	AAC CAC AGC TGG GAT TAC CAT T	180
12	GGC CAG TGG CAC AAA AGA CAG GCT	CCC TGG GCA CTG GTC CGG CGC A	181
	CAC CAC ACA TCA CTG CTG GTG C	GGC ACT GGT GAT CAG TTT GGG AGA	200
13	CCC TTT TCC CCA GGC TGA CGC AAA	GTC TAA AGC AGG CCA AGA CAA ATG	133
14	CTG GAA GGT ATT CCA GTT ACA TAT GA	ACC CAT GAA GGC TGT GCC AGC TGC	239
15	CTT TCC ATC CCA AAC AAT TCC T	CCC CAC CAT CCC CCA TGC AGT	174
16	GAG CCA GAG CCC TTC ACA AGG TCC CCT	CCC TTG GCC AAC TTA CCA CAA G	351
17	CTG GAT GGC TTG GCA TGG TGC AG	GGG TGG CGG GGA GTA GGG GGT G	224
	GCC CAG GGC CAG CTG CCC AGC T	CTG TAT ATG TAG GTG CCT TAT ACA TG	228
18	AGG GTC TGA AAC CCC CAG GGT CA	CCC AGC TGG CTT CAG GGA CAA A	162
19	GGC TCG AGG CCA AAG GCT GCT	G CTA GGG CAG AGG GCT GCC CGG	225
20	GGC ATT CAC AGG CCC TGA GGT GGG	CTT TCC AGC TGG AGA CCT CCT TTC C	155
21	TCC AGG CTT CAT GTC CAC CTT GTC T	TCT CCC GCA CCG GCA ATG GGT	174
22	GTC CCC AAC AGT GGG GAG CTG TTC	CCG CCT CCC ACT CCC TGG TGG	123
23	TTG AAA AGG GCA TGT GCT CTG GG	CAC ATC ATG GGT GAT GGC CAT	282
24	CTC AAG CGA GGT ACA GAA TTA AAT GA	GGG CTT TCA GAT GCA GAC ACT GAT	54
25	GCC TGT CTG ATC TCC CTG TGT GA	CCT GGA GCC TGA GTG GCC CCT C	138
26	CCA TGC TGG GGC CTC TGA GAA C	GGC TCT GAT GGC TGG CCA TGT G	105
27	CCC TGC TGA GCA CTT TCC ATT TG	GCT TCT CCG TCC AGC TGA CTT GTA	271
28	GCT GGC TGG AAG ACA GAG GTG C	GGT GAT CTG GAA GAG GCA CAG C	280

	AAG TGG GAG GCT GGC ATC GAC	GTG CTC TCC TCC GTG GCC ACG C	263
	GAG CCC AGC CGT GGG CAT CCT	GTC CCC ACT CAC CAT GGG CAG	268
	CCA ACC AGA TAA GCC TCA TCA ACA	CCG CCT GCT GAC GGA AGA GGA	264
	TGC TGC AAC GCT CTT TGA AGC AT	AAA GGC TGC TTT TCA GTG TGT CCT	300

2.7.2. Real-Time PCR Primer Sequences

Primer Sequences *SCN5A* upstream fragments and Reference Genes [23]

Position	*Forward Primer (5' → 3')*	*Reverse Primer (5' → 3')*	*Amplicon length (bp)*
***SCN5A* upstream *-1845 to -1610* (fragment I)**	AGCTTCATTCTGAGGCCGAG	GTACAGACGGATGGACCACA	237
***SCN5A* upstream *-1964 to -1853* (fragment II)**	AGTGAAAACCCCACTTCTGCTA	GCAAACTGACATTGGGTCAAGC	112
***SCN5A* upstream *-1606 to -1469* (fragment III)**	CAGACACCCCACTCAACTCG	GGGTGTGGGGCTTCGTTG	138
***GPR15* Reference Gene [23]**	GGTCCCTGGTGGCCTTAATT	TTGCTGGTAATGGGCACACA	101
***ZNF80* Reference Gene [23]**	CTGTGACCTGCAGCTCATCCT	TAAGTTCTCTGACGTTGACTGATGTG	120

3. CHAPTER 3 – GENETIC MODIFIERS AS RISK FACTORS FOR LONG QT SYNDROME AND SUDDEN CARDIAC DEATH

3.1. Abstract

Sequence variants in the ion channel genes *KCNH2* and *SCN5A* may cause the cardiac disorder long QT syndrome (LQTS) which is characterized by a prolonged QT interval on the electrocardiogram (ECG) and cardiac events such as syncopes and sudden cardiac death (SCD). This disorder is further associated with an incomplete penetrance and a variable expressivity among *KCNH2*- or *SCN5A*-mutation carriers. In recent years, it became clear that common genetic variants, if associated with a mutation, may modulate disease severity in LQTS.

In the *SCN5A* gene of a 17 years old female who died during sleep, the variants A572D and H558R were identified. It has been shown previously that sodium channels with both variants in *"cis"* position exhibit a LQTS-like dysfunction. DNA-haplotyping was performed and revealed that both variants reside on the same allele in case of the deceased female. Therefore, it can be assumed that *SCN5A*-A572D in association with the common variant H558R on the same allele might be responsible for the sudden cardiac death of the female.

In a female patient with a clinically diagnosed LQTS and a family history of sudden cardiac death, the mutation *KCNH2*-E876X was identified. Family members were carriers of the same mutation and the common variant *KCNH2*-K897T. This common variant is associated with QTc interval variability and is proposed to function as a genetic modifier of LQTS disease severity. Family members carrying both variants exhibited only a mild QTc prolongation in resting ECG and experienced a syncope only once in their lifetime. However, it can only be speculated whether the common *KCNH2* variant K897T modifies disease severity in the investigated family.

3.2. Introduction

The congenital long QT syndrome (LQTS) is an inherited cardiac disease with a prevalence of approximately 1/2000 [1]. This disorder is characterized by prolongation of the QT interval on the electrocardiogram (ECG) (Fig. 26B) due to delayed ventricular repolarization (Fig. 26B); it is further associated with syncopes and sudden cardiac death (SCD) as a result of torsades des pointes (TdP) ventricular tachycardia (VT) [2].

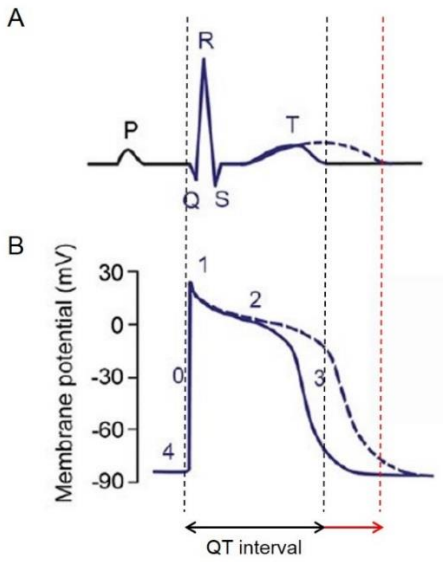

Fig. 26: The cardiac electrical activity.

(A) Prolongation of the QT interval on a surface electrocardiogram. (B) Corresponding prolongation of the action potential duration. Phase 0: depolarization, phase 1: fast repolarization, phase 2: plateau, phase 3: terminal repolarization, phase 4: resting (Modified from Amin et al. [3]).

Mutations in 15 different genes coding for ion channels and their accessory subunits have been linked to different types of LQTS [4]. Approximately 90% of genotype-positive cases carry a mutation in *KCNQ1* (42-54%, LQTS type 1, LQT1), *KCNH2* (35-45%, LQTS type 2, LQT2) or *SCN5A* (1.7-8%, LQTS type 3, LQT3) [5–7].

LQT2-linked loss-of-function mutations in the KCNH2-encoded hERG ($K_v11.1$) channel lead to a decrease in the rectifier K^+ current (I_{Kr}) [6,8]. LQT3 associated gain-of-function mutations in the *SCN5A* gene, which encodes the α-subunit of the cardiac sodium channel $Na_v1.5$, may affect the fast inactivation of the channel resulting in a late depolarizing Na^+ current (I_{Na}) [9]. Thus, LQT-associated mutations delay the repolarization of the ventricular action potential, either through a decrease of the repolarizing current (LQT2) or due to increasing the depolarizing current (LQT3).

In recent years, it became evident that carriership of a mutation in the LQTS-susceptibility genes often fails to predict the clinical phenotype, since some carriers remain asymptomatic (incomplete penetrance), some only show QTc prolongation without cardiac events, whereas others experience serious cardiac events at an early age (variable expressivity) [10]. It is known that LQTS is a disorder with many non-genetic factors, amongst which age and sex [11,12], modifying the clinical phenotype. Furthermore, it has become clear that common genetic variants (with a minor allele frequency (MAF) > 5%), if associated with a mutation, modulate the disease severity in LQTS [3]. These common variants, which may even influence the QTc duration in the general population, can be located in the same or in a different gene. Single nucleotide polymorphisms (SNPs) in the coding regions of LQTS-related genes such as *KCNH2* K897T [13–16] and *SCN5A* H558R [16] are known to influence the QT interval. In addition, SNPs in non-coding regions (introns, 3'UTR) of *KCNQ1* are also reported to modify QTc duration [3,17].

In the current study, we present familial, clinical and genetic evidence underlining the important issue, that common genetic variants may modify the expressivity of LQTS in mutation carriers and that this mechanism may aggravate or otherwise mitigate the risk of SCD.

3.3. Material and Methods

3.3.1. Clinical characteristics and genetic analysis

Case 1:

A 17 years old female died suddenly and unexpected during sleep. Since no pathological findings were obtained by medico-legal autopsy a genetic analysis was carried out. Genomic DNA was extracted from blood samples using standard phenol chloroform procedures. Targeted mutational analysis including the major LQTS, BrS and CPVT related genes *KCNQ1* (NG_008935), *KCNH2* (NG_008916), *SCN5A* (NG_008934), *KCNE1* (NG_009091), *KCNE2* (NG_008804), *KCNJ2* (NG_008798), *SCN4B* (NG_011710), *HCN4* (NG_009063) and 20 exons (3, 8, 14, 15, 44-47, 49, 83, 88, 90, 93, 96, 97, 100-103, 105) of *RyR2* (NG008799) as well as the major ARVC genes *PKP2* (NG_009000), *DSG2* (NG_007072), *DSC2* (NG_008208) and *DSP* (NG_008803) was performed using polymerase chain reaction (PCR) with published [18–20] and own primers (primer sequences upon request). After direct sequencing of the amplicons, the sequencing products were examined using a 3130xl Genetic Analyzer (Applied Biosystems, Germany). Analysis of the sequence data was done using the SeqScape v2.5 software (Applied Biosystems, Germany). As this analysis revealed a potentially pathogenic variant, the first-degree relatives were encouraged to seek genetic counselling. After providing informed consent of the father and the sister of the SCD victim, blood samples were collected and analysed as described above. The mother died due a non-cardiac cause.

Case 2:

A 30 years old female experienced seizures and a recurrent Torsade de pointes (TdP) tachycardia. Under hypoxic and QT-prolonging medication a LQTS (Romano-Ward-Syndrome) was unmasked. Genetic analysis revealed a heterozygous mutation E876X (c.2626G>T) in exon 12 of the *KCNH2* gene. The attending physician gave the advice for an implantable cardioverter defibrillator (ICD). Because of the autosomal dominant inheritance of the LQTS and given the fact that a 58 years old aunt of the index patient had died due to SCD, the first-degree relatives were recommended to seek genetic counselling and undergo cardiological assessment including resting and exercise ECG. Standard criteria for the diagnosis of LQTS [21,22] were used as described. The corrected QT interval (QTc) was calculated using Bazett's formula. According to the ESC guidelines [23] a clinical LQTS diagnosis is considered in patients with unexplained syncope and QTc ≥ 460 ms in repeated 12-lead ECGs. After obtaining informed consent of five family members, blood samples were collected and exclusively exon 12 of the *KCNH2* gene was analysed. The genetic analysis was performed as described in case 1.

3.3.2. H558R and A572D haplotyping (case 1)

The genetic analysis in case 1 revealed a double heterozygous carriership of the variants H558R and A572D in the *SCN5A* gene of the SCD victim. The common polymorphism H558R is known to be a modifying variant that can alter the phenotypic effects of other *SCN5A* variants. To determine if D572 existed on the same allele as H558 or R558 a polymerase chain reaction (PCR) of *SCN5A* exon 12 was performed using the forward (5'-GCCAGTGGCACAAAAGACAGGCT-3') and the reverse primer (5'-GGAACTGCTGATCAGTTTGGGAGA-3') as described by Tester et al. [24]. The amplification products were digested with the restriction enzyme Tsp45I (New England BioLabs, Frankfurt, Germany) which cleaves only the D572 allele (5'-GTSAC-3'). The digestion products were

separated on a 2% agarose gel; the 275 bp band was excised from the agarose gel, purified using the QIAquick Gel Extraction Kit (Qiagen, Hilden, Germany) and sequenced.

3.4. Results

3.4.1. Case 1: Analysis of the *SCN5A* gene

A targeted postmortem mutational analysis of the major LQTS, BrS, CPVT and ARVC related genes using PCR followed by direct sequencing revealed the heterozygous variant A572D (c.1715C>A, rs36210423) as well as the polymorphism H558R (c.1673A>G, rs1805124) in the *SCN5A* gene of the deceased female (Fig. 28A). The variant A572D has a minor allele frequency (MAF) of 0,37% in the European population (ExAC database) and is associated with a susceptibility to develop LQTS [24,25]. Both, variant and polymorphism, are localized to the DI-DII interdomain linker of $Na_v1.5$ [26] (Fig. 27A); this part of the $Na_v1.5$ channel is relatively non-conserved among different species (Fig. 27B).

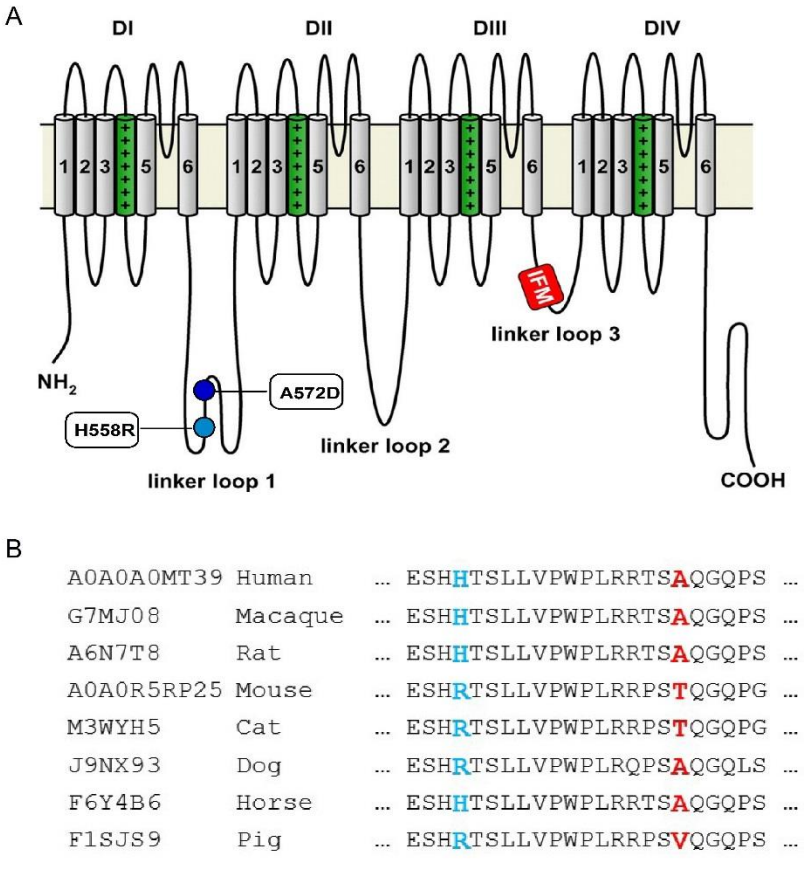

Fig. 27: Location of the *SCN5A* variants H558R and A572D.

(A) Schematic representation of a $Na_v1.5$ α-subunit. The polymorphism H558R and the variant A572D are located in the intracellular linker loop 1 of the cardiac sodium channel. DI-DIV are the four homologous domains of the α-subunit (modified from Abriel et al. [27]). (B) Alignment of a part of the *SCN5A* amino acid sequence from different species. The position H558 is highlighted in blue and the position A572 is indicated in red.

Tester et al. [24] demonstrated that the *SCN5A* variant D572 is invariably linked to the common polymorphism R558 meaning both variants residing on the same allele ("*cis*" position). To verify if R558 and D572 existed on the same allele in case of the deceased female, haplotyping as described by Tester et al. [24] was performed (Fig. 28). The A572D heterozygote sample yielded gel bands of 518 bp (representing the non-cleaved A572 allele), 275 bp (representing the 5'-end of the cleaved D572 allele) and 243 bp (representing the 3'-end of the cleaved D572 allele) (Fig 28B). Sequencing of the 275 bp fragment demonstrated that the variant D572 was in fact in "*cis*" position to the polymorphism R558 (Fig. 28C).

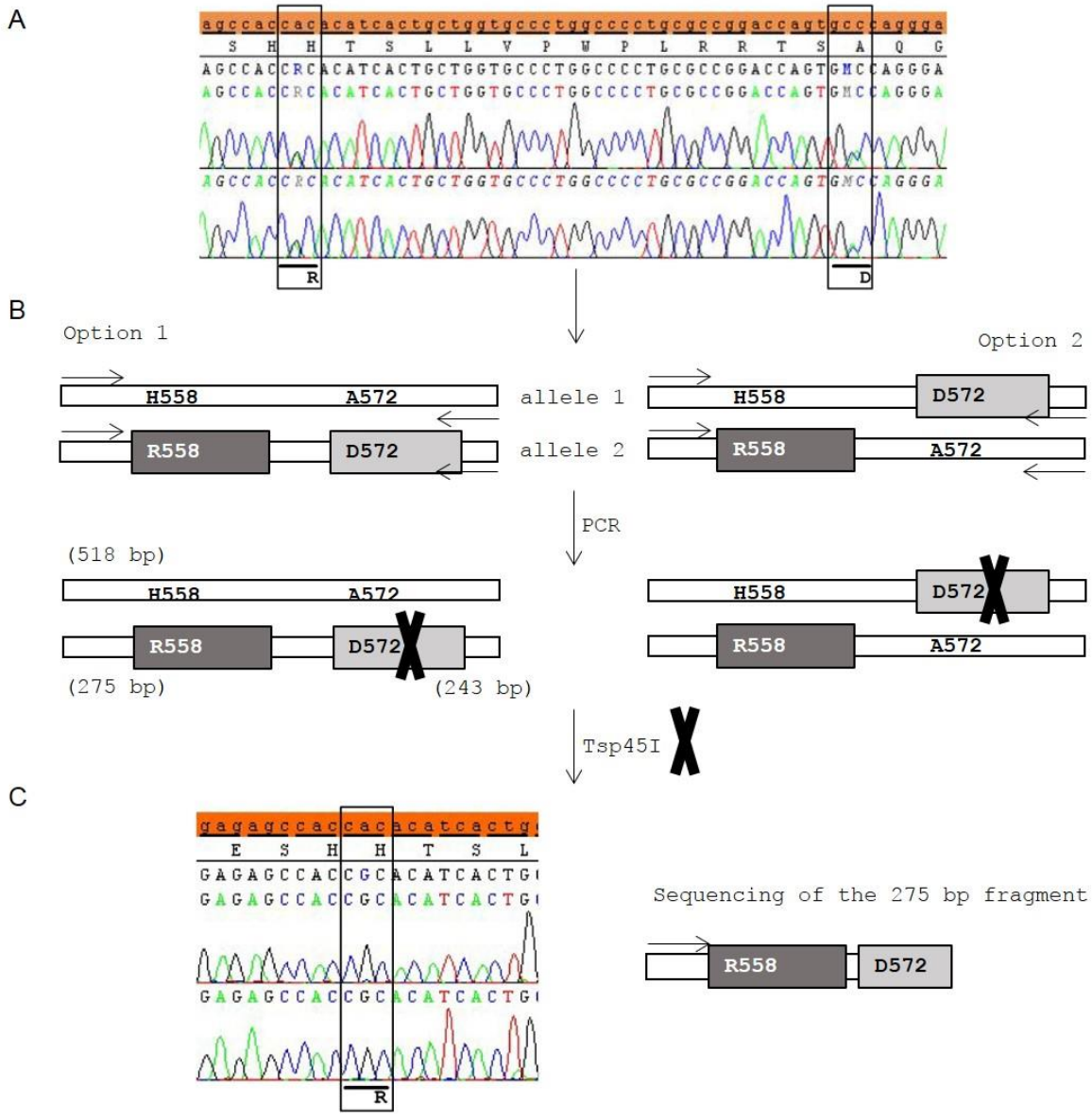

Fig. 28: H558R and A572D haplotyping.

(A) Sequence analysis of the *SCN5A* gene revealed two heterozygous nucleotide changes c.1673A>G (H558R) and c.1715C>A (A572D) in the SCD victim. Highlighted in orange is the *SCN5A* reference sequence. H = Histidine, R = Arginine, A = Alanine, D = Aspartic acid. (B) The two *SCN5A* sequence variants existed either on the same (option 1) or on different alleles (option 2). After PCR amplification, the products were digested with the restriction enzyme Tsp45I which cleaved only the D572 allele. Numbers in parentheses indicate the expected fragment size on an agarose gel. (C) Sequencing of the 275 bp fragment revealed that the polymorphism R558 was on the same allele as the variant D572.

In case of the father and the sister of the deceased female exclusively exon 12 of the *SCN5A* gene was analysed. Both carried neither the polymorphism H558R nor the variant A572D (Fig. 29). Hence, the sequence variants could be passed on by the mother of the SCD victim, who had already died due to non-cardiac causes, or arose *de novo*.

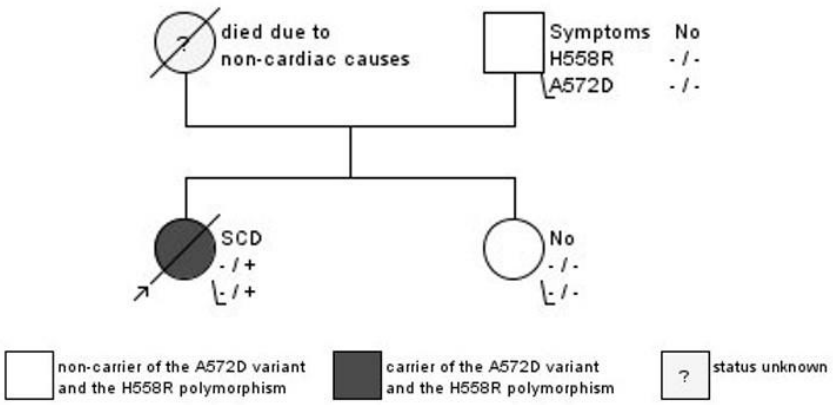

Fig. 29: Family pedigree of the deceased female, case 1.

Square symbols indicate males, round symbols females and slashed symbols mark deceased individuals. The arrow indicates the index patient. SCD = Sudden Cardiac Death.

3.4.2. Case 2: Clinical characteristics

The index patient (Fig. 31A, IV.1), a 30 years old female, experienced recurrent seizures and TdP arrhythmias. The clinical diagnosis of a LQTS was confirmed by an externally performed genetic analysis, which identified a heterozygous mutation E876X (c.2626G>T) in exon 12 of the *KCNH2* gene. Further evaluation of the family history revealed that one aunt (III.4) had died due to sudden cardiac death at the age of 58. The mother (III.1) and two uncles (III.2 and III.3) of the index patient experienced a syncope once in their lifetime. The QTc was marginally prolonged (III.1: 450 ms, III.2: 444 ms and III.3: 436 ms). Exercise ECG testing was performed and showed a QTc prolongation during the recovery phase in III.2 (549 ms) and III.3 (566 ms); the QTc in III.1 was shortened (300 ms). The sister (IV.2) of the index patient had no syncopal episode so far and the QTc was 430 ms. The cousin (IV.3) reported a history of 3-4 syncopes at a young age, but these were rather non-vasovagal. Resting and exercise ECG showed normal QTc intervals, 390 ms and 420 ms, respectively.

3.4.3. Case 2: *KCNH2* mutation analysis

The female index patient carried the very rare variant E876X in exon 12 of the *KCNH2* gene. The mutation, which was first identified in a large cohort of unrelated LQTS patients [28], creates a stop codon through a nucleotide change from guanine to thymine at position 2626 (**G**AG → **T**AG) in the sequence and leads to a deletion of 283 amino acids in the hERG protein (Fig.30). Genotyping of the mother (III.1) for the *KCNH2*-E876X mutation revealed a homozygous carriership of this mutation (Fig. 31B). However, the genetic results were not consistent with the cardiological findings of a moderate QTc prolongation. Therefore, a point mutation in the primer binding site of the wildtype allele was considered. Amplification of *KCNH2* exon 12 with an alternative forward (5'-GGGCAAAATCACATTGGGGG-3') and reverse (5'-AGGTCTGAGGCCTGGGTAAA-3') primer identified the heterozygous state of the

E876X mutation (Fig. 31C). Additionally, the new primer pair detected a heterozygous nucleotide change (A**A**G → A**C**G) at position 2690 leading to the substitution of lysine at the residue 897 to threonine in the resulting protein (Fig. 31C). The polymorphism K897T is classified as a common variant (MAF ~24% in the European population, ExAC database) that is proposed as a genetic modifier in LQTS [3].

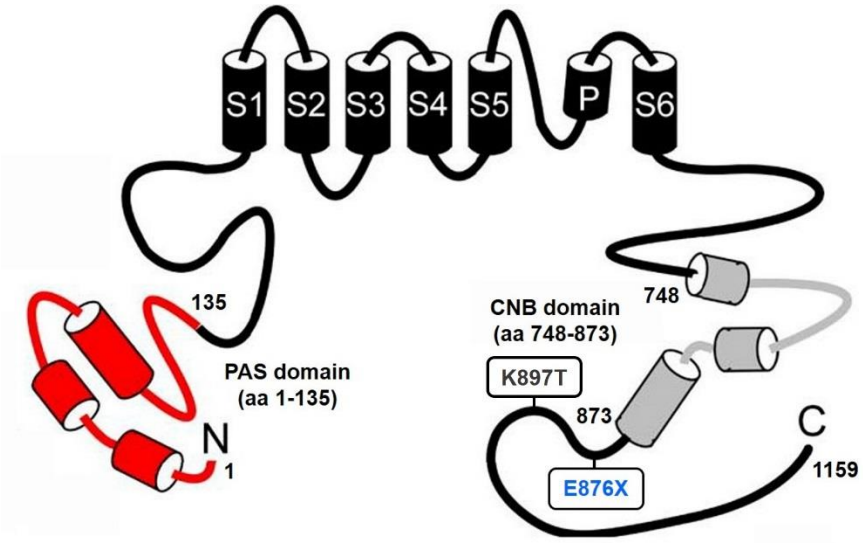

Fig. 30: Topology of the hERG channel and location of the E876X mutation and the K897T polymorphism.

Schematic topology of the hERG channel illustrating the relative positioning of channel regions and domains. The mutation is located at the distal C-terminus of the channel and leads to a deletion of 283 amino acids. PAS = Per-Arnt-Sim domain, S1-S6 = Transmembrane helices, P = Pore helix, CNB = Cyclic-nucleotide-binding homology domain, aa = amino acids, E = Glutamic acid, X = Stop (modified from Gustina et al. [29]).

3.4.4. Case 2: Segregation of the *KCNH2* variants

By family screening *KCNH2*-E876X and -K897T were detected in two uncles (III.2 and III.3) of the index patient. The sister (IV.2) and cousin (IV.3) were genotyped for the K897T polymorphism. Analysis of the family pedigree as well as of the sequence data indicated that the mutation E876X and the polymorphism K897T exist on separate *KCNH2* alleles. No material for a genetic analysis of the deceased aunt (III.4) exist.

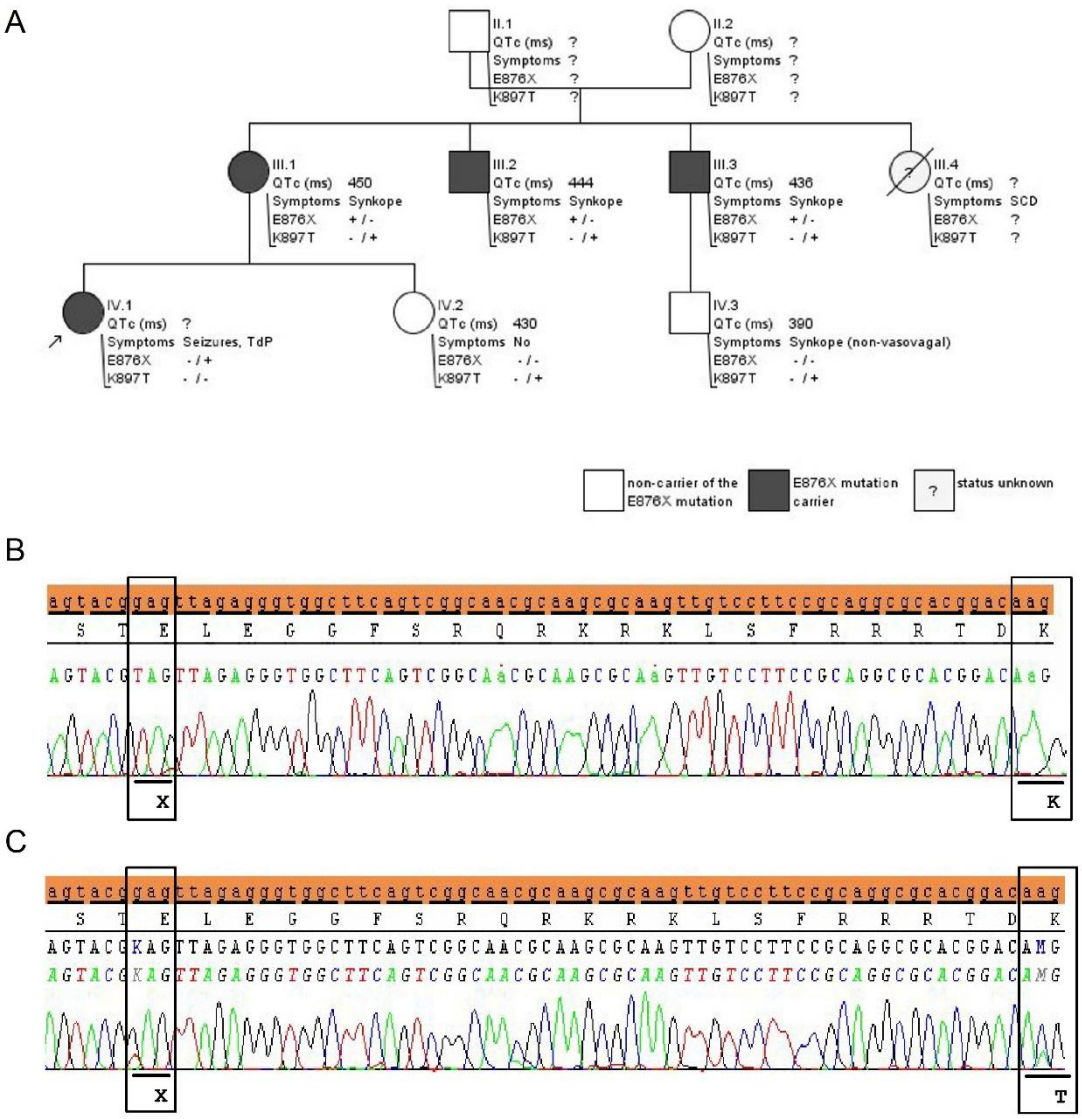

Fig. 31: Identification of the *KCNH2* E876X mutation and the K897T polymorphism, case 2.

(A) Pedigree structure of the affected family. Square symbols indicate males, round symbols females and slashed symbols mark deceased individuals. The Roman numerals indicate the generation number, Arabic numerals each individual in a given generation. The arrow indicates the index patient. SCD = Sudden Cardiac Death. (B) DNA analysis of the mother (III.1) with the generally used primers revealed a homozygous G → T transition at position 2626 of *KCNH2*. The A → C change at nucleotide position 2690 was not detected. (C) Amplification with an alternative primer pair and subsequent sequence analysis identified both heterozygous nucleotide changes leading to the amino acid substitutions E876X and K897T in the resulting protein. E = glutamic acid, X = stop, K = lysine, T = threonine.

3.5. Discussion

In the present study, we describe the identification of a rare variant together with a common variant in a case of sudden cardiac death and in a LQTS-affected family with a history of sudden cardiac death. The findings provide evidence that common variants may modulate disease severity of LQTS and possibly enhance or weaken the risk for sudden cardiac death.

In case of the 17-year-old female who died suddenly during sleep (case 1), two heterozygous variants, A572D and H558R, were identified in the *SCN5A* gene. Medico-legal autopsy, including toxicological and histological investigations, revealed no pathological findings. Genetic screening of the father and the sister of the deceased revealed that they were non-carriers of both variants. The mother of the SCD victim had already died due to non-cardiac causes. The *SCN5A* variant A572D is classified as a rare variant with a MAF of 0.37% in the European population (ExAC database) and is furthermore associated with the susceptibility to develop LQTS [24,25,28]. The common *SCN5A* variant H558R, with a MAF of ~23% in the European population (ExAc database), has been shown previously to modify the phenotype of other *SCN5A* variants [30,31] and is known to influence the QT interval [16].

In a recent study Ortiz-Bonnin et al. [25] identified the *SCN5A*-A572D variant in a patient with an unclear cardiological phenotype and functionally characterized the variant in *Xenopus laevis* oocytes. They showed that oocytes expressing the A572D variant exhibited a significant gain-of-function phenotype (slower inactivation, faster recovery from inactivation) which might have the ability to prolong the cardiac action potential. However, based on the discordance between the clinical and the *in vitro* phenotype they classified *SCN5A*-A572D as a variant of unknown significance. Furthermore, they hypothesized that this variant may be influenced by other factors modifying the clinical phenotype. Tester et al. [24] performed functional studies of *SCN5A*-A572D in the context of the common *SCN5A* variant H558R in HEK293 cells. They observed that HEK293 cells expressing D572/R558-containing sodium channels (both variants in *"cis"* position) exhibited a LQT3-like dysfunction. In contrast to the study of Ortiz-Bonnin et al. [25] no gating kinetic or current density differences compared with wild-type channels were detected in cells expressing the *SCN5A* variant D572 alone or in the setting of H558 (D572/H558).

Considering these results, it can be concluded that *SCN5A*-A572D in association with the common variant H558R on the same allele could cause LQT3 and might be responsible for the sudden cardiac death of the 17 years old female. It cannot be ruled out that other genetic or non-genetic factors might have influenced disease severity.

In the second case the index patient was a 30-year-old female with a clinically diagnosed LQTS and a family history of sudden cardiac death. Genetic analysis identified a heterozygous mutation E876X in the *KCNH2* gene. Genetic screening of the family members of the index patient revealed heterozygous carriership of this mutation in the mother and in two uncles. Additionally, they were genotyped for the heterozygous *KCNH2* polymorphism K897T. The sister and cousin of the index patient were carriers of the *KCNH2*-K897T polymorphism but not of the mutation. Evaluation of the family history revealed the sudden cardiac death of a 58-year-old aunt of the index patient; regrettably, no medico-legal autopsy or genetic testing was performed.

The *KCNH2*-E876X mutation was first identified in a large study cohort of LQTS patients [28] and leads to a C-terminal truncation of the hERG channel. Functional studies of this *KCNH2* variant are not available, but Teng et al. [32] performed a clinical and electrophysiological characterization of a comparable *KCNH2* mutation R863X, which also causes a deletion of the distal C-terminus of the hERG protein. They demonstrated that *KCNH2*-R863X failed to form functional hERG channels contributing to a prolongation of the QT interval [32]. On the basis

of these results, the same effect could be assumed for the *KCNH2* mutation E876X identified in the affected family.

The common variant *KCNH2*-K897T (MAF ~24% in the European population, ExAc database) is associated with QTc interval variability in the general population [13,14,16,33–35] and is proposed to serve as a genetic modifier of LQTS disease severity [15,36]. However, there is an apparent inconsistency among the different studies. Considering genome-wide association studies (GWAS), in Western European [13,14,16] and North American [33] study cohorts *KCNH2*-K897T shortened the QTc interval, whereas in Finnish cohorts [34,35] the QTc interval was prolonged; thus, the discordant findings may be population-specific. Crotti et al. [15] studied a LQTS family with the *KCNH2*-A1116V mutation and demonstrated that disease was only manifested in individuals who co-inherited the minor T allele of the K897T variant on the non-mutant *KCNH2* allele (variants in *"trans"* position); family members with *KCNH2*-A1116V alone were asymptomatic with a mild QTc prolongation. Controversially, Zhang et al. [36] showed in a LQTS family that two variants in *KCNH2*, the mutation A490T and the common variant K897T, interact with each other in *"cis"* orientation (minor T allele of K897T on the mutant *KCNH2* allele). They concluded this *"cis"* orientation of both variants leads to a shortened QT interval and less severe symptoms and therefore to a reduced risk of LQTS.

Whether the common *KCNH2* variant K897T modifies disease severity in the investigated family can only be speculated. All three *KCNH2*-E876X mutation carriers with the minor T allele of K897T in *"trans"* position exhibited only a mild QTc prolongation in resting ECG and experienced a syncope only once in their lifetime. By contrast, the index patient carrying the *KCNH2*-E876X mutation alone experienced seizures and a recurrent Torsade de pointes (TdP) tachycardia; unfortunately, a QTc was not available. Therefore, it can be hypothesized that the minor T allele of the common variant *KCNH2*-K897T could play a protective role on QTc prolongation. However, there are some limitations for this hypothesis. The studied family was very small and the presence of additional QTc-modifying variants in other ion channel genes cannot be excluded. Furthermore, studying the functional effect of the mutation in combination with the common variant on the electrophysiological behaviour of the hERG channel may provide insights into the mechanism of QTc prolongation or shortening.

In summary, the results underline the important issue that additional genetic modifications, like common genetic variants in the same gene, may influence the expressivity of LQTS in *KCNH2*- and *SCN5A*-mutation carriers and this could be an important aspect for risk stratification. Nevertheless, further studies concerning the functional consequences of polymorphism/mutation interactions are needed.

3.6. References

1. Schwartz PJ, Stramba-Badiale M, Crotti L, Pedrazzini M, Besana A, Bosi G, et al. Prevalence of the congenital long-QT syndrome. Circulation. 2009; 120: 1761–1767.
2. Schwartz PJ, Moss AJ, Vincent GM, Crampton RS. Diagnostic criteria for the long QT syndrome. An update. Circulation. 1993; 88: 782–784.
3. Amin AS, Pinto YM, Wilde AAM. Long QT syndrome: beyond the causal mutation. J Physiol (Lond). 2013; 591: 4125–4139.
4. Mizusawa Y, Horie M, Am Wilde A. Genetic and Clinical Advances in Congenital Long QT Syndrome. Circ J. 2014; 78: 2827–2833.
5. Splawski I, Shen J, Timothy KW, Vincent GM, Lehmann MH, Keating MT. Genomic structure of three long QT syndrome genes: KVLQT1, HERG, and KCNE1. Genomics. 1998; 51: 86–97.
6. Curran ME, Splawski I, Timothy KW, Vincen G, Green ED, Keating MT. A molecular basis for cardiac arrhythmia. HERG mutations cause long QT syndrome. Cell. 1995; 80: 795–803.
7. Wang Q, Zhizhong L, Jiaxiang S and Keating MT. Genomic Organization of the Human SCN5A Gene Encoding the Cardiac Sodium Channel. Genomics. 1996; 34: 9–16.
8. Sanguinetti MC, Jiang C, Curran ME, Keating MT. A mechanistic link between an inherited and an acquired cardiac arrhythmia. HERG encodes the IKr potassium channel. Cell. 1995; 81: 299–307.
9. Wang Q, Shen J, Splawski I, Atkinson D, Li Z, Robinson JL, et al. SCN5A mutations associated with an inherited cardiac arrhythmia, long QT syndrome. Cell. 1995; 80: 805–811.
10. Giudicessi JR, Ackerman MJ. Determinants of incomplete penetrance and variable expressivity in heritable cardiac arrhythmia syndromes. Transl Res. 2013; 161: 1–14.
11. Locati EH, Zareba W, Moss AJ, Schwartz PJ, Vincent GM, Lehmann MH, et al. Age- and Sex-Related Differences in Clinical Manifestations in Patients With Congenital Long-QT Syndrome. Findings From the International LQTS Registry. Circulation. 1998; 97: 2237–2244.
12. Sakaguchi T, Shimizu W, Itoh H, Noda T, Miyamoto Y, Nagaoka I, et al. Age- and genotype-specific triggers for life-threatening arrhythmia in the genotyped long QT syndrome. J Cardiovasc Electrophysiol. 2008; 19: 794–799.
13. Bezzina C. A common polymorphism in KCNH2 (HERG) hastens cardiac repolarization. Cardiovascular Research. 2003; 59: 27–36.
14. Pfeufer A. Common Variants in Myocardial Ion Channel Genes Modify the QT Interval in the General Population: Results From the KORA Study. Circulation Research. 2005; 96: 693–701.
15. Crotti L, Lundquist AL, Insolia R, Pedrazzini M, Ferrandi C, Ferrari GM de, et al. KCNH2-K897T is a genetic modifier of latent congenital long-QT syndrome. Circulation. 2005; 112: 1251–1258.
16. Gouas L, Nicaud V, Berthet M, Forhan A, Tiret L, Balkau B, et al. Association of KCNQ1, KCNE1, KCNH2 and SCN5A polymorphisms with QTc interval length in a healthy population. Eur J Hum Genet. 2005; 13: 1213–1222.
17. Amin AS, Giudicessi JR, Tijsen AJ, Spanjaart AM, Reckman YJ, Klemens CA, et al. Variants in the 3' untranslated region of the KCNQ1-encoded Kv7.1 potassium channel modify disease severity in patients with type 1 long QT syndrome in an allele-specific manner. European Heart Journal. 2012; 33: 714–723.

18. Splawski I, Shen J, Timothy KW, Lehmann MH, Priori S, Robinson JL, et al. Spectrum of Mutations in Long-QT Syndrome Genes. KVLQT1, HERG, SCN5A, KCNE1, and KCNE2. Circulation. 2000; 102: 1178–1185.
19. Tiso N, Stephan DA, Nava A, Bagattin A, Devaney JM, Stanchi F, Larderet G, Brahmbhatt B, Brown K, Bauce B, Muriago M, Basso C, Thiene G, Danieli GA, Rampazzo A. Identification of mutations in the cardiac ryanodine receptor gene in families affected with arrhythmogenic right ventricular cardiomyopathy type 2 (ARVD2). Human Molecular Genetics. 2001; 10: 189–194.
20. Lu C-W, Lin J-H, Rajawat YS, Jerng H, Rami TG, Sanchez X, et al. Functional and clinical characterization of a mutation in KCNJ2 associated with Andersen-Tawil syndrome. J Med Genet. 2006; 43: 653–659.
21. Schwartz PJ, Moss AJ, Vincent GM, Crampton RS. Diagnostic criteria for the long QT syndrome. An update. Circulation. 1993; 88: 782–784.
22. Sy RW, van der Werf C, Chattha IS, Chockalingam P, Adler A, Healey JS, et al. Derivation and validation of a simple exercise-based algorithm for prediction of genetic testing in relatives of LQTS probands. Circulation. 2011; 124: 2187–2194.
23. Priori SG, Blomstrom-Lundqvist C, Mazzanti A, Blom N, Borggrefe M, Camm J, et al. 2015 ESC Guidelines for the management of patients with ventricular arrhythmias and the prevention of sudden cardiac death: The Task Force for the Management of Patients with Ventricular Arrhythmias and the Prevention of Sudden Cardiac Death of the European Society of Cardiology (ESC). Endorsed by: Association for European Paediatric and Congenital Cardiology (AEPC). European Heart Journal. 2015; 36: 2793–2867.
24. Tester DJ, Valdivia C, Harris-Kerr C, Alders M, Salisbury BA, Wilde AA, et al. Epidemiologic, molecular, and functional evidence suggest A572D-SCN5A should not be considered an independent LQT3-susceptibility mutation. Heart Rhythm. 2010; 7: 912–919.
25. Ortiz-Bonnin B, Rinne S, Moss R, Streit AK, Scharf M, Richter K, et al. Electrophysiological characterization of a large set of novel variants in the SCN5A-gene: identification of novel LQTS3 and BrS mutations. Pflugers Arch. 2016; 468: 1375–1387.
26. Paulussen A, Matthijs G, Gewillig M, Verhasselt P, Cohen N, Aerssens J. Mutation analysis in congenital Long QT Syndrome--a case with missense mutations in KCNQ1 and SCN5A. Genet Test. 2003; 7: 57–61.
27. Abriel H. Roles and regulation of the cardiac sodium channel Na v 1.5: recent insights from experimental studies. Cardiovascular Research. 2007; 76: 381–389.
28. Tester DJ, Will ML, Haglund CM, Ackerman MJ. Compendium of cardiac channel mutations in 541 consecutive unrelated patients referred for long QT syndrome genetic testing. Heart Rhythm. 2005; 2: 507–517.
29. Gustina AS, Trudeau MC. hERG potassium channel gating is mediated by N- and C-terminal region interactions. The Journal of General Physiology. 2011; 137: 315–325.
30. Shinlapawittayatorn K, Du XX, Liu H, Ficker E, Kaufman ES, Deschênes I. A common SCN5A polymorphism modulates the biophysical defects of SCN5A mutations. Heart Rhythm. 2011; 8: 455–462.
31. Kauferstein S, Kiehne N, Peigneur S, Tytgat J, Bratzke H. Cardiac channelopathy causing sudden death as revealed by molecular autopsy. International Journal of Legal Medicine. 2013; 127: 145–151.
32. Teng S, Ma L, Dong Y, Lin C, Ye J, Bahring R, et al. Clinical and electrophysiological characterization of a novel mutation R863X in HERG C-terminus associated with long QT syndrome. J Mol Med (Berl). 2004; 82: 189–196.

33. Newton-Cheh C, Guo C-Y, Larson MG, Musone SL, Surti A, Camargo AL, et al. Common genetic variation in KCNH2 is associated with QT interval duration: the Framingham Heart Study. Circulation. 2007; 116: 1128–1136.
34. Pietila E, Fodstad H, Niskasaari E, Laitinen P PJ, Swan H, Savolainen M, et al. Association between HERG K897T polymorphism and QT interval in middle-aged Finnish women. Journal of the American College of Cardiology. 2002; 40: 511–514.
35. Koskela J, Laiho J, KaHonen M, Rontu R, Lehtinen R, Viik J, et al. Potassium channel KCNH2 K897T polymorphism and cardiac repolarization during exercise test: The Finnish Cardiovascular Study. Scand J Clin Lab Invest. 2008; 68: 31–38.
36. Zhang X, Chen S, Zhang L, Liu M, Redfearn S, Bryant RM, et al. Protective effect of KCNH2 single nucleotide polymorphism K897T in LQTS families and identification of novel KCNQ1 and KCNH2 mutations. BMC Med Genet. 2008; 9: 87.

4. SUMMARY

Sudden death (SD) is defined as a natural and unexpected event in apparently healthy persons that occurs within the first hour after onset of symptoms. Nearly 85% of all sudden deaths are of cardiac origin, called sudden cardiac death (SCD). In individuals > 55 years old about 80% of SCD cases are a consequence of a coronary heart disease whereas in the young adult population (< 40 years old) SCD is often caused by a primary arrhythmia syndrome in a structurally normal heart. Among these syndromes are the two main ion channel diseases: long QT syndrome (LQTS) and Brugada syndrome (BrS). Since these diseases are of genetic origin, relatives of SCD victims or clinically affected patients may be at risk, despite being asymptomatic. Furthermore, within affected families variable expressivity and incomplete penetrance of the clinical phenotype are frequent.

The present thesis describes the identification and characterization of sequence variants in the cardiac ion channel genes *KCNH2* and *SCN5A.* The variants were found in sudden cardiac death victims, in patients with ion channel diseases and in their family members. The results support the growing awareness that carriership of a single mutation often fails to predict the clinical phenotype and that additional genetic modifications may influence the clinical manifestation of the disease.

Sequence variants in the *KCNH2* gene, which encodes the α-subunit of the voltage-gated potassium channel hERG, may cause a prolonged repolarization of the cardiac action potential (prolonged QT interval on the ECG) either through disruption of channel gating or reduction of intracellular trafficking to the plasma membrane.

In a LQTS patient the mutation L69P in the PAS domain of the hERG channel was identified. Electrophysiological studies in HEK293 cells expressing the hERG-L69P mutant channel unveiled a reduced channel function compared to cells expressing the WT channel. Additionally, the cellular distribution of EGFP-tagged hERG-WT and hERG-L69P mutant channels in HEK293 cells was monitored by CLSM. The GFP fluorescence in hERG-L69P expressing cells was stronger in intracellular compartments than in the plasma membrane. Furthermore, a comparative quantification of isolated plasma membrane patches showed that the relative fluorescence intensity of the hERG-L69P mutant was about 50% reduced compared to that of hERG-WT. These results indicate that the mutation L69P causes both functional and trafficking defects of the hERG channel. Incubation of hERG-L69P mutant expressing HEK293 cells at 27°C, which should promote protein folding, did not improve channel trafficking. Three additional channel variants (L69A, L69D and L69G) exhibited larger currents than the hERG-L69P mutant but with different deactivation kinetics compared to the WT channel. In summary, these data suggest that an amino acid exchange at position 69 in the PAS domain of the hERG protein has a negative effect on channel kinetics as well as on channel trafficking, which supports the clinical diagnosis of a LQTS.

In a female patient with a clinically diagnosed LQTS the mutation *KCNH2*-E876X was identified. The index patient experienced seizures and a recurrent Torsade de pointes (TdP) tachycardia. Three family members carried the common variant *KCNH2*-K897T in addition to the *KCNH2*-E876X mutation; they exhibited only a mild QTc prolongation in resting ECG and experienced a syncope only once in their lifetime. The effect of *KCNH2*-K897T on the QTc interval is controversially discussed. Additionally, this variant is proposed to function as a genetic modifier of LQTS disease severity. In case of the studied family it can be hypothesized that the common *KCNH2* variant K897T modulates disease severity, but this remains to be elucidated.

The *SCN5A* gene encodes the α-subunit of the cardiac sodium channel $Na_v1.5$. Mutations in the *SCN5A* gene cause a change in the cardiac action potential either through an increase (gain-of-function mutations, LQTS) or a decrease of the depolarizing sodium current (loss-of-function mutations, BrS).

In a case of SCD of a 16-year-old female genetic analysis identified a heterozygous *SCN5A* variant E1053K, which was previously associated with BrS as well as with LQTS. Genetic screening of the family members revealed a heterozygous carriership of the variant in her mother and in her cousin of second degree; the aunt of the deceased was a homozygous carrier of the *SCN5A*-E1053K variant. Surprisingly, neither a heterozygous nor the homozygous carrier of the variant exhibited any pathological cardiac phenotype assuming additional genetic factors in the *SCN5A* gene of the SCD victim. MLPA analysis identified a heterozygous deletion in the promotor region of *SCN5A* of the deceased but not in other family members. To further localize the deletion in the 5' upstream region of the *SCN5A* gene, a RT-qPCR was performed, which confirmed the deletion in a region extending from position -1845 to -1610 upstream of the major transcription initiation site. It is hypothesized that variants in the promoter region may affect transcriptional activity of the *SCN5A* gene and thereby modulate the susceptibility to arrhythmia syndromes. In conclusion, the results suggest that *SCN5A*-E1053K is not an independent pathogenic variant but in association with additional genetic modifications might contribute to an increased risk for SCD.

In a second SCD case two heterozygous variants, A572D and H558R, were identified in the *SCN5A* gene of a 17 years old female. *SCN5A*-A572D was previously associated with a susceptibility to develop LQTS but rather in combination with other genetic modifications. In a previous study, it was shown *SCN5A*-A572D in association with the common variant H558R on the same allele (*"cis"* position) cause a LQTS-like dysfunction in HEK293 cells. To verify if both variants were located on the same allele in case of the deceased female, DNA haplotyping was performed. This analysis revealed that A572D and H558R were in fact in *"cis"* position on the *SCN5A* gene. It can be concluded that D572 in the setting of R558 on the same allele might be responsible for the sudden cardiac death of the young female.

5. ZUSAMMENFASSUNG

Der plötzliche Tod ist definiert als ein natürliches und unerwartetes Ereignis bei zuvor gesund erscheinenden Personen, welches innerhalb der ersten Stunde nach Beginn der Symptome auftritt. Fast 85% aller plötzlichen Todesfälle sind kardialen Ursprungs; daher wird vom plötzlichen Herztod gesprochen („sudden cardiac death“, SCD). Bei älteren Personen (> 55 Jahre) sind etwa 80% der SCD-Fälle eine Folge einer koronaren Herzerkrankung, während bei jüngeren Menschen (<40 Jahre) häufig ein primäres Arrhythmiesyndrom bei strukturell unauffälligem Herzen vorliegt. Zu diesen Arrhythmiesyndromen gehören die beiden wichtigsten Ionenkanalerkrankungen: das Long QT-Syndrom (LQTS) und das Brugada-Syndrom (BrS). Da diese Erkrankungen häufig eine genetische Ursache haben, können Angehörige von SCD-Opfern oder von klinisch auffälligen Personen, obwohl sie asymptomatisch sind, gefährdet sein. Darüber hinaus beobachtet man innerhalb der betroffenen Familien häufig eine unvollständige Penetranz und eine variable Expressivität des klinischen Phänotyps.

Die vorliegende Arbeit beschreibt die Identifizierung und Charakterisierung von Sequenzvarianten in den kardialen Ionenkanalgenen *KCNH2* und *SCN5A*. Die Identifizierung von Sequenzvarianten erfolgte bei am plötzlichen Herztod verstorbenen Personen, bei Patienten mit Ionenkanalerkrankungen und deren Familienangehörigen. Die Ergebnisse legen nahe, dass eine genetische Variante nicht immer einen klinischen Phänotyp hervorrufen muss und zusätzlich genetische Modifikationen vorliegen können, welche die klinische Ausprägung einer Erkrankung beeinflussen.

Sequenzvarianten im *KCNH2* Gen, das für die α-Untereinheit des spannungsabhängigen Kaliumkanals hERG kodiert, können zu einer Verlängerung des kardialen Aktionspotentials (verlängertes QT-Intervall im EKG) führen; der Grund hierfür kann entweder in einer funktionellen Störung des Kanals liegen oder die Folge eines verminderten intrazellulären Transports des Kanals zur Plasmamembran sein.

In einem LQTS-Patienten wurde in der PAS-Domäne des hERG Kanals die Mutation L69P detektiert. Elektrophysiologische Studien an HEK293 Zellen zeigten, dass Zellen, welche die hERG-L69P Mutante exprimierten, im Vergleich zu Zellen, die den hERG-WT exprimierten, eine reduzierte Kanalleitfähigkeit besitzen. Zusätzlich wurde mittels CLSM die zelluläre Verteilung von GFP-markierten hERG-WT und hERG-L69P Kanälen in HEK293 Zellen untersucht. Bei der hERG-L69P Mutante war die Fluoreszenzintensität in den intrazellulären Kompartimenten stärker als in der Plasmamembran. Darüber hinaus wurde die Fluoreszenzintensität von isolierten Plasmamembran-Fragmenten quantifiziert und verglichen; dies zeigte, dass die Fluoreszenzintensität der hERG-L69P Mutante im Vergleich zum hERG-WT um etwa 50% reduziert war. Diese Ergebnisse deuten darauf hin, dass die L69P Mutation sowohl eine funktionelle Störung des hERG Kanals verursacht, als auch dessen Transport zur Plasmamembran beeinflusst. Die Verwendung einer erniedrigten Inkubationstemperatur von 27°C, was die Proteinfaltung begünstigen sollte, führte nicht zu einem gesteigerten Transport des hERG-L69P Kanals zur Plasmamembran. Bei den zusätzlichen hERG Varianten (L69A, L69D und L69G) konnten im Vergleich zur hERG-L69P Mutante größere Ströme gemessen werden, allerdings mit einer veränderten Deaktivierungskinetik verglichen mit dem hERG-WT. Zusammenfassend lässt sich feststellen, dass ein Aminosäureaustausch an Position 69 in der PAS-Domäne des hERG Proteins sowohl die Kinetik als auch den Transport des hERG Kanals beeinflusst, was sich mit der klinischen Diagnose eines LQTS vereinbaren lässt.

Bei einer Patientin mit einem klinisch diagnostizierten LQTS wurde im *KCNH2* Gen die Mutation E876X identifiziert. Die Indexpatientin litt unter Krampfanfällen und einer wiederkehrenden Torsade de pointes (TdP) Tachykardie. Bei drei Familienangehörigen wurde

zusätzlich zur Mutation die häufige *KCNH2* Variante K897T detektiert; die QTc-Zeit im Ruhe-EKG war nur grenzwertig verlängert und bei allen kam es nur einmal im Leben zu einer Synkope. Der Einfluss der Variante *KCNH2*-K897T auf das QTc-Intervall wird kontrovers diskutiert. Es wird zudem vermutet, dass diese häufige genetische Variante die Schwere einer LQTS-Erkrankung modifiziert. Dieser Mechanismus wird auch im Falle der untersuchten Familie angenommen, dies bedarf aber noch weiterer Abklärung.

Das *SCN5A* Gen codiert für die α-Untereinheit des kardialen Natriumkanals Nav1.5. Mutationen im *SCN5A* Gen führen entweder zu einer Zunahme (Funktionsgewinn-Mutation, LQTS) oder zu einer Abnahme (Funktionsverlust-Mutation, BrS) des depolarisierenden Natriumstromes und bewirken dadurch eine Veränderung des kardialen Aktionspotentials.

Im Fall des plötzlichen Herztodes eines 16-jährigen Mädchens wurde im *SCN5A* Gen die heterozygote Variante E1053K detektiert, die zuvor schon mit dem BrS als auch mit dem LQTS assoziiert war. Eine genetische Untersuchung der Familienangehörigen zeigte, dass die Mutter der Verstorbenen und ein Cousin zweiten Grades heterozygote Träger der Variante sind; bei einer Tante der Verstorbenen konnte die *SCN5A* Variante E1053K in homozygoter Form nachgewiesen werden. Überraschenderweise zeigten weder ein heterozygoter Träger noch die homozygote Trägerin der Variante bei einer kardiologischen Untersuchung einen pathologischen Phänotyp; es wurde daher vermutet, dass bei der Verstorbenen zusätzliche genetische Modifikationen vorliegen. Mittels einer MLPA-Analyse wurde eine heterozygote Deletion im Promotorbereich des *SCN5A* Gens der Verstorbenen identifiziert, welche jedoch nicht in anderen Familienangehörigen nachgewiesen werden konnte. Um die Deletion in der 5‘-Richtung gelegenen Region des *SCN5A* Gens zu bestätigen und näher eingrenzen zu können, wurde ein RT-qPCR durchgeführt. Die Deletion konnte bestätigt werden und liegt zwischen Position -1845 bis -1610 vor der Transkriptionsstartstelle. Es wird vermutet, dass Sequenzvarianten im Promotorbereich des *SCN5A* Gens die Transkriptionsaktivität desselben beeinflussen und dadurch das Arrhythmierisiko erhöhen. Im vorliegenden Fall deuten die Ergebnisse darauf hin, dass *SCN5A*-E1053K keine unabhängige pathogene Variante ist, sondern in Verbindung mit zusätzlichen genetischen Modifikationen das Risiko eines plötzlichen Herztodes erhöht.

In einem zweiten SCD Fall eines 17-jährigen Mädchens, wurden, ebenfalls im *SCN5A* Gen, zwei heterozygote Sequenzvarianten, A572D und H558R, identifiziert. Es wird vermutet, dass *SCN5A*-A572D in Kombination mit anderen genetischen Modifikationen das Risiko ein LQTS zu entwickeln erhöht. In einer früheren Studie konnte gezeigt werden, dass *SCN5A*-A572D in Verbindung mit der häufigen Variante H558R auf dem gleichen Allel (*„cis“*-Position) in HEK293-Zellen eine LQTS-ähnliche Dysfunktion verursacht. Um zu testen, ob im vorliegenden Fall ebenfalls beide Varianten auf demselben Allel vorlagen, wurde eine DNA-Haplotypisierung durchgeführt. Diese Analyse bestätigte die *„cis“*-Position der beiden Varianten A572D und H558R auf dem *SCN5A* Gen. Es kann angenommen werden, dass D572 in Verbindung mit R558 auf dem gleichen Allel des *SCN5A* Gens bei dem plötzlichen Herztod der jungen Frau ursächlich gewesen sein könnte.

6. LIST OF FIGURES

7. LIST OF ABBREVATIONS

µM	micromolar
3D	three dimensional
Å	Ångström
AA	amino acid
ATP	adenosine triphosphate
bp	base pair
BrS	Brugada syndrome
$CaCl_2$	calcium chloride
CCD	cardiac conduction disease
CLSM	confocal laser scanning microscopy
CNBD	cyclic nucleotide-binding domain
DCM	dilated cardiomyopathy
ddH_2O	double-distilled water
DMEM	Dulbecco's modified eagle medium
DMSO	dimethyl sulfoxide
DNA	deoxyribonucleic acid
ECG	electrocardiogram
EGFP	enhanced green fluorescent protein
EGTA	ethylene glycol tetraacetic acid
ER	endoplasmatic reticulum
ExAC	Exome Aggregation Consortium
GFP	green fluorescent protein
GPR15	G-protein coupled receptor 15
HEK293	human embryonic kidney cells
HEPES	4-(2-hydroxyethyl) piperazine-1-ethanesulfonic acid
hERG	human ether-a-go-go related gene
I-V	current-voltage
ICD	implantable cardioverter defibrillator
I_{Kr}	rapidly activating delayed rectifier potassium current
I_{Na}	sodium current
KCl	potassium chloride
KCNH2	potassium voltage-gated channel subfamily H member 2
KCNQ1	potassium voltage-gated channel subfamily Q member 1
KOH	potassium hydroxide
LQTS	long QT syndrome
MAF	minor allele frequency
MLPA	Multiplex Ligation-dependent Probe Amplification
mM	millimolar
MΩ	Megaohm
MRI	Magnetic Resonance Imaging
mV	millivolt
n	number
n.d.	not determined
nA	nanoampere
NaCl	sodium chloride
NCBI	National Center of Biotechnology
p	probability
pA	picoampere
PAS	Per-Arnt-Sim
PBS	phosphate buffered saline
PDB	Protein Data Bank
PDL	poly-D-lysine
qPCR	quantitative PCR
SCD	sudden cardiac death
SCN5A	sodium voltage-gated channel alpha subunit 5
SD	standard deviation
SNP	single nucleotide polymorphism
SSS	sick sinus syndrome
TdP	Torsade des pointes tachycardia
U	Units
WT	wildtype
ZNF80	zinc finger protein 80

8. OWN WORK

Experiments, data analysis and writing of the present thesis with exception of the following items, were all done by myself.

- The *KCNH2*-L69P mutation (Chapter 1) was first identified in the thesis of Nadine Kiehne, TU Darmstadt, 2011.

- Patch clamp recordings of the hERG-L69P mutant at 37°C and 27°C (Chapter 1) were part of the bachelor thesis of Johanna Schäfer, TU Darmstadt, 2014.

- ECG data shown in Fig. 21 (Chapter 2) were provided by Dr. Britt-Maria Beckmann, Medizinische Klinik 1, Klinikum der Ludwig-Maximilians-Universität, München.

- MLPA analysis (Chapter 2) was in part performed by Stella Rose (Hochschule, Bonn-Rhein-Sieg) during her bachelor thesis at the Institut für Rechtsmedizin, Frankfurt, 2014.

- Clinical data of the *KCNH2*-E876X-family (Chapter 3) were provided by Prof. Dr. Thomas Neumann, Kerckhoff-Klinik, Abteilung für Elektrophysiologie, Bad Nauheim.

9. EHRENWÖRTLICHE ERKLÄRUNG

Ich erkläre hiermit ehrenwörtlich, dass ich die vorliegende Arbeit entsprechend den Regeln guter wissenschaftlicher Praxis selbstständig und ohne unzulässige Hilfe Dritter angefertigt habe. Sämtliche aus fremden Quellen direkt oder indirekt übernommenen Gedanken sowie sämtliche von Anderen direkt oder indirekt übernommenen Daten, Techniken und Materialien sind als solche kenntlich gemacht. Die Arbeit wurde bisher bei keiner anderen Hochschule zu Prüfungszwecken eingereicht.

Darmstadt, den _____

_____

Tina Jenewein

10. DANKSAGUNG

Zum Abschluss möchte ich mich bei allen herzlich bedanken, die zum Gelingen dieser Arbeit beigetragen haben:

Prof. Dr. Gerhard Thiel, für die Betreuung und Begutachtung dieser Arbeit. Für die Möglichkeit die elektrophysiologischen Messungen in seinem Arbeitskreis durchzuführen und für das stetige Interesse und die Unterstützung dieser Arbeit über einen so langen Zeitraum.

Prof. Dr. Ralf Galuske, für die sofortige Bereitschaft das Koreferat zu übernehmen.

PD Dr. Silke Kauferstein, für die externe Betreuung und Begutachtung der Arbeit und für ihre langjährige Unterstützung und Motivation.

Prof. Dr. Marcel Verhoff und besonders seinem Vorgänger, **Prof. Dr. Hansjürgen Bratzke**, für die Ermöglichung der Arbeit durch die Bereitstellung sämtlicher Geräte und Materialien; **Prof. Dr. Dietrich Mebs** für das Korrekturlesen der Arbeit.

Dr. Brigitte Hertel, für ihre große Hilfsbereitschaft, ihre Unterstützung bei der Auswertung der hERG Daten und die schönen Tage in der AG Thiel

Anne Berthold für die vielen Stunden am CLSM und **Johanna Schäfer** für die Messung der hERG-L69P Mutante und die gemeinsamen Tage am Patch-Platz.

Dr. Stephanie Biel für die gemeinsame Zeit während der Promotion und die gegenseitige Hilfe.

Svenja Schütt für ihre langjährige Freundschaft und die schöne Zeit im Labor; bei allen Kollegen im DNA-Labor für das freundschaftliche Arbeitsklima.

Meiner Familie – **Stefan, Malin und Eline**, für euer Verständnis, eure Unterstützung und Geduld und vor allem eure Liebe! Tausend Dank an Stefan, der oft an mir verzweifelt ist, mich aber immer uneingeschränkt unterstützt und motiviert hat!

Meinen Eltern – ihr seid in meinem Herzen.

11. CURRICULUM VITAE

Name	Tina Jenewein
Date of birth	03.01.1978
Place of birth	Frankfurt am Main

Experience

Since 01/2013	**Doctoral programme**, Technische Universität Darmstadt, Fachbereich Biologie
06/2011-12/2012	**Research assistant**, Institut für Rechtsmedizin, Abteilung Forensische Genetik, Frankfurt am Main
11/2008-10/2010	**Research assistant**, Institut für Rechtsmedizin, DNA-Abteilung, München
03/2007-10/2008	**Research assistant**, Institut für Rechtsmedizin, DNA-Abteilung, Frankfurt am Main
06/2006-02/2007	**Research assistant**, Sanofi-Aventis, Abteilung Metabolism and Pharmacokinetics, Frankfurt am Main

Education

10/2000-02/2006	**Studies in biology**, Johann Wolfgang Goethe-Universität, Frankfurt am Main Diploma thesis: “Untersuchungen zum Gentransfer in dem moderat halophilen Bakterium *Halobacillus halophilus*“ (Institut für Mikrobiologie, Prof. Dr. V. Müller)
10/1997-10/2000	**Apprenticeship** for medical technical assistant, staatliche Schule für technische Assistenten in der Medizin, Klinikum der Johann Wolfgang Goethe-Universität, Frankfurt am Main
09/1988 – 07/1997	Freiherr-vom-Stein Gymnasium, Frankfurt am Main
09/1984 – 07/1988	Friedrich-Fröbel-Grundschule, Frankfurt am Main

Talks

2013	92. Jahrestagung der DGRM, Saarbrücken,

	“Charakterisierung kardialer Sequenzveränderungen als Grundlage einer gezielten genetischen Beratung”
2012	91. Jahrestagung der DGRM, Freiburg “Genomic rearrangements in cardiac genes – a possible cause for sudden cardiac death?”

Workshops

2012	PhD course: Sudden Cardiac Death, Department of Forensic Medicine, Kopenhagen, Dänemark

C:\Users\Jenewein\Documents\Dissertation\finale Versionen\M.docx